Toulouse limit for the nonequilibrium Kondo impurity: Currents, noise spectra, and magnetic properties

Avraham Schiller
Department of Physics, The Ohio State University, Columbus, Ohio 43210-1106

Selman Hershfield
Department of Physics and National High Magnetic Field Laboratory, University of Florida, P.O. Box 118440, Gainesville, Florida 32611
(Received 2 April 1998)

We present an exact solution to the nonequilibrium Kondo problem, based on a special point in the parameter space of the model where both the Hamiltonian and the operator describing the nonequilibrium distribution can be diagonalized simultaneously. Through this solution we are able to compute the differential conductance, spin current, charge-current noise, and magnetization, for arbitrary voltage bias. The differential conductance shows the standard zero-bias anomaly and its splitting under an applied magnetic field. A detailed analysis of the scaling properties at low temperature and voltage is presented. The spin current is independent of the sign of the voltage. Its direction depends solely on the sign of the magnetic field and the asymmetry in the transverse coupling to the left and right leads. The charge-current noise can exceed $2eI_c$ for a large magnetic field, where I_c is the charge current. This is not seen in noninteracting quantum problems, but occurs here because of the tunneling of pairs of electrons. The finite-frequency noise spectrum has singularities at $\hbar\Omega = \pm 2\,\mathrm{eV}$, which cannot be explained in terms of noninteracting electrons. These singularities are traced to a different type of pair process involving the simultaneous creation or annihilation of two scattering states. The impurity susceptibility has three characteristic peaks as a function of magnetic field, two of which are due to interlead processes and one is due to intralead processes. Although the solvable point is only one point in the parameter space of the nonequilibrium Kondo problem, we expect it to correctly describe the strong-coupling regime of the model for arbitrary antiferromagnetic coupling constants and to be qualitatively correct as one leaves the strong-coupling regime. [S0163-1829(98)02442-4]

I. INTRODUCTION

The interplay between strong correlations and mesoscopic systems is an active area of research. Systems being studied experimentally and theoretically include quasi-one-dimensional wires,[1] mesoscopic superconductors,[2] quantum Hall devices,[3] quantum dots,[4] and other quantum impurities. In some cases, the reduced dimensionality of the system leads to new physics, while in other cases it allows one to probe known physical phenomena in new ways. One system which falls in the latter category is tunneling through a Kondo impurity. The tunneling spectroscopy allows one to directly probe the Kondo resonance that develops at low temperature due to the screening of the impurity spin by the conduction electrons.

The phenomena of tunneling through a Kondo impurity has a long history. It was first discovered by accident in the early 1960s,[5] when magnetic impurities were present in tunnel junctions between two normal metals.[6] A zero-bias anomaly was seen, which enhanced the conductance at low voltages. Shortly after the original experiments, Appelbaum[7] and Anderson[7] developed a perturbative theory which captured the essential features of the experiment: a zero-bias conductance that increased logarithmically with decreasing temperature and a zero-bias anomaly which split in the presence of a sufficiently large magnetic field. Although quite successful in explaining the qualitative and in some cases the quantitative results, the Appelbaum-Anderson theory is perturbative and hence cannot describe the strong-coupling regime of the Kondo effect. Experimentally, it is now possible to access this regime for a single magnetic impurity both in metallic point contacts[8] and in quantum dots.[9]

Despite the wide range of many-body techniques[10] that have been applied in recent years to get at the strong-coupling regime of the nonequilibrium Kondo model, there are still no rigorous results for the nonequilibrium state. This is to be contrasted with the equilibrium case, which is exactly solvable using the Bethe ansatz.[11] In this paper, we present an exact solution of the nonequilibrium problem at a special point in the parameter space of the nonequilibrium Kondo model, related to the Toulouse limit[12] of the ordinary Kondo problem and the Emery-Kivelson[13] solution of the two-channel Kondo model. We give both the details of the solution and an extensive discussion of the results, some of which have been reported earlier in a short publication.[14]

One of the primary advantages of a solvable point is that many different observables can be computed. In the nonequilibrium Kondo problem, the calculations have focused exclusively on the charge current and differential conductance. In addition to the differential conductance for the charge current, we compute the spin current through the impurity, the charge-current noise as a function of voltage, temperature, and frequency, and the impurity magnetization and susceptibility. As far as we know, the spin current, noise, and magnetization have not been studied before in the context of the nonequilibrium Kondo problem.

 ©1998 The American Physical Society

In particular, because one can calculate so many observables at the solvable point, new and surprising physics is revealed. We find that the spin current is independent of the sign of the applied voltage, and its direction is determined by the asymmetry in the transverse coupling to the left and to the right leads. The charge-current shot noise in an applied magnetic field can actually exceed the Poisson value of $2eI_c$ (I_c is the charge current), which we are able to explain by virtual processes involving the tunneling of pairs of electrons with opposite spin. As a function of frequency, we find a new set of singularities in the noise spectrum at $\Omega=\pm 2eV/\hbar$, i.e., twice the conventional frequencies. Such singularities have no analog in noninteracting systems, and are associated with particle-particle and hole-hole excitations for the scattering states, which are the elementary excitations of the system. Finally, even in the case of the nonlinear differential conductance, we are able to compute the scaling curve at low temperature and low voltage, and show that it is distinct from that of the resonant-level model.

An important aspect of this paper is the unique approach to nonequilibrium interacting quantum problems. With the conventional approaches, one starts with a well-defined initial density matrix ρ_0 describing an unperturbed system in equilibrium. The expectation value of a given operator $\hat{A}$ at some later time t is obtained by switching on the interactions that drive the system out of equilibrium and evolving the operator in the Heisenberg representation:

$$\rho_0=\frac{e^{-\beta(\mathcal{H}_0-Y_0)}}{\mathrm{Tr}\{e^{-\beta(\mathcal{H}_0-Y_0)}\}}, \tag{1.1}$$

$$\langle \hat{A}(t)\rangle=\mathrm{Tr}\{\rho_0\hat{A}(t)\}. \tag{1.2}$$

Here $\mathcal{H}_0$ is the unperturbed part of the Hamiltonian, and Y_0 is an operator describing the nonequilibrium condition (e.g., a chemical-potential difference). Each of the standard nonequilibrium Green-function techniques[15,16] represents a different way of implementing the time evolution in Eq. (1.2). Specifically, a nonequilibrium steady state is reached by setting the initial time to be infinitely far in the past and assuming that correlation functions decay in time.

Recently, under the same assumption that correlation functions decay in time, an equivalent operator equation has been derived for the steady-state nonequilibrium density matrix:[17]

$$[Y,\mathcal{H}]=i\eta(Y_0-Y), \tag{1.3}$$

$$\langle \hat{A}\rangle=\frac{\mathrm{Tr}\{e^{-\beta(\mathcal{H}-Y)}\hat{A}\}}{\mathrm{Tr}\{e^{-\beta(\mathcal{H}-Y)}\}}. \tag{1.4}$$

Here η is a positive infinitesimal introduced to ensure appropriate boundary conditions. It does not enter any physical quantities. In Eqs. (1.3) and (1.4), the task of implementing the time evolution in Eq. (1.2) has been replaced with that of (i) solving Eq. (1.3) for the Y operator and (ii) evaluating averages with respect to $e^{-\beta(\mathcal{H}-Y)}$. In practice, Eq. (1.3) is solved by constructing the many-body scattering states for the problem at hand,[17] which illustrates the added complexity in solving for the nonequilibrium state: In addition to diagonalizing the Hamiltonian, one must work in a particular many-body basis set that simultaneously diagonalizes the (yet-to-be-determined) Y operator.

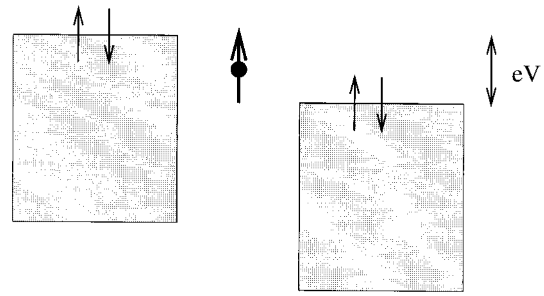

FIG. 1. Schematic description of the physical system. We consider a tunnel junction that consists of two leads of noninteracting spin-1/2 electrons and a spin-1/2 impurity moment placed in between the two leads. Tunneling across the junction takes place by way of the impurity moment, via an exchange interaction between the impurity spin and the conduction electrons in both leads. The effect of an applied voltage bias is to fix a chemical-potential difference $\mu_L-\mu_R=eV$ between the two Fermi seas.

In this paper, we demonstrate by explicit calculation the equivalence of the two approaches to nonequilibrium for the nontrivial problem of tunneling through a Kondo impurity. In particular, after transforming both $\mathcal{H}$ and Y_0 to quadratic forms, we compute all observables in two distinct ways: one using conventional nonequilibrium Green-function techniques and the other by finding the many-body scattering states and solving Eqs. (1.3) and (1.4). Both approaches are exact and give identical results; however, each technique has advantages and disadvantages. For example, in the case of the charge-current noise it is easier to obtain final expressions using the Green-function technique, but their physical interpretation is more transparent in the scattering-state representation. Since this is one solution in a potentially larger class of nonequilibrium problems, we explain in detail each of the techniques used.

The organization of the rest of the paper is as follows: In Sec. II we introduce the model. In Sec. III we present the mapping onto an equivalent noninteracting nonequilibrium problem, which is solved in turn in Sec. IV. Sections V, VI, VII, and VIII contain detailed discussions of the charge current, spin current, charge-current noise, and impurity magnetization, respectively, the main results of which are summarized in Sec. IX. Technical details and a comprehensive set of analytic expressions for the physical observables are provided in four appendixes.

II. MODEL AND ITS LIMITS

A. Model

The physical system under consideration is shown schematically in Fig. 1. It consists of left (L) and right (R) leads of noninteracting spin-1/2 electrons, which interact via an exchange coupling with a spin-1/2 impurity moment placed in between the two leads. In the standard fashion,[18] the conduction-electron channels that couple to the impurity are reduced to one-dimensional fields $\psi_{\alpha\sigma}(x)$, where $\alpha=L,R$ and $\sigma=\uparrow,\downarrow$ are the lead and spin indices, respectively. Here we have linearized the conduction-electron dispersion around the Fermi level: $\epsilon_k=\hbar v_F k$, where ϵ_k and k are measured relative to the Fermi level and Fermi wave number, respectively. x is a fictitious position variable conjugate to k.

In terms of the one-dimensional fields, the exchange interaction with the impurity spin, $\vec{\tau}$, takes place via the conduction-electron spin densities at the origin:

$$\vec{s}_{\alpha\beta}=\frac{1}{2}\sum_{\sigma,\sigma'}\psi^{\dagger}_{\alpha\sigma}(0)\vec{\sigma}_{\sigma,\sigma'}\psi_{\beta\sigma'}(0). \tag{2.1}$$

The two diagonal elements $\vec{s}_{LL}$ and $\vec{s}_{RR}$ are independent spin densities for the left and right leads, respectively, while the spinlike operators $\vec{s}_{LR}$ and $\vec{s}_{RL}$ introduce tunneling between the leads. The system is driven out of equilibrium by applying a voltage bias V across the junction. This fixes a chemical-potential difference $\mu_L-\mu_R=eV$ between the two Fermi seas, causing a steady-state charge current to flow in the direction of the applied bias. We assume that the voltage drops entirely in the region between the two metallic leads—a reasonable assumption given that the resistance of the tunnel junction is much larger than that of the leads.

Thus, the most general form of the Hamiltonian $\mathcal{H}$ and the nonequilibrium condition Y_0 is

$$\mathcal{H}=i\hbar v_F\sum_{\alpha=L,R}\sum_{\sigma=\uparrow,\downarrow}\int_{-\infty}^{\infty}\psi^{\dagger}_{\alpha\sigma}(x)\,\frac{\partial}{\partial x}\psi_{\alpha\sigma}(x)dx + \sum_{\alpha,\beta=L,R}\sum_{\lambda=x,y,z}J^{\alpha\beta}_{\lambda}s^{\lambda}_{\alpha\beta}\tau^{\lambda}-\mu_B g_i H\tau^{z}, \tag{2.2}$$

$$Y_0=\frac{eV}{2}\sum_{\sigma}\int_{-\infty}^{\infty}[\psi^{\dagger}_{L\sigma}\psi_{L\sigma}-\psi^{\dagger}_{R\sigma}\psi_{R\sigma}]dx, \tag{2.3}$$

where we have allowed for different couplings $J^{\alpha\beta}_{\lambda}=J^{\beta\alpha}_{\lambda}$ between the conduction electrons and the impurity spin, and also for a local magnetic field H. Here μ_B and g_i are the magneton Bohr and impurity Landé g factor, respectively. Note that in Eq. (2.2) we have omitted for conciseness the electrostatic potential energy on each lead, $U_{\alpha}=-eV_{\alpha}$. This contribution to the Hamiltonian can easily be incorporated within our approach, but has no effect on the physical quantities under consideration as long as eV is much smaller than the conduction-electron bandwidth. The latter is assumed throughout the paper to be the largest energy scale in the problem.

For $J^{\alpha\beta}_{\lambda}=J>0$, Eqs. (2.2) and (2.3) reduce to the standard nonequilibrium Kondo problem, treated perturbatively by Appelbaum[7] and Anderson.[7] Here we take a different approach. Rather then setting all coupling constants equal to one another and starting at weak coupling, we identify a special point in the parameter space of the model where it can be solved exactly. Specifically, we show that the Hamiltonian (2.2) together with the nonequilibrium condition (2.3) can be solved for arbitrary bias V in that region of the $J^{\alpha\beta}_{\lambda}$ parameter space where

$$J^{\alpha\beta}_{x}=J^{\alpha\beta}_{y}\equiv J^{\alpha\beta}_{\perp}, \tag{2.4}$$

$$J^{LR}_{z}=J^{RL}_{z}=0, \tag{2.5}$$

and

$$J^{LL}_{z}=J^{RR}_{z}\equiv J_z \tag{2.6}$$

with $J_z=2\pi\hbar v_F$. This provides the first exact solution of a nonequilibrium Kondo model, from which both universal and nonuniversal features of Kondo-assisted tunneling can be extracted. Before proceeding with details of our solution, let us first examine the meaning of Eqs. (2.5) and (2.6).

B. Scaling equations

We begin by asking, how restrictive are the above constraints on the longitudinal Kondo couplings? To answer this question we focus on the $V=0$ equilibrium case and use Anderson's poor man's scaling[19] to derive scaling equations for the Kondo couplings. Our objective is to determine under which circumstances is a nonzero J^{LR}_{z} coupling generated as the bandwidth is reduced.

To lowest order in the couplings, the scaling equations are

$$\frac{dJ^{LL}_{z}}{dl}=\frac{1}{2\pi\hbar v_F}[(J^{LL}_{\perp})^2+(J^{LR}_{\perp})^2],$$

$$\frac{dJ^{RR}_{z}}{dl}=\frac{1}{2\pi\hbar v_F}[(J^{RR}_{\perp})^2+(J^{LR}_{\perp})^2],$$

$$\frac{dJ^{LR}_{z}}{dl}=\frac{1}{2\pi\hbar v_F}(J^{RR}_{\perp}+J^{LL}_{\perp})J^{LR}_{\perp}, \tag{2.7}$$

with a similar set of equations for the transverse couplings $J^{\alpha\beta}_{\perp}$. Here $l=\ln(E_0/E)$ is the logarithm of the renormalized bandwidth E and E_0 is the bare bandwidth. Starting with $J^{LR}_{z}=0$, a nonzero J^{LR}_{z} coupling is generated from Eqs. (2.7) unless the two leads are decoupled to begin with or if $J^{RR}_{\perp}+J^{LL}_{\perp}=0$. Moreover, $J^{LL}_{z}\neq J^{RR}_{z}$ is also generated from Eqs. (2.7) if the bare transverse couplings $J^{LL}_{\perp}$ and $J^{RR}_{\perp}$ differ in magnitude. Only in two special cases do we find that both $J^{LR}_{z}=0$ and $J^{LL}_{z}=J^{RR}_{z}$ remain stable upon scaling. This occurs if the bare Kondo couplings satisfy either

$$J^{LL}_{\perp}=J^{RR}_{\perp}\quad\text{and}\quad J^{LR}_{\perp}=0 \tag{2.8}$$

or

$$J^{LL}_{\perp}=-J^{RR}_{\perp}. \tag{2.9}$$

As we shall see in the next subsection, these two cases correspond to two distinct two-channel[20] limits of the Hamiltonian of Eq. (2.2).

Hence, with the exception of conditions (2.8) and (2.9), scaling trajectories for our model flow to a nonzero longitudinal coupling J^{LR}_{z} and also to $J^{LL}_{z}\neq J^{RR}_{z}$ if the bare transverse couplings satisfy $|J^{LL}_{\perp}|\neq|J^{RR}_{\perp}|$.

C. Limits of the Hamiltonian

Next we recast the Hamiltonian in a form more suitable for identifying its various limits. Using the spinor notation

$$\Psi_{\sigma}(x)=\begin{pmatrix}\psi_{R\sigma}\\ \psi_{L\sigma}\end{pmatrix}, \tag{2.10}$$

the Kondo interaction in Eq. (2.2) is written as

$$\mathcal{H}_{Kondo}=\frac{1}{2}[\Psi_{\uparrow}^{\dagger}(0)\hat{J}_z\Psi_{\uparrow}(0)-\Psi_{\downarrow}^{\dagger}(0)\hat{J}_z\Psi_{\downarrow}(0)]\tau^z + \frac{1}{2}\Psi_{\uparrow}^{\dagger}(0)\hat{J}_{\perp}\Psi_{\downarrow}(0)\tau^- + \frac{1}{2}\Psi_{\downarrow}^{\dagger}(0)\hat{J}_{\perp}\Psi_{\uparrow}(0)\tau^+, \tag{2.11}$$

where

$$\hat{J}_z=\begin{pmatrix} J_z^{RR} & J_z^{RL} \\ J_z^{LR} & J_z^{LL}\end{pmatrix}, \quad \hat{J}_{\perp}=\begin{pmatrix} J_{\perp}^{RR} & J_{\perp}^{RL} \\ J_{\perp}^{LR} & J_{\perp}^{LL}\end{pmatrix}. \tag{2.12}$$

Here $\tau^{\pm}=\tau^x \pm i\tau^y$ are the standard raising and lowering operators for the impurity spin: $\tau^{\lambda}=\frac{1}{2}\sigma^{\lambda}$, where σ^{λ} is a Pauli matrix. In general, $\hat{J}_z$ and $\hat{J}_{\perp}$ are two symmetric matrices which need not commute with one another. Thus, while each matrix can be diagonalized separately, it might not be possible to diagonalize them simultaneously.

This is the point where conditions (2.5) and (2.6) come into play. Subject to Eqs. (2.5) and (2.6), the longitudinal-coupling matrix $\hat{J}_z$ is simply proportional to the unity matrix, leaving only $\hat{J}_{\perp}$ to be diagonalized. This can be achieved by carrying out the linear transformation

$$\begin{pmatrix}\psi_{1\sigma}\\ \psi_{2\sigma}\end{pmatrix}=\hat{T}\begin{pmatrix}\psi_{R\sigma}\\ \psi_{L\sigma}\end{pmatrix}, \tag{2.13}$$

where

$$\hat{T}=\frac{1}{\sqrt{(J_{\perp}^{LR})^2+\lambda^2}}\begin{pmatrix}\lambda & -J_{\perp}^{LR}\\ J_{\perp}^{LR} & \lambda\end{pmatrix} \tag{2.14}$$

and

$$\lambda=\frac{1}{2}(J_{\perp}^{LL}-J_{\perp}^{RR})+\frac{1}{2}\sqrt{(J_{\perp}^{LL}-J_{\perp}^{RR})^2+4(J_{\perp}^{LR})^2}. \tag{2.15}$$

In terms of the new conduction-electron channels $\psi_{1\sigma}$ and $\psi_{2\sigma}$, the Kondo interaction reduces to

$$\mathcal{H}_{Kondo}=J_z s_1^z\tau^z+J_{\perp 1}(s_1^x\tau^x+s_1^y\tau^y) + J_z s_2^z\tau^z+J_{\perp 2}(s_2^x\tau^x+s_2^y\tau^y), \tag{2.16}$$

where

$$J_{\perp 1,2}=\frac{1}{2}(J_{\perp}^{LL}+J_{\perp}^{RR})\mp\frac{1}{2}\sqrt{(J_{\perp}^{LL}-J_{\perp}^{RR})^2+4(J_{\perp}^{LR})^2} \tag{2.17}$$

are the eigenvalues of the $\hat{J}_{\perp}$ matrix and

$$\vec{s}_i=\frac{1}{2}\sum_{\sigma,\sigma'}\psi_{i\sigma}^{\dagger}(0)\vec{\sigma}_{\sigma,\sigma'}\psi_{i\sigma'}(0), \quad i=1,2, \tag{2.18}$$

are the spin-density operators corresponding to conduction-electron channels 1 and 2.

Thus, the Hamiltonian has the form of a generalized two-channel Kondo model,[20] with an additional channel anisotropy in the transverse coupling. In particular, the conventional isotropic two-channel model (i.e., with two *equivalent* channels) is recovered when either $J_{\perp 1}=J_{\perp 2}$ or $J_{\perp 1}=-J_{\perp 2}$. In terms of the bare model parameters, these two limits correspond to conditions (2.8) and (2.9), respectively.

What are the two channels in each of these two limits? For $J_{\perp}^{LL}=J_{\perp}^{RR}$ and $J_{\perp}^{LR}=0$, Eq. (2.8), the two leads are decoupled. Hence the channels are just the right and left leads, which obviously carry no current. For $J_{\perp}^{LL}=-J_{\perp}^{RR}$, Eq. (2.9), one needs first to make $J_{\perp 1}$ equal to $J_{\perp 2}$ by attaching a minus phase to one of the fermion fields, say, $\psi_{1\uparrow}(x)$. The physical picture depends then in a continuous manner on the interplay between $J_{\perp}^{LR}$ and $J_{\perp}^{LL}-J_{\perp}^{RR}$. When $|J_{\perp}^{LR}|\ll|J_{\perp}^{LL}-J_{\perp}^{RR}|$, the system approaches a limit where the leads are again decoupled. The channels are basically the right and left leads, with minor mixing of the two leads. Mixing of the leads gradually increases as $J_{\perp}^{LR}$ becomes comparable to $J_{\perp}^{LL}-J_{\perp}^{RR}$. Eventually, for $|J_{\perp}^{LR}|\gg|J_{\perp}^{LL}-J_{\perp}^{RR}|$, the channels are (i) spin-up electrons in the left lead and spin-down electrons in the right lead and (ii) spin-down electrons in the left lead and spin-up electrons in the right lead.

As soon as $J_{\perp 1}\neq\pm J_{\perp 2}$, our model departs from its two-channel limits and becomes that of a two-channel Kondo impurity with channel anisotropy. The extent of anisotropy between the channels can be continuously tuned by varying the different transverse couplings. An opposite limit is reached when one of the $J_{\perp 1}$, $J_{\perp 2}$ couplings vanishes. This may be regarded as an effective one-channel limit, as only one conduction-electron channel undergoes spin-flip scattering. In terms of the original parameters of the model, this case is described by the condition

$$J_{\perp}^{LL}J_{\perp}^{RR}=(J_{\perp}^{LR})^2. \tag{2.19}$$

In equilibrium, we can actually show that the above limit is equivalent to the ordinary one-channel Kondo Hamiltonian (see Appendix A). We further note that Eq. (2.19) is always satisfied when the Hamiltonian of Eq. (2.2) is derived from an Anderson impurity model via a Schrieffer-Wolff transformation.[21] We therefore expect the effective one-channel limit of Eq. (2.19) to best describe the conventional Appelbaum-Anderson model.[7] Further support for this interpretation will later emerge in the course of our solution. It should be emphasized, though, that our particular choice of model parameters cannot be the outcome of a Schrieffer-Wolff transformation, as the latter generates equal transverse and longitudinal couplings. This relation is obviously violated within our model since J_z^{LR} is set equal to zero.

D. Magnetic field

Finally, a few words are in order on the magnetic field. When an external magnetic field acts on the conduction-electron spins, it polarizes their spins. This generates a net bulk magnetization in each lead, which modifies the effective field seen by the impurity. H in our model should therefore be viewed as the *overall* effective magnetic field seen by the impurity—applied and induced.

To make the discussion quantitative, consider a weak external magnetic field H_{ext} acting on all spin degrees of freedom. When coupled to the spins of the conduction electrons, H_{ext} induces in each lead a bulk magnetization equal to

$$M_{bulk} = \frac{1}{2}(\mu_B g_e)^2 \rho_0 H_{ext}. \tag{2.20}$$

Here g_e and $\rho_0 = (2\pi\hbar v_F)^{-1}$ are the conduction-electron Landé g factor and density of states, respectively. The impurity spin, being coupled to M_{bulk} through the Kondo interaction, thus experiences an induced magnetic field of magnitude

$$H_{ind} = -g_i^{-1} g_e J_z \rho_0 H_{ext}, \tag{2.21}$$

which acts to reduce the overall field seen by the impurity. Hence, inasmuch as impurity-related quantities are concerned, the effect of a magnetic field acting on the conduction-electron spins can be fully absorbed into a renormalization of the local field that couples to the impurity spin according to[22]

$$H = H_{ext} + H_{ind} = (1 - g_i^{-1} g_e J_z \rho_0) H_{ext}. \tag{2.22}$$

[In the case where $J_z^{LL} \neq J_z^{RR}$, one needs to replace J_z in Eq. (2.22) with $(J_z^{LL} + J_z^{RR})/2$.]

As can be seen from Eq. (2.22), there is really only one physical parameter which determines the effect of a magnetic field on impurity-related quantities, and that is $\Delta E_{mag} \equiv \mu_B g_i H$. There are two approaches one could take towards determining this parameter: (i) One could deduce it experimentally, e.g., from the measured Zeeman splitting in the differential conductance. (ii) One could determine the effective field H from the applied magnetic field H_{ext} and the model parameters entering the renormalization factor of Eq. (2.22), i.e., g_i, g_e, J_z^{LL}, J_z^{RR}, and ρ_0. At the solvable point, the renormalization factor actually vanishes if $g_e = g_i$. Even more surprising, it becomes negative if $g_e > g_i$. In this paper we take the first approach and regard $\mu_B g_i H$ in Eq. (2.2) as an independent parameter to be determined directly from experiment.

III. MAPPING ONTO A NONINTERACTING NONEQUILIBRIUM PROBLEM

In this section, we present the mapping of Eqs. (2.2) and (2.3) onto an equivalent noninteracting nonequilibrium problem. Normally, mapping of an interacting quantum-mechanical problem onto a noninteracting one means that one can perform a canonical transformation to reduce the Hamiltonian to a quadratic form. For a nonequilibrium problem, in addition to the Hamiltonian the transformation must also preserve the quadratic form of Y_0, or else the task of finding Y and diagonalizing $\mathcal{H} - Y$ remains a true many-body problem. This sets an added constraint, which often prevents the extension of successful mappings in equilibrium to the nonequilibrium state. Equations (2.2) and (2.3) provide a rare example where such an extension is possible.

The reduction of $\mathcal{H}$ and Y_0 to quadratic forms relies on bosonizing the one-dimensional fields.[23,24] The derivation presented below is a generalization of the Emery-Kivelson solution of the two-channel Kondo model,[13] designed to account for the extra channel-symmetry-breaking terms present in our model. Here, although the natural degrees of freedom for describing the Kondo interaction were seen in the previous section to be $\psi_{1\sigma}$ and $\psi_{2\sigma}$, we shall work directly with the left- and right-lead electrons as these couple more transparently to the applied voltage.

Following Emery and Kivelson[13] we introduce four different boson fields

$$\Phi_{\alpha\sigma}(x) = \sqrt{\pi}\left\{ \int_{-\infty}^{x} \Pi_{\alpha\sigma}(x')dx' + \phi_{\alpha\sigma}(x) \right\}, \tag{3.1}$$

to account for the four different left-moving fermion species entering Eqs. (2.2) and (2.3). Here $\phi_{\alpha\sigma}(x)$ and $\Pi_{\alpha\sigma}(x)$ are real, conjugate boson fields satisfying standard commutation relations:

$$[\phi_{\alpha\sigma}(x), \Pi_{\alpha'\sigma'}(x')] = i\delta_{\alpha,\alpha'}\delta_{\sigma,\sigma'}\delta(x-x'). \tag{3.2}$$

The left-moving fermions are expressed as[23,24]

$$\psi_{\alpha\sigma}(x) = \frac{e^{i\varphi_{\alpha\sigma}}}{\sqrt{2\pi a}} e^{-i\Phi_{\alpha\sigma}(x)}, \tag{3.3}$$

where a^{-1} is an ultraviolet momentum cutoff, corresponding to a lattice spacing. The additional phases $\varphi_{\alpha\sigma}$ are required to assure that the different fermion species anticommute with one another. Our choices for these phases are

$$\varphi_{L\uparrow} = \pi \int_{-\infty}^{\infty} [\psi_{L\downarrow}^{\dagger}\psi_{L\downarrow} + \psi_{R\uparrow}^{\dagger}\psi_{R\uparrow} + \psi_{R\downarrow}^{\dagger}\psi_{R\downarrow}]dx,$$

$$\varphi_{L\downarrow} = \pi \int_{-\infty}^{\infty} [\psi_{R\uparrow}^{\dagger}\psi_{R\uparrow} + \psi_{R\downarrow}^{\dagger}\psi_{R\downarrow}]dx,$$

$$\varphi_{R\uparrow} = \pi \int_{-\infty}^{\infty} \psi_{R\downarrow}^{\dagger}\psi_{R\downarrow}dx, \tag{3.4}$$

and $\varphi_{R\downarrow} = 0$. Alternatively, Eqs. (3.4) can be written directly in terms of the Φ fields, by replacing each $\psi_{\alpha\sigma}^{\dagger}(x)\psi_{\alpha\sigma}(x)$ above with $\nabla\Phi_{\alpha\sigma}(x)/(2\pi)$.

Using the well-known prescriptions for bosonizing,[23,24] both the Hamiltonian and Y_0 are expressed in terms of the four boson fields $\Phi_{\alpha\sigma}(x)$. The $\Phi_{\alpha\sigma}(x)$ are used in turn to construct four new boson fields, corresponding to collective charge, spin, flavor (left minus right), and spin-flavor modes:

$$\Phi_c = \frac{1}{2}(\Phi_{L\uparrow} + \Phi_{L\downarrow} + \Phi_{R\uparrow} + \Phi_{R\downarrow}),$$

$$\Phi_s = \frac{1}{2}(\Phi_{L\uparrow} - \Phi_{L\downarrow} + \Phi_{R\uparrow} - \Phi_{R\downarrow}),$$

$$\Phi_f = \frac{1}{2}(\Phi_{L\uparrow} + \Phi_{L\downarrow} - \Phi_{R\uparrow} - \Phi_{R\downarrow}),$$

$$\Phi_{sf} = \frac{1}{2}(\Phi_{L\uparrow} - \Phi_{L\downarrow} - \Phi_{R\uparrow} + \Phi_{R\downarrow}). \tag{3.5}$$

Similar combinations also apply to each of $\phi_\nu(x)$, $\Pi_\nu(x)$, and the phases φ_ν ($\nu = c,s,f,sf$). The latter can also be written directly in terms of the new collective fields, for example,

$$\varphi_f=\frac{1}{4}\int_{-\infty}^{\infty}[2\nabla\Phi_c(x)-\nabla\Phi_f(x)-\nabla\Phi_{sf}(x)]dx, \quad (3.6)$$

$$\varphi_{sf}=\frac{1}{4}\int_{-\infty}^{\infty}[\nabla\Phi_f(x)-\nabla\Phi_{sf}(x)]dx. \quad (3.7)$$

Introducing for convenience the shorthand notation $\chi_\nu=\Phi_\nu(0)-\varphi_\nu$, we notice that χ_s commutes with both χ_f and χ_{sf}. Thus, the Hamiltonian $\mathcal{H}$ and the nonequilibrium operator Y_0 are written as

$$\mathcal{H}=\frac{\hbar v_F}{4\pi}\sum_{\nu=c,s,f,sf}\int_{-\infty}^{\infty}(\nabla\Phi_\nu)^2dx+\frac{J^+}{\pi a}[-\tau^x\sin(\chi_s)+\tau^y\cos(\chi_s)]\cos(\chi_{sf})-\frac{J^-}{\pi a}[\tau^x\cos(\chi_s)+\tau^y\sin(\chi_s)]\sin(\chi_{sf})-\frac{J_\perp^{LR}}{\pi a}[\tau^x\cos(\chi_s)+\tau^y\sin(\chi_s)]\sin(\chi_f)+\frac{J_z}{2\pi}\nabla\Phi_s(0)\tau^z-\mu_Bg_iH\tau^z \quad (3.8)$$

and

$$Y_0=\frac{eV}{2\pi}\int_{-\infty}^{\infty}\nabla\Phi_f(x)dx, \quad (3.9)$$

where $J^\pm$ are the even and odd combinations:

$$J^\pm=\frac{1}{2}(J_\perp^{LL}\pm J_\perp^{RR}). \quad (3.10)$$

A crucial feature of the bosonized Hamiltonian is that χ_s enters the spin-flip terms of Eq. (3.8) only as an effective angle of rotation. Hence it can be conveniently removed[13] by rotating both $\mathcal{H}$ and Y_0 about the z axis: $\mathcal{H}'=U\mathcal{H}U^\dagger$, $Y_0'=UY_0U^\dagger$, with $U=\exp[i\chi_s\tau^z]$. Y_0, being proportional to $\nabla\Phi_f(x)$, is unaffected by the canonical transformation; however, the Hamiltonian simplifies to[13]

$$\mathcal{H}'=\frac{\hbar v_F}{4\pi}\sum_{\nu=c,s,f,sf}\int_{-\infty}^{\infty}(\nabla\Phi_\nu)^2dx+\frac{J^+}{\pi a}\tau^y\cos(\chi_{sf})-\frac{J^-}{\pi a}\tau^x\sin(\chi_{sf})-\frac{J_\perp^{LR}}{\pi a}\tau^x\sin(\chi_f)+\left[\frac{J_z}{2\pi}-\hbar v_F\right]\nabla\Phi_s(0)\tau^z-\mu_Bg_iH\tau^z. \quad (3.11)$$

At this point we transform to a new fermion representation. To this end, we first express the τ spin in terms of a fermion operator:

$$d=i\tau^x-\tau^y=i\tau^+. \quad (3.12)$$

The Bose fields are then ‘‘refermionized’’ according to

$$\psi_f(x)=\frac{e^{i\pi d^\dagger d}}{\sqrt{2\pi a}}e^{-i[\Phi_f(x)-\varphi_f]}, \quad (3.13)$$

$$\psi_{sf}(x)=\frac{e^{i\pi d^\dagger d}}{\sqrt{2\pi a}}e^{-i[\Phi_{sf}(x)-\varphi_{sf}]}, \quad (3.14)$$

with similar expressions for $\psi_c(x)$ and $\psi_s(x)$. Here the $i\pi d^\dagger d$ phase takes care of the anticommutation relations between the d fermion and the $\psi_\nu(x)$ fields, while φ_f and φ_{sf} [see Eqs. (3.6) and (3.7)] guarantee that the flavor and spin-flavor fermions anticommute. The remaining anticommutation relations involving either $\psi_c(x)$ or $\psi_s(x)$ are easily taken care of by slightly modifying the phases φ_c and φ_s.

Once these steps are completed, the Hamiltonian $\mathcal{H}'$ and the nonequilibrium operator Y_0' acquire the following fermion forms:

$$\mathcal{H}'=i\hbar v_F\sum_{\nu=c,s,f,sf}\int_{-\infty}^{\infty}\psi_\nu^\dagger(x)\frac{\partial}{\partial x}\psi_\nu(x)dx+\frac{J^+}{2\sqrt{2\pi a}}[\psi_{sf}^\dagger(0)+\psi_{sf}(0)](d^\dagger-d)+\frac{J_\perp^{LR}}{2\sqrt{2\pi a}}[\psi_f^\dagger(0)-\psi_f(0)](d^\dagger+d)+\frac{J^-}{2\sqrt{2\pi a}}[\psi_{sf}^\dagger(0)-\psi_{sf}(0)](d^\dagger+d)+[\mu_Bg_iH-(J_z-2\pi\hbar v_F){:}\psi_s^\dagger(0)\psi_s(0){:}](d^\dagger d-1/2) \quad (3.15)$$

and

$$Y_0'=eV\int_{-\infty}^{\infty}\psi_f^\dagger(x)\psi_f(x)dx. \quad (3.16)$$

Here ${:}\psi_s^\dagger(0)\psi_s(0){:}$ means normal ordering with respect to the unperturbed ψ_s Fermi sea. Strictly speaking, Y_0' and the kinetic-energy terms of $\mathcal{H}'$ are also normal ordered; however, normal ordering of these terms is left implicit since it merely amounts to shifting Y_0' and $\mathcal{H}'$ by constants. By contrast, normal ordering of $\psi_s^\dagger(0)\psi_s(0)$ is essential, as this combination multiplies the operator $d^\dagger d-1/2$.

The solvable line is readily identified from Eqs. (3.15) and (3.16). Upon setting $J_z=2\pi\hbar v_F$, both the Hamiltonian and the nonequilibrium operator Y_0' reduce to quadratic forms. Hence the strongly interacting nonequilibrium Kondo problem maps onto a noninteracting one, which may be regarded as the *nonequilibrium analog* of the Toulouse limit.[12]

Although noninteracting, the resulting nonequilibrium problem is somewhat unconventional in the sense that $\mathcal{H}'$ does not conserve the overall number of transformed fermions (not to be confused with the original electrons in the problem). Moreover, it involves the combinations

$$\hat{a}=\frac{d+d^\dagger}{\sqrt{2}}, \quad \hat{b}=\frac{d^\dagger-d}{i\sqrt{2}}, \quad (3.17)$$

which are Majorana fermions.[13] The Majorana fermions satisfy $\hat{a}^2=\hat{b}^2=1/2$ instead of zero as for usual fermions, a fact that will have important implications later on. If $H=0$ and the $J_\perp^{\alpha\beta}$ parameters are such that only one of $\hat{a}$ or $\hat{b}$ couples to the ψ fermions, $\mathcal{H}'$ reduces to the Emery-Kivelson[13] limit of the two-channel Kondo Hamiltonian. Recalling the definition of $J^\pm$, Eq. (3.10), this is seen to occur when either Eq. (2.8) or Eq. (2.9) is satisfied, i.e., for each of the two two-channel limits identified in the previous section.

IV. SOLUTION OF THE NONINTERACTING NONEQUILIBRIUM PROBLEM

At this stage both $\mathcal{H}'$ and Y_0' are quadratic, hence the nonequilibrium problem can be solved exactly. We shall do so using two independent routes: (A) by explicitly constructing the Y' operator in terms of scattering-state operators and (B) by standard diagrammatic techniques. The latter approach will require a specific decomposition of the Hamiltonian into a perturbation $\mathcal{H}_1'$ and an unperturbed part $\mathcal{H}_0'$. Since both formulations employed are exact, they must coincide when applied to any physical observable. This will provide us with a critical check as to the correctness of our results.

A. Explicit construction of the Y' operator

The first thing to recognize is that $Y' = UYU^\dagger$ obeys the operator equation

$$[Y',\mathcal{H}'] = i\eta(Y_0' - Y'), \tag{4.1}$$

which follows from applying the canonical transformation U to both sides of Eq. (1.3). Y' is therefore composed of scattering-state operators.[17]

For a standard single-particle scattering problem, scattering states are eigenstates of the Schrödinger equation obeying suitable boundary conditions.[25] They are given as solutions of the corresponding Lippmann-Schwinger equation. Within second quantization, an analogous equation may be written down for the scattering-state operators, which in this case simply create electrons in the scattering states. For a noninteracting problem, the two representations are equivalent, due to the one-to-one correspondence between single-particle states in first quantization and creation operators in second quantization. However, as soon as interactions are switched on, the scattering-state operators acquire complicated many-body components that can no longer be described in terms of single-particle states. Even in our case, where $\mathcal{H}'$ is quadratic in fermion operators, the scattering-state operators do not conserve the number of particles and thus have no first-quantization analog.

Equations (3.15) and (3.16) contain four species of fermion fields, yet both ψ_c and ψ_s are decoupled from the d fermion and the Y_0' operator for $J_z = 2\pi\hbar v_F$. As a result, only ψ_f and ψ_{sf} need to be considered when computing impurity-related quantities such as the current. Restricting our attention to the latter fields, we introduce their Fourier transforms

$$\psi_\nu^\dagger(x) = \frac{1}{\sqrt{L}} \sum_k \psi_{\nu,k}^\dagger e^{ikx} \quad (\nu = f, sf). \tag{4.2}$$

Here L is the size of the system, and k takes the discrete values $k = 2\pi n/L$. The Fourier components satisfy

TABLE I. Definition of energy scales and symbols used in the solution of the nonequilibrium Kondo model. Here $J_\perp^{\alpha\beta}$ are the transverse Kondo couplings from Eq. (2.2), $J^\pm$ are the even and odd combinations defined in Eq. (3.10), and a is an ultraviolet momentum cutoff, corresponding to a lattice spacing. Physically, the energy scales Γ_a and Γ_b play the role of Kondo temperatures at the solvable point. The remaining energies show up as coefficients in the expansion of physical operators in terms of the scattering-state operators (see Table II) and as prefactors in the final expressions for physical quantities.

Symbol	Definition
Γ_a	$[(J_\perp^{LR})^2 + (J^-)^2]/4\pi a\hbar v_F$
Γ_b	$(J^+)^2/4\pi a\hbar v_F$
Γ_1	$(J_\perp^{LR})^2/4\pi a\hbar v_F$
Γ_2	$(J^-)^2/4\pi a\hbar v_F$
Γ_L	$(J_\perp^{LL})^2/4\pi a\hbar v_F$
Γ_R	$(J_\perp^{RR})^2/4\pi a\hbar v_F$
Γ_m	$J_\perp^{LR} J^-/4\pi a\hbar v_F$
Γ_p	$J_\perp^{LR} J^+/4\pi a\hbar v_F$

$$\{\psi_{\nu,k}^\dagger, \psi_{\nu',k'}\} = \delta_{k,k'}\delta_{\nu,\nu'}. \tag{4.3}$$

Rewriting Eqs. (3.15) and (3.16) for $J_z = 2\pi\hbar v_F$ in terms of the $\psi_{\nu,k}$ operators yields

$$\begin{aligned}\mathcal{H}' = &\sum_{\nu=f,sf}\sum_k \epsilon_k \psi_{\nu,k}^\dagger \psi_{\nu,k} - i\mu_B g_i H \hat{a}\hat{b} \\ &+ i\frac{J^+}{2\sqrt{\pi a L}}\sum_k (\psi_{sf,k}^\dagger + \psi_{sf,k})\hat{b} \\ &+ \frac{J_\perp^{LR}}{2\sqrt{\pi a L}}\sum_k (\psi_{f,k}^\dagger - \psi_{f,k})\hat{a} \\ &+ \frac{J^-}{2\sqrt{\pi a L}}\sum_k (\psi_{sf,k}^\dagger - \psi_{sf,k})\hat{a}\end{aligned} \tag{4.4}$$

and

$$Y_0' = eV\sum_k \psi_{f,k}^\dagger \psi_{f,k}, \tag{4.5}$$

where ϵ_k is equal to $\hbar v_F k$.

The scattering-state operators for the flavor and spin-flavor channels, $c_{f,k}^\dagger$ and $c_{sf,k}^\dagger$, respectively, are defined by the operator equation[17]

$$[c_{\nu,k}^\dagger, \mathcal{H}'] = -\epsilon_k c_{\nu,k}^\dagger + i\eta(\psi_{\nu,k}^\dagger - c_{\nu,k}^\dagger), \tag{4.6}$$

in which the positive infinitesimal η is introduced to guarantee appropriate boundary conditions. Due to the quadratic nature of $\mathcal{H}'$, one can solve these equations exactly. Leaving the details of the derivation to Appendix B, here we present their solutions.

In writing the solutions for the scattering-state operators of Eq. (4.6), we use the notation specified in Table I. The two basic energy scales in the problem are

$$\Gamma_a = \frac{1}{4\pi a\hbar v_F}[(J_\perp^{LR})^2 + (J^-)^2] \tag{4.7}$$

and

$$\Gamma_b = \frac{1}{4\pi a\hbar v_F}(J^+)^2, \tag{4.8}$$

which play the role of Kondo temperatures at the solvable point.[13] It is also useful to define the matrix function

$$G(z) \equiv \begin{bmatrix} G_{aa} & G_{ab} \\ G_{ba} & G_{bb} \end{bmatrix} = \frac{1}{(z \pm i\Gamma_a)(z \pm i\Gamma_b) - (\mu_B g_i H)^2} \times \begin{bmatrix} z \pm i\Gamma_b & -i\mu_B g_i H \\ i\mu_B g_i H & z \pm i\Gamma_a \end{bmatrix}, \tag{4.9}$$

where upper (lower) signs correspond to z in the upper (lower) half plane. Although not apparent at this point, $G(z)$ will turn out to be the Majorana Green function (see next subsection). Notice that G is diagonal in the a-b basis only for a zero magnetic field, in which case Γ_a and Γ_b are the spectral broadenings of the $\hat{a}$ and $\hat{b}$ spectral functions, respectively. In particular, the effective one-channel limit of Eq. (2.19) corresponds to the case where $\Gamma_a = \Gamma_b$, which features, in accordance with the ordinary one-channel scenario, only a single Kondo scale. Using the above Majorana Green function, the scattering-state operators are given by

$$c_{f,k}^\dagger = \psi_{f,k}^\dagger + \frac{J_\perp^{LR}}{2\sqrt{\pi a L}}[G_{aa}(\epsilon_k + i\eta)\hat{\alpha}_k + G_{ba}(\epsilon_k + i\eta)\hat{\beta}_k], \tag{4.10}$$

$$c_{sf,k}^\dagger = \psi_{sf,k}^\dagger + \frac{J^-}{2\sqrt{\pi a L}}[G_{aa}(\epsilon_k + i\eta)\hat{\alpha}_k + G_{ba}(\epsilon_k + i\eta)\hat{\beta}_k] - i\frac{J^+}{2\sqrt{\pi a L}}[G_{ab}(\epsilon_k + i\eta)\hat{\alpha}_k + G_{bb}(\epsilon_k + i\eta)\hat{\beta}_k]. \tag{4.11}$$

To keep the notation concise, we have introduced in Eqs. (4.10) and (4.11) two k-dependent operators

$$\hat{\alpha}_k = \hat{a} + \frac{J_\perp^{LR}}{2\sqrt{\pi a L}}\sum_{k'}\left(\frac{\psi_{f,k'}^\dagger}{\epsilon_k - \epsilon_{k'} + i\eta} - \frac{\psi_{f,k'}}{\epsilon_k + \epsilon_{k'} + i\eta}\right) + \frac{J^-}{2\sqrt{\pi a L}}\sum_{k'}\left(\frac{\psi_{sf,k'}^\dagger}{\epsilon_k - \epsilon_{k'} + i\eta} - \frac{\psi_{sf,k'}}{\epsilon_k + \epsilon_{k'} + i\eta}\right) \tag{4.12}$$

and

$$\hat{\beta}_k = \hat{b} + i\frac{J^+}{2\sqrt{\pi a L}}\sum_{k'}\left(\frac{\psi_{sf,k'}^\dagger}{\epsilon_k - \epsilon_{k'} + i\eta} + \frac{\psi_{sf,k'}}{\epsilon_k + \epsilon_{k'} + i\eta}\right). \tag{4.13}$$

One can directly confirm at this point that the scattering-state operators given above satisfy the commutation relations of Eq. (4.6) for a general $\eta \neq 0$, not only $\eta \to 0^+$ as is implicitly assumed throughout our treatment. Further, $c_{f,k}^\dagger$ and $c_{sf,k}^\dagger$ obey standard anticommutation relations

$$\{c_{\nu,k}^\dagger, c_{\nu',k'}\} = \delta_{k,k'}\delta_{\nu,\nu'}, \quad \{c_{\nu,k}, c_{\nu',k'}\} = 0. \tag{4.14}$$

Hence, despite being composed of both creation and annihilation operators of the bare Fermi degrees of freedom, $c_{f,k}^\dagger$ and $c_{sf,k}^\dagger$ are fermion creation operators.

As one might expect from Eqs. (4.6) and (4.14), the transformed Hamiltonian is diagonal in the scattering-state basis. Indeed, one can rigorously show that

$$\mathcal{H}' = \sum_k \epsilon_k (c_{f,k}^\dagger c_{f,k} + c_{sf,k}^\dagger c_{sf,k}) \tag{4.15}$$

by replacing all scattering-state operators in Eq. (4.15) with their explicit expressions, Eqs. (4.10) and (4.11). After some lengthy but straightforward algebra, Eq. (4.15) is found in this manner to be identical to Eq. (4.4).

The main strength of the scattering-state formalism, though, lies in the Y' operator, which is solved directly in diagonal form. Up to an insignificant constant, Y' is given by

$$Y' = eV\sum_k c_{f,k}^\dagger c_{f,k}, \tag{4.16}$$

which again can be verified rigorously. To see this one needs to substitute Y' from Eq. (4.16) into the operator equation (4.1) and exploit some basic properties of the scattering-state operators. A complete derivation of this important result is provided in Appendix C. Thus, as previously argued in Ref. 17, Y' is obtained from Y_0' by simply replacing all bare fermion operators that appear in Y_0' with their scattering-state counterparts.

Having obtained and diagonalized the operator $\mathcal{H}' - Y'$, our nonequilibrium Kondo problem is nearly solved. All that remains to be done is to express the physical observables, whose steady-state averages we wish to compute, in terms of the scattering-state operators. Once this step is completed, averages with respect to $e^{-\beta(\mathcal{H}' - Y')}$ are readily carried out. In Table II we list a few basic operator identities, which serve as building blocks for constructing physical operators. Each of these entries may be verified directly using Eqs. (4.10) and (4.11). The physical observables of interest include the charge and spin currents $\hat{I}_c$ and $\hat{I}_s$, respectively, and the impurity magnetization $M^z = \mu_B g_i \tau^z$. To identify the new representations of these operators, it is necessary to go back to the initial description of the system in terms of left- and right-lead electrons.

Consider first the charge current $\hat{I}_c$. The charge current measures the rate at which electric charge increases on the left lead or, equivalently, the rate at which electric charge decreases on the right lead (for a Kondo impurity, the two are identical). Therefore, the charge current from right to left (which amounts to e times the number current from left to right) is given by

$$\hat{I}_c = \frac{ie}{2\hbar}[\hat{N}_{L\uparrow} + \hat{N}_{L\downarrow} - \hat{N}_{R\uparrow} - \hat{N}_{R\downarrow}, \mathcal{H}], \tag{4.17}$$

TABLE II. Expansion of useful operator combinations in terms of the scattering-state operators. Here $c^{\dagger}_{f,k}$ and $c^{\dagger}_{sf,k}$ are the scattering-state operators for the flavor and spin-flavor channels, respectively, $J^{LR}_{\perp}$ is the transverse Kondo coupling for flipping the impurity spin while tunneling an electron across the junction, $J^{\pm}$ are the even and odd combinations of Eq. (3.10), and $G_{\alpha\beta}$ are the corresponding components of the Majorana Green function, Eq. (4.9). The different Γ's are defined in Table I.

Operator	Expansion in terms of scattering-state operators
$\hat{a}$	$(4\pi aL)^{-1/2}\Sigma_k\{J^{LR}_{\perp}G_{aa}(\epsilon_k-i\eta)c^{\dagger}_{f,k}+[J^{-}G_{aa}(\epsilon_k-i\eta)+iJ^{+}G_{ba}(\epsilon_k-i\eta)]c^{\dagger}_{sf,k}\}$ $+(4\pi aL)^{-1/2}\Sigma_k\{J^{LR}_{\perp}G_{aa}(\epsilon_k+i\eta)c_{f,k}+[J^{-}G_{aa}(\epsilon_k+i\eta)-iJ^{+}G_{ab}(\epsilon_k+i\eta)]c_{sf,k}\}$
$\hat{b}$	$(4\pi aL)^{-1/2}\Sigma_k\{J^{LR}_{\perp}G_{ab}(\epsilon_k-i\eta)c^{\dagger}_{f,k}+[J^{-}G_{ab}(\epsilon_k-i\eta)+iJ^{+}G_{bb}(\epsilon_k-i\eta)]c^{\dagger}_{sf,k}\}$ $+(4\pi aL)^{-1/2}\Sigma_k\{J^{LR}_{\perp}G_{ba}(\epsilon_k+i\eta)c_{f,k}+[J^{-}G_{ba}(\epsilon_k+i\eta)-iJ^{+}G_{bb}(\epsilon_k+i\eta)]c_{sf,k}\}$
$L^{-1/2}\Sigma_k(\psi^{\dagger}_{f,k}+\psi_{f,k})$	$L^{-1/2}\Sigma_k(c^{\dagger}_{f,k}+c_{f,k})$
$L^{-1/2}\Sigma_k(\psi^{\dagger}_{sf,k}+\psi_{sf,k})$	$L^{-1/2}\Sigma_k\{\Gamma_pG_{ab}(\epsilon_k-i\eta)c^{\dagger}_{f,k}+[1+\frac{1}{4}(\Gamma_L-\Gamma_R)G_{ab}(\epsilon_k-i\eta)+i\Gamma_bG_{bb}(\epsilon_k-i\eta)]c^{\dagger}_{sf,k}\}$ $+L^{-1/2}\Sigma_k\{\Gamma_pG_{ba}(\epsilon_k+i\eta)c_{f,k}+[1+\frac{1}{4}(\Gamma_L-\Gamma_R)G_{ba}(\epsilon_k+i\eta)-i\Gamma_bG_{bb}(\epsilon_k+i\eta)]c_{sf,k}\}$
$L^{-1/2}\Sigma_k(\psi^{\dagger}_{sf,k}-\psi_{sf,k})$	$L^{-1/2}\Sigma_k\{i\Gamma_mG_{aa}(\epsilon_k-i\eta)c^{\dagger}_{f,k}+[1+\frac{1}{4}(\Gamma_L-\Gamma_R)G_{ab}(\epsilon_k-i\eta)+i\Gamma_2G_{aa}(\epsilon_k-i\eta)]c^{\dagger}_{sf,k}\}$ $+L^{-1/2}\Sigma_k\{i\Gamma_mG_{aa}(\epsilon_k+i\eta)c_{f,k}+[-1+\frac{1}{4}(\Gamma_L-\Gamma_R)G_{ab}(\epsilon_k+i\eta)+i\Gamma_2G_{aa}(\epsilon_k+i\eta)]c_{sf,k}\}$

where $\hat{N}_{\alpha\sigma}$ is the number operator for electrons with spin σ on lead α. Upon carrying out the canonical transformation U, this maps onto

$$\hat{I}'_c \equiv U\hat{I}_cU^{\dagger}=\frac{ie}{\hbar}[\hat{N}_f,\mathcal{H}'], \tag{4.18}$$

with $\hat{N}_f=\Sigma_k\psi^{\dagger}_{f,k}\psi_{f,k}$ being the flavor-fermion number operator.

The spin-current operator is obtained in a similar fashion. $\hat{I}_s$ is defined as the difference in number currents for the spin-up and spin-down electrons. Alternatively, $\hat{I}_s$ measures the rate at which magnetization flows across the tunnel junction. In steady state, the outgoing spin current from the left lead is equal to the incoming spin current for the right lead, and hence the steady-state spin current from left to right is written in a symmetric manner as

$$\hat{I}_s=\frac{i}{2\hbar}[\hat{N}_{L\uparrow}-\hat{N}_{L\downarrow}-\hat{N}_{R\uparrow}+\hat{N}_{R\downarrow},\mathcal{H}]. \tag{4.19}$$

This translates under the canonical transformation to

$$\hat{I}'_s \equiv U\hat{I}_sU^{\dagger}=\frac{i}{\hbar}[\hat{N}_{sf},\mathcal{H}'], \tag{4.20}$$

where $\hat{N}_{sf}=\Sigma_k\psi^{\dagger}_{sf,k}\psi_{sf,k}$ is the spin-flavor number operator. Finally, the impurity magnetization is unaffected by the canonical transformation and remains equal to $M^z=\mu_B g_i\tau^z$.

To complete our solution, the explicit expressions for $\hat{I}'_c$, $\hat{I}'_s$, and M^z in terms of the Majorana and ψ fermions are gathered in Table III. These may be easily expanded in terms of scattering-state operators using the operator identities listed in Table II. The resultant expressions, although cumbersome, are straightforward to work with when evaluating averages with respect to $e^{-\beta(\mathcal{H}'-Y')}$. Such averages will be used extensively in the next few sections, where a variety of physical quantities and response functions are computed.

B. Diagrammatic solution

In this subsection, we solve the quadratic nonequilibrium problem defined by $\mathcal{H}'$ and Y'_0 using the nonequilibrium Green-function technique. Because the problem is quadratic, one is able to sum all diagrams exactly, providing an alternative solution to the noninteracting problem. This approach is equivalent to the one presented in the previous subsection and must give the same result for any physical observable.

A key step in applying this approach is to choose a practical decomposition of the Hamiltonian into an unperturbed part and a perturbation, where all processes that drive the system out of equilibrium are contained within the latter part. The initial density matrix is taken accordingly to be

$$\rho_0=\frac{e^{-\beta(\mathcal{H}_0-Y_0)}}{\mathrm{Tr}\{e^{-\beta(\mathcal{H}_0-Y_0)}\}}, \tag{4.21}$$

where $\mathcal{H}_0$ is the unperturbed part of the Hamiltonian, and Y_0 is the same nonequilibrium operator that enters the Y-operator formalism.[17]

To make our choice for $\mathcal{H}_0$ physically transparent, we go back to the initial description of the system in terms of left-

TABLE III. Expansion of transformed operators describing physical observables in terms of the Majorana and ψ fermions. Here $J^{LR}_{\perp}$ is the transverse Kondo coupling for processes combining flipping of the impurity spin with tunneling of an electron across the junction. $J^{\pm}$ are the even and odd combinations of Eq. (3.10).

Observable	Symbol	Operator
Charge current	$\hat{I}'_c=$	$i\dfrac{eJ^{LR}_{\perp}}{2\hbar\sqrt{\pi aL}}\sum_k(\psi^{\dagger}_{f,k}+\psi_{f,k})\hat{a}$
Spin current	$\hat{I}'_s=$	$i\dfrac{J^{-}}{2\hbar\sqrt{\pi aL}}\Sigma_k(\psi^{\dagger}_{sf,k}+\psi_{sf,k})\hat{a}$
Magnetization	$M^z=$	$-\dfrac{J^{+}}{2\hbar\sqrt{\pi aL}}\Sigma_k(\psi^{\dagger}_{sf,k}-\psi_{sf,k})\hat{b}$ $i\mu_Bg_i\hat{a}\hat{b}$

and right-lead electrons. Typically, $\mathcal{H}_1$ is chosen such that $\mathcal{H}_0$ and ρ_0 are diagonal single-particle operators. For a nonequilibrium Kondo problem, this means starting with two disconnected leads at different chemical potentials and treating all components of the Hamiltonian involving the magnetic impurity as a perturbation. Here we use a slightly different decomposition, for reasons that will become clear shortly. In addition to the kinetic-energy terms for each lead, we also include within $\mathcal{H}_0$ the longitudinal Kondo terms:

$$\mathcal{H}_0 = i\hbar v_F \sum_{\alpha=L,R} \sum_{\sigma=\uparrow,\downarrow} \int_{-\infty}^{\infty} \psi^\dagger_{\alpha\sigma}(x)\, \frac{\partial}{\partial x}\, \psi_{\alpha\sigma}(x)dx + J_z(s^z_{LL}+s^z_{RR})\tau^z. \tag{4.22}$$

This is a valid choice for $\mathcal{H}_0$ since Eq. (4.22) conserves the number of conduction electrons on both the left and right leads, and hence the two leads have well-defined, independent chemical potentials.

To determine how $\mathcal{H}_0 - Y_0$ transforms under the canonical transformation U, it is sufficient to set the transverse Kondo couplings and the local magnetic field to zero in Eqs. (4.4) and (4.5). This leads to

$$\rho_0' \equiv U\rho_0 U^\dagger = \frac{e^{-\beta(\mathcal{H}_0'-Y_0')}}{\mathrm{Tr}\{e^{-\beta(\mathcal{H}_0'-Y_0')}\}}, \tag{4.23}$$

with

$$\mathcal{H}_0' - Y_0' = \sum_k (\epsilon_k - eV)\psi^\dagger_{f,k}\psi_{f,k} + \sum_{\nu=c,s,sf} \sum_k \epsilon_k \psi^\dagger_{\nu,k}\psi_{\nu,k}. \tag{4.24}$$

The advantage of choosing $\mathcal{H}_0$ of Eq. (4.22) is now apparent: ρ_0' rather than ρ_0 takes the desired form of a diagonal single-particle density matrix, providing us with a representation in which both ρ_0' and $\mathcal{H}'$ have simple noninteracting forms.

We are now in position to apply perturbation theory with respect to $J_\perp^{LR}$, J^+, J^-, and H.[26] The main ingredients of the theory are the greater, lesser, retarded, and advanced Majorana Green functions, which are defined according to[27]

$$G^>_{\alpha\beta}(t,t') = \langle \hat{\alpha}(t)\hat{\beta}(t')\rangle, \tag{4.25}$$

$$G^<_{\alpha\beta}(t,t') = \langle \hat{\beta}(t')\hat{\alpha}(t)\rangle, \tag{4.26}$$

$$G^{r,a}_{\alpha\beta}(t,t') = \mp i\theta(\pm t \mp t')\langle\{\hat{\alpha}(t),\hat{\beta}(t')\}\rangle. \tag{4.27}$$

Here α,β are either a or b. For convenience, we represent hereafter all Majorana Green functions in terms of 2×2 matrices, with the convention that indices 1 and 2 correspond to a and b, respectively.

Due to time-translational invariance, all four response functions listed above depend on the single time argument $\Delta t = t - t'$. It is therefore advantageous to switch over to the energy domain, by introducing the Fourier transforms with respect to $\Delta t/\hbar$. The corresponding unperturbed retarded and advanced Majorana Green functions have the form

$$G_0^{r,a}(\epsilon) = \frac{1}{\epsilon \pm i\eta} I, \tag{4.28}$$

where I is the 2×2 unity matrix. The unperturbed flavor-channel Green functions are

$$g^<_{f,k}(\epsilon) = 2\pi\delta(\epsilon-\epsilon_k)f(\epsilon_k - eV), \tag{4.29}$$

$$g^>_{f,k}(\epsilon) = 2\pi\delta(\epsilon-\epsilon_k)f(eV-\epsilon_k), \tag{4.30}$$

$$g^{r,a}_{f,k}(\epsilon) = \frac{1}{\epsilon - \epsilon_k \pm i\eta}. \tag{4.31}$$

Similar expressions apply to the spin-flavor fermions; only V is set equal to zero.

Using standard diagrammatics, all Majorana self-energies are derived from contractions of the sort $\langle(\psi^\dagger \pm \psi)(\psi^\dagger \pm \psi)\rangle$. These are most conveniently handled in the wideband limit, where the simple relation

$$\frac{1}{L}\sum_k \frac{1}{\epsilon - \epsilon_k \pm i\eta} = \frac{1}{2\pi\hbar v_F}\int \frac{d\epsilon_k}{\epsilon-\epsilon_k \pm i\eta} = \mp\frac{i}{2\hbar v_F} \tag{4.32}$$

can be used to obtain the retarded and advanced self-energies

$$\Sigma^{r,a}(\epsilon) = \begin{bmatrix} \mp i\Gamma_a & -i\mu_B g_i H \\ i\mu_B g_i H & \mp i\Gamma_b \end{bmatrix} \tag{4.33}$$

and the greater and lesser self-energies

$$\Sigma^{>,<}(\epsilon) = \begin{bmatrix} 2\Gamma_1 f_{eff}(\mp\epsilon) + 2\Gamma_2 f(\mp\epsilon) & 0 \\ 0 & 2\Gamma_b f(\mp\epsilon) \end{bmatrix}. \tag{4.34}$$

Here Γ_a and Γ_b are the two Kondo scales defined in Eqs. (4.7) and (4.8), respectively, while Γ_1 is equal to $(J_\perp^{LR})^2/4\pi a\hbar v_F$ and Γ_2 is equal to $(J^-)^2/4\pi a\hbar v_F$. The function $f_{eff}(\epsilon)$, which enters the greater and lesser self-energies, is an effective distribution function that depends explicitly on the applied bias:

$$f_{eff}(\epsilon) = \frac{f(\epsilon+eV)+f(\epsilon-eV)}{2}. \tag{4.35}$$

For zero bias $f_{eff}(\epsilon)$ reduces to the ordinary Fermi-Dirac distribution function, while for finite bias it has two separate steps at $\epsilon = \pm eV$.

With the self-energies listed above, the retarded and advanced Green functions $G^{r,a}(\epsilon) = [\epsilon - \Sigma^{r,a}(\epsilon)]^{-1}$ are equal to the two analytic pieces of Eq. (4.9):

$$G^{r,a}(\epsilon) = G(\epsilon \pm i\eta). \tag{4.36}$$

The greater and lesser Green functions are given by the matrix products[28]

$$G^{>,<}(\epsilon) = G^r(\epsilon)\Sigma^{>,<}(\epsilon)G^a(\epsilon). \tag{4.37}$$

Equations (4.33)–(4.37) are the central result of this subsection. Together they provide us with exact, closed-form expressions for the different Majorana Green functions, which in turn can be used to compute observables such as the charge and spin currents, the charge-current noise spectrum, the impurity magnetization, and the impurity susceptibility. The latter quantities will be discussed in detail in the following sections.

V. CHARGE CURRENT

The first observable we compute is the charge current across the junction. Using the results of the previous two subsections we obtain the exact differential-conductance curve, which features a zero-bias anomaly that splits in the presence of a magnetic field. We analyze in detail the scaling properties of the differential conductance at low temperature and low voltage, and compare it to that of the noninteracting resonant-level model.

A. Derivation

The time-averaged charge current $I_c(V)$ may be calculated using either the scattering-state approach, developed in the previous section, or in the framework of standard diagrammatic techniques. In the former approach, one uses the operator identities listed in Tables II and III to expand the charge-current operator $\hat{I}_c'$ in terms of scattering-state operators. The charge current then follows from averaging $\hat{I}_c'$ with respect to $e^{-\beta(\mathcal{H}'-Y')}$:[17]

$$I_c(V)=\langle \hat{I}_c'\rangle=\frac{\mathrm{Tr}\{e^{-\beta(\mathcal{H}'-Y')}\hat{I}_c'\}}{\mathrm{Tr}\{e^{-\beta(\mathcal{H}'-Y')}\}}. \tag{5.1}$$

From Eqs. (4.15) and (4.16) we have

$$\mathcal{H}'-Y'=\sum_k (\epsilon_k-eV)c_{f,k}^{\dagger}c_{f,k}+\sum_k \epsilon_k c_{sf,k}^{\dagger}c_{sf,k}, \tag{5.2}$$

where $c_{f,k}^{\dagger}$, $c_{sf,k}^{\dagger}$ are standard Fermi operators. Hence the average in Eq. (5.1) is readily carried out using

$$\langle c_{f,k}^{\dagger}c_{f,k}\rangle=f(\epsilon_k-eV),\quad \langle c_{sf,k}^{\dagger}c_{sf,k}\rangle=f(\epsilon_k), \tag{5.3}$$

where $f(\epsilon)$ is the ordinary Fermi-Dirac distribution function.

The diagrammatic calculation of $I_c(V)$ is only slightly more complicated. Defining

$$G_{fk,a}^{>}(t,t')=\langle[\psi_{f,k}^{\dagger}(t)+\psi_{f,k}(t)]\hat{a}(t')\rangle, \tag{5.4}$$

the charge current is expressed as

$$I_c(V)=i\frac{eJ_{\perp}^{LR}}{2\hbar\sqrt{\pi aL}}\sum_k G_{fk,a}^{>}(t,t). \tag{5.5}$$

Switching to energy variables, $G_{fk,a}^{>}(\epsilon)$ is evaluated along the same lines as the Majorana Green functions using perturbation theory with respect to $J_{\perp}^{LR}$, J^{+}, J^{-}, and H. With the aid of Eq. (4.32) one obtains

$$\frac{1}{\sqrt{L}}\sum_k G_{fk,a}^{>}(\epsilon)=\frac{J_{\perp}^{LR}}{2v_F\hbar\sqrt{\pi a}}G_{aa}^{a}(\epsilon)\times[f(\epsilon+eV)-f(\epsilon-eV)], \tag{5.6}$$

from which the equal-time function follows as an integral over all ϵ. The resultant expression for the charge current is identical to that obtained using the scattering-state approach. It takes the familiar form of the integral of a spectral function times the difference of two Fermi functions, the spectral function here being that of the $\hat{a}$ Majorana fermion:

$$I_c(V)=\frac{e\Gamma_1}{2\pi\hbar}\int_{-\infty}^{\infty}A_a(\epsilon)[f(\epsilon-eV)-f(\epsilon+eV)]d\epsilon, \tag{5.7}$$

$$A_a(\epsilon)=-\mathrm{Im}\left\{\frac{\epsilon+i\Gamma_b}{(\epsilon+i\Gamma_a)(\epsilon+i\Gamma_b)-(\mu_B g_i H)^2}\right\}. \tag{5.8}$$

Three comments should be made about Eqs. (5.7) and (5.8). First, the arguments of the Fermi functions in Eq. (5.7) are shifted by $2eV$, not eV as in conventional expressions [see, e.g., Eq. (5.23) for the resonant-level model]. This is because we are working with flavor excitations, which have a chemical potential of eV instead of $eV/2$. Physically, when an electron is transferred from the right lead to the left one the number of flavor fermions is increased by 1, but the potential energy cost is equal to eV. The energy for creating a flavor fermion is therefore equal to eV rather than $eV/2$.

Second, the spectral function $A_a(\epsilon)$ in Eq. (5.7) is not that of the impurity spin in the original Hamiltonian. Instead, by inverting the canonical transformation U one sees that the Majorana fermion $\hat{a}$ corresponds to a composite of impurity and conduction-electron degrees of freedom. Consequently, there is no simple relation between $A_a(\epsilon)$ and the ordinary impurity-spin spectral function.

The third point to notice is that, at the solvable point, both the temperature and voltage enter into the charge current only through the Fermi functions, not via the spectral function which is independent of both V and T. This stems from the quadratic nature of the problem at the solvable point. As one goes away from the solvable point, the voltage and temperature will explicitly enter the spectral function as well.[29]

Equation (5.7) can further be written in closed form using the digamma function $\psi(z)$.[30] A single expression covering all parameter regimes of our model is provided in Appendix D, Eq. (D1). Here we mention only two important cases: (i) For a zero magnetic field, $A_a(\epsilon)$ is independent of Γ_b and has the shape of a Lorentzian with half-width Γ_a. Hence, after integration, the charge current becomes

$$I_c(V)=\frac{e\Gamma_1}{\pi\hbar}\mathrm{Im}\left\{\psi\left(\frac{1}{2}+\frac{\Gamma_a+ieV}{2\pi k_BT}\right)\right\}. \tag{5.9}$$

(ii) For $\Gamma_a=\Gamma_b$—corresponding to the effective one-channel limit—a nonzero magnetic field splits $A_a(\epsilon)$ into two identical Lorentzians centered about $\pm\mu_B g_i H$, each with a half-width of Γ_a. The charge current then takes the form

$$I_c(V)=\frac{e\Gamma_1}{2\pi\hbar}\mathrm{Im}\left\{\psi\left(\frac{1}{2}+\frac{\Gamma_a+ieV+i\mu_B g_i H}{2\pi k_BT}\right)+\psi\left(\frac{1}{2}+\frac{\Gamma_a+ieV-i\mu_B g_i H}{2\pi k_BT}\right)\right\}. \tag{5.10}$$

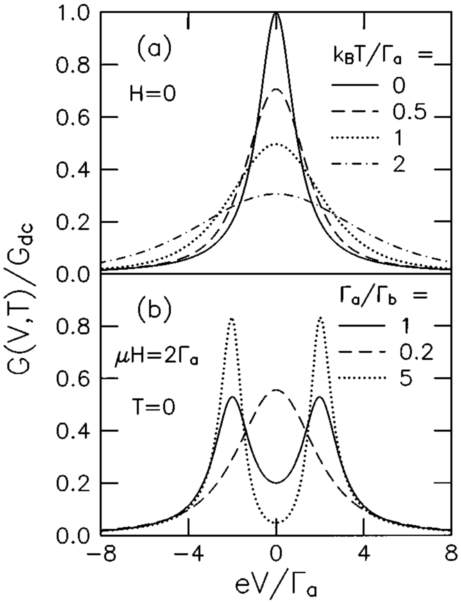

FIG. 2. The differential conductance $G(V,T)=dI_c/dV$ as a function of V (a) for zero magnetic field and different temperatures; the effect of T is to smear and reduce the peak height; and (b) at $T=0$ and $\mu_B g_i H=2\Gamma_a$, for different ratios of Γ_a to Γ_b. For either $\Gamma_a \ll \Gamma_b$ or $\Gamma_b \ll \Gamma_a$, two-channel limits are approached. This shows up in $G(V,0)$ as resonant transmission ($\Gamma_a \ll \Gamma_b$) or resonant reflection ($\Gamma_b \ll \Gamma_a$). Here $G_{dc}=e^2\Gamma_1/\pi\hbar\Gamma_a$ is the $T=0$, $H=0$ conductance, and $\mu=\mu_B g_i$.

B. Differential conductance

Figures 2 and 3 show the differential conductance $G(V,T)=dI_c/dV$ as a function of bias, for different temperatures and model parameters. We begin with the case of a zero magnetic field, shown in Fig. 2(a). Differentiation of Eq. (5.9) with respect to V yields

$$G(V,T)=\frac{e^2}{\pi\hbar}\frac{\Gamma_1}{2\pi k_B T}\,\mathrm{Re}\left\{\psi^{(1)}\left(\frac{1}{2}+\frac{\Gamma_a+ieV}{2\pi k_B T}\right)\right\}, \tag{5.11}$$

where $\psi^{(1)}(z)=d\psi/dz$ is the trigamma function.[30] At zero temperature, Eq. (5.11) reduces to a Lorentzian with half-width Γ_a and a zero-bias conductance equal to $G(0,0)=e^2\Gamma_1/\pi\hbar\Gamma_a$. For $\Gamma_1=\Gamma_a$, the zero-temperature conductance is thus optimal. It corresponds to one e^2/h conductance quanta per spin channel. For $\Gamma_1<\Gamma_a$, this value is suppressed by a factor of Γ_1/Γ_a, reflecting an asymmetry in the transverse coupling of the impurity to the two leads.

The effect of raising the temperature is mainly to smear and reduce the peak height. Specifically, using the asymptotic expansion[30] of $\psi^{(1)}(z)$ one finds, in accordance with Fermi-liquid behavior, that the conductance decreases quadratically with T at temperatures small compared to Γ_a:

$$G(0,T)=\frac{e^2\Gamma_1}{\pi\hbar\Gamma_a}\left[1-\frac{\pi^2}{3}\left(\frac{k_B T}{\Gamma_a}\right)^2+O(T^4)\right]. \tag{5.12}$$

Next we switch on a nonzero magnetic field, causing the energy scale Γ_b to enter the charge current. At $T=0$, the differential conductance is simply proportional to $A_a(eV)$. The effect of a magnetic field is thus seen along the following lines: for $H=0$, the differential conductance has the shape of a Lorentzian with half-width Γ_a; a nonzero magnetic field gradually broadens the zero-field resonance until it splits at a critical field $\mu_B g_i H_c=\Gamma_b/\sqrt{2+\Gamma_a/\Gamma_b}$; for $H>H_c$, the differential conductance is split. There are two symmetric resonances at a finite bias, accompanied by a minimum rather than a maximum at zero voltage. For large fields $\mu_B g_i H \gg \Gamma_a, \Gamma_b$, the two resonances are centered about $eV=\pm\mu_B g_i H$, each with a half-width of $(\Gamma_a+\Gamma_b)/2$.

In Fig. 2(b) we show the differential conductance for a moderately large magnetic field $\mu_B g_i H=2\Gamma_a$ at zero temperature and different ratios of Γ_a to Γ_b. For $\Gamma_a=\Gamma_b$, a nonzero magnetic field simply splits the zero-field resonance into two symmetric Lorentzians centered about $\pm\mu_B g_i H$. Similar magnetic splittings have also been observed in experiments[8,9] and will later appear in other physical quantities.

For either $\Gamma_a \ll \Gamma_b$ or $\Gamma_b \ll \Gamma_a$, the system approaches one of the two two-channel limits discussed in Sec. II. For $\Gamma_a \ll \Gamma_b$ the two-channel limit of Eq. (2.8) is approached, whereas for $\Gamma_b \ll \Gamma_a$ the limit of Eq. (2.9) is approached. Notice that the differential conductance in Fig. 2(b) is quite different for these two limits. For $\Gamma_a \ll \Gamma_b$, there is a single resonance at zero bias. Splitting of this resonance occurs at $\mu_B g_i H \approx \Gamma_b/\sqrt{2}$—i.e., at a Zeeman energy much *larger* than the zero-field half-width Γ_a. In the opposite limit, $\Gamma_b \ll \Gamma_a$, splitting takes place already at $\mu_B g_i H_c \approx \Gamma_b\sqrt{\Gamma_b/\Gamma_a}$, corresponding to a Zeeman energy much *smaller* than Γ_a (and possibly also Γ_b). Hence by the time $\mu_B g_i H \sim \Gamma_a$, as in Fig. 2(b), a sharp minimum rather than a maximum has developed at zero bias. Note that in the extreme limit $\Gamma_b=0$

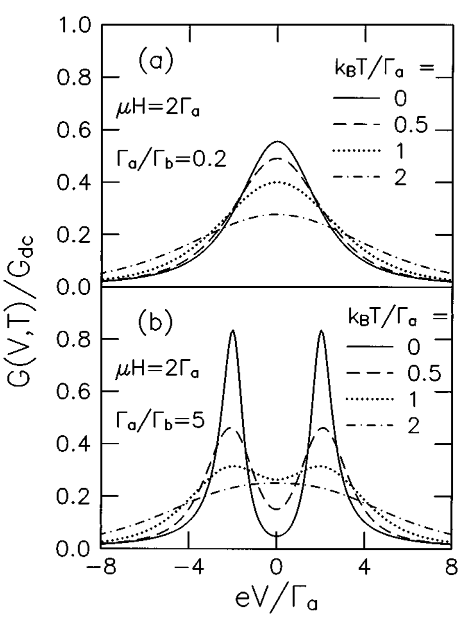

FIG. 3. The differential conductance as a function of V, for $\mu_B g_i H=2\Gamma_a$ and different temperatures. The ratio Γ_a/Γ_b is equal to 0.2 and 5 in (a) and (b), respectively. As in Fig. 2(a), the effect of a finite temperature is to broaden and smear the $T=0$ structure, resulting in a nonmonotonic temperature dependence of the conductance in (b). $G_{dc}=e^2\Gamma_1/\pi\hbar\Gamma_a$ is the $T=0$, $H=0$ conductance, while $\mu=\mu_B g_i$.

there is actually perfect reflection: $G(0,0)$ identically vanishes for arbitrary nonzero magnetic fields.

This difference between the two two-channel limits stems from the fact that the charge current samples the $\hat{a}$ Majorana fermion by way of the ψ_f fermions, while a magnetic field couples the $\hat{a}$ and $\hat{b}$ Majorana fermions. In the case of $\Gamma_b \ll \Gamma_a$ one is thus probing a broad resonance which is coupled to a narrow one, leading to resonant reflection. In the opposite case one is probing directly the narrow resonance, leading to resonant transmission.

Finally, the effect of raising the temperature for a nonzero magnetic field is summarized in Fig. 3. As in Fig. 2(a), a finite temperature basically broadens and smears the $T=0$ structure. For $H>H_c$, this results in a nonmonotonic temperature dependence of the zero-voltage conductance, as exemplified in Fig. 3(b). $G(0,T)$ first increases with T at low temperature, before decreasing with T at higher temperature.

C. Scaling of the differential conductance with V/T

An important aspect of having an exact solution is the possibility to extract universal behavior. Recently, there has been considerable interest in scaling properties of the differential conductance with V/T for Kondo scatterers, following experiments on zero-bias anomalies in ballistic metal point contacts.[31] It has been argued[31] that the observed anomalies are due to two-channel Kondo scattering from two-level systems, corresponding to the Hamiltonian of Eq. (2.2) with an additional flavor index. In support of this interpretation, a scaling ansatz for the differential conductance with V/T has been suggested and compared to the experiment.[32] Subsequent perturbative calculations on a related model[33] showed nice agreement between theory and experiment, but revealed at the same time also finite-temperature corrections to scaling. Since one expects scaling to hold equally well for the Hamiltonian in Eq. (2.2) (although with different exponents and different scaling curves—see discussion below), we can exploit our exact solution to make a quantitative statement about scaling.

For the Hamiltonian of Eq. (2.2), a quadratic temperature dependence is expected for the low-temperature zero-bias conductance. Indeed, this is what we find at the solvable point, Eq. (5.12), including in the two-channel limit $\Gamma_b=0$ (in the opposite limit $\Gamma_a=0$, the current is zero). This suggests a scaling function of the form

$$F(V,T)=\frac{G(0,T)-G(V,T)}{BT^2}, \tag{5.13}$$

where B is a model-dependent constant, defined from the expansion $G(0,T)=G(0,0)-BT^2+O(T^3)$. Specifically, within our solution $B=e^2k_B^2\pi\Gamma_1/3\hbar\Gamma_a^3$. The basic assumption[32] is that $F(V,T)$ reduces to a universal function of V/T at temperatures and voltages well below the Kondo temperature.

In Eq. (5.13), the power T^α entering the denominator is $\alpha=2$ for a Fermi liquid, whereas in Ref. 32 it is $\alpha=1/2$, corresponding to the non-Fermi-liquid fixed point of the two-channel Kondo model.[34] Similar power laws must also show up in the corresponding scaling curves in order for the scaling ansatz to be true. This follows from the fact that

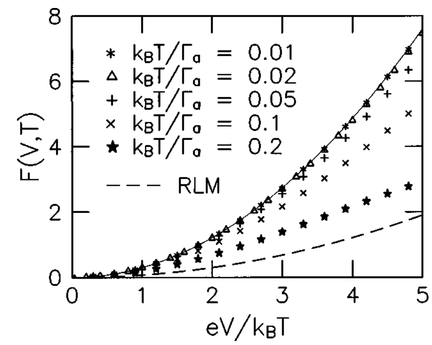

FIG. 4. $F(V,T)=[G(0,T)-G(V,T)]/BT^2$ as a function of eV/k_BT for different temperatures. Here $B=e^2k_B^2\pi\Gamma_1/3\hbar\Gamma_a^3$ is a model-dependent coefficient, defined by the expansion $G(0,T)=G(0,0)-BT^2+O(T^3)$. The solid line corresponds to the first term in Eq. (5.14). Deviations from scaling occur already for $k_BT/\Gamma_a=0.05$. For comparison, the dashed line shows the corresponding low-T, low-V scaling function for the $E_f=0$ noninteracting resonant-level model [Eq. (5.28) with $r=0$], which is a factor of 4 smaller than the first term in Eq. (5.14).

$G(0,T)-G(V,T)$ has a well-defined zero-temperature limit, which implies that if V is kept fixed and T goes to zero, then $F(V,T)$ diverges like $T^{-\alpha}$. Coupled to the assumption that in the scaling regime $F(V,T)$ depends solely on V/T, this demands proportionality to $(V/T)^\alpha$ for $T\ll V$.

In Figure 4 we show a scaling plot of the differential conductance. Clearly, at low enough temperature all curves collapse onto a single line, confirming that $F(V,T)$ indeed reduces to a universal function of V/T. However, even at temperatures small compared to the Kondo temperature, Γ_a, there are substantial deviations from scaling. These come from the fact that $F(V,T)$ for low V and low T can be expanded as

$$F(V,T)=\frac{3}{\pi^2}\left(\frac{eV}{k_BT}\right)^2-6\left(\frac{eV}{\Gamma_a}\right)^2-\frac{3}{\pi^2}\left(\frac{eV}{\Gamma_a}\right)^2\left(\frac{eV}{k_BT}\right)^2+\cdots. \tag{5.14}$$

Hence scaling is violated already by the second term.

Beyond the deviations from scaling, Eq. (5.14) contains an explicit prediction for the universal part of the scaling function, which could be tested experimentally. Specifically, at sufficiently low temperature and voltage, $F(V,T)$ approaches the model-independent curve $3(eV/\pi k_BT)^2$. As we shall argue below, this is an important characteristic of Kondo-assisted tunneling, distinguishing it from ordinary resonant tunneling (see discussion in Sec. V D). Moreover, it holds also for samples with several impurities, provided (i) interactions between different impurities are unimportant and (ii) T and V are sufficiently small compared to all Kondo temperatures in the system. To see this we use the basic approach of Ref. 32. For many independent impurities, the conductance signal is additive:

$$G(V,T)=\sum_i G_i(V,T). \tag{5.15}$$

Here i runs over the different impurities. In particular, Eq. (5.15) implies that

$$G(0,T)=G(0,0)-T^2\sum_i B_i+O(T^3) \tag{5.16}$$

and

$$G(0,T)-G(V,T)=\frac{3}{\pi^2}\left(\frac{eV}{k_B}\right)^2\sum_i B_i+\cdots . \tag{5.17}$$

Hence, to leading order in V and T, the scaling function

$$\frac{G(0,T)-G(V,T)}{BT^2}=\frac{3}{\pi^2}\left(\frac{eV}{k_BT}\right)^2 \tag{5.18}$$

remains unchanged with respect to the single-impurity result. The effect of a distribution of Kondo temperatures enters only beyond the leading-order term.

For a nonzero magnetic field, there is no analogous universal scaling with H/T. This is because the effect of a magnetic field depends explicitly on the ratio of Γ_a to Γ_b. Here we choose to focus on the effective one-channel limit $\Gamma_a=\Gamma_b$, which is expected to be the most relevant case. To include a nonzero magnetic field, we extend the definition of the scaling function F according to

$$F(V,T,H)=\frac{G(0,T,0)-G(V,T,H)}{BT^2}, \tag{5.19}$$

where B is defined, as before, from the zero-field expansion: $G(0,T,0)=G(0,0,0)-BT^2+O(T^3)$. Upon combining Eqs. (5.10) and (5.14) one finds

$$F(V,T,H)=\frac{3}{\pi^2}\left[\left(\frac{eV}{k_BT}\right)^2+\left(\frac{\mu_Bg_iH}{k_BT}\right)^2\right]+\cdots , \tag{5.20}$$

assuming k_BT, eV, and μ_Bg_iH are all much smaller than Γ_a. Thus, for $\Gamma_a=\Gamma_b$, an identical scaling is found with eV/k_BT and μ_Bg_iH/k_BT.

D. Comparison with the resonant-level model

It is instructive to compare our results for the charge current in the Kondo model to the I-V curve due to ordinary resonant tunneling. In the noninteracting resonant-level model, electrons tunnel between two Fermi seas (leads) via a localized electronic level $f_\sigma^\dagger$ placed in between the two leads. Resonant tunneling occurs as the energy of the level, E_f, crosses the chemical potential of one of the leads, producing a peak in the differential conductance. The model is described by the Hamiltonian

$$\mathcal{H}=\sum_{\alpha=L,R}\sum_{k,\sigma}\epsilon_k c_{k\alpha\sigma}^\dagger c_{k\alpha\sigma}+E_f\sum_\sigma f_\sigma^\dagger f_\sigma + \sum_{\alpha=L,R}\frac{t_\alpha}{\sqrt{L}}\sum_{k,\sigma}\{c_{k\alpha\sigma}^\dagger f_\sigma+\text{H.c.}\}, \tag{5.21}$$

in which $c_{kL\sigma}^\dagger$ ($c_{kR\sigma}^\dagger$) creates a conduction electron with wave number k and spin projection σ on the left (right) lead, t_α are the matrix elements for hopping between the localized level and the leads, L is the size of the system, and E_f—the energy of the level—is measured relative to the average chemical potential $(\mu_L+\mu_R)/2$. The latter is taken to be our reference energy. Note that E_f itself is generally voltage dependent, if the level sits physically closer to one lead than the other. For consistency with the Kondo Hamiltonian of Eq. (2.2), the electrostatic potential energy on each lead, $U_\alpha=-eV_\alpha$, has been omitted from Eq. (5.21). In both models this bears no effect on the physical quantities under investigation, as the conduction-electron bandwidth is assumed to be much larger than the applied bias.

Solution of the resonant-level model features two basic energy scales

$$\gamma_L=2\pi\rho_Lt_L^2,\quad \gamma_R=2\pi\rho_Rt_R^2, \tag{5.22}$$

corresponding to the tunneling rates from the localized level to the left and right leads, respectively. Here ρ_α is the conduction-electron density of states per unit length on lead α. The width of the localized level, γ, is related to the tunneling rates through $\gamma=\gamma_L+\gamma_R$.

For an applied voltage bias such that $\mu_L-\mu_R=eV$, the steady-state current flowing from right to left is given by

$$I^{RLM}(V)=2\frac{e}{\pi\hbar}\left(\frac{\gamma_L\gamma_R}{\gamma_L+\gamma_R}\right)\int_{-\infty}^{\infty}d\epsilon\frac{\gamma/2}{(\epsilon-E_f)^2+(\gamma/2)^2}\times\left[f\left(\epsilon-\frac{eV}{2}\right)-f\left(\epsilon+\frac{eV}{2}\right)\right]. \tag{5.23}$$

Here the factor of 2 comes from the two possible spin orientations of the electrons. This expression for the current closely resembles the charge current in our Kondo model, Eq. (5.7), for a zero magnetic field. The two notable differences are the explicit dependence of $I^{RLM}(V)$ on the position of the level and, as noted earlier, the eV shift between the arguments of the two Fermi functions (compared to $2eV$ in the Kondo model).

The resonant-level energy E_f has no analog in the Kondo problem, as the Abrikosov-Suhl resonance is always pinned in equilibrium at the Fermi level. In that respect, the Kondo model is best described by the case where E_f is fixed in equilibrium at zero energy. For a Kondo impurity, though, only the chemical potential difference $\mu_L-\mu_R$ is relevant to transport properties, reflecting the lack of charge fluctuations on the impurity site. By contrast, $\mu_L+\mu_R$ explicitly enters the resonant-level current through the definition of E_f.

In general, E_f has the form $E_f=E_f^{(0)}+reV$, where $E_f^{(0)}$ denotes the equilibrium ($V=0$) position of the resonant level, and $-1/2<r<1/2$ parametrizes the electrostatic potential energy on the level site. For a linear potential drop across the junction, r basically measures the physical distance of the level from the center of the junction. Specifically, $r=\pm1/2$ describes a level adjacent to one of the leads, whereas $r=0$ corresponds to a level that sits midway between the two leads.

The differential conductance for the resonant-level model is obtained by differentiating Eq. (5.23) with respect to V. At zero temperature this gives a differential-conductance curve that is generally a superposition of two Lorentzians: one centered about $2E_f^{(0)}/(1-2r)$ with half-width $\gamma/(1-2r)$ and the other centered about $-2E_f^{(0)}/(1+2r)$ with half-width $\gamma/(1+2r)$. Only in two cases does one recover a single Lorentzian centered about $V=0$ which can possibly emulate the Kondo-model result: (i) If $E_f=0$ (i.e., $E_f^{(0)}=r=0$) and (ii) if $E_f=\pm eV/2$ (i.e., $E_f^{(0)}=0$ and $r=\pm 1/2$). In the following we analyze in detail these two cases, comparing their respective I-V curves with that of the nonequilibrium Kondo model.

To this end, it is useful to introduce the function

$$C(x,y)=2\,\mathrm{Im}\left\{\psi\left(\frac{1}{2}+\frac{1+ix}{2\pi y}\right)\right\}, \tag{5.24}$$

which allows a unified representation of the relevant currents:

$$I_c(V)=\frac{e\Gamma_1}{2\pi\hbar}C\left(\frac{eV}{\Gamma_a},\frac{k_BT}{\Gamma_a}\right) \tag{5.25}$$

for the Kondo model with zero magnetic field,

$$I^{RLM}(V)=2\,\frac{e\gamma_L\gamma_R}{\pi\hbar\gamma}C\left(\frac{eV}{\gamma},\frac{2k_BT}{\gamma}\right) \tag{5.26}$$

for the $E_f=0$ resonant-level model and

$$I^{RLM}(V)=\frac{e\gamma_L\gamma_R}{\pi\hbar\gamma}C\left(\frac{2eV}{\gamma},\frac{2k_BT}{\gamma}\right) \tag{5.27}$$

for the resonant-level model with $E_f=\pm eV/2$.

For $E_f=\pm eV/2$, the currents $I^{RLM}(V)$ and $I_c(V)$ are indistinguishable. This is because one can always identify $\gamma/2$ and $2\gamma_L\gamma_R/\gamma$ for the resonant-level model with Γ_a and Γ_1, respectively, for the Kondo model, to make the two I-V curves identical. In particular, the condition $\Gamma_1=\Gamma_a$ for perfect zero-temperature conductance in the Kondo model translates to $\gamma_L=\gamma_R$ for the resonant-level model. Also for $E_f=0$ the two currents are indistinguishable, but only at zero temperature. The necessary mapping of model parameters in this case involves identifying γ with Γ_a and $4\gamma_L\gamma_R/\gamma$ with Γ_1. This equivalence of the two I-V curves breaks down as soon as T is nonzero, as the temperature for the $E_f=0$ resonant-level model is effectively twice as large as that for the corresponding Kondo model [compare Eqs. (5.25) and (5.26) with the above identification of model parameters]. As explained below, this fundamental difference between the two models is directly probed by the scaling function $F(V,T)$.

Going back to general model parameters $E_f^{(0)}$ and r, we analyze the scaling function of Eq. (5.13) for the resonant-level model. For $E_f^{(0)}\neq 0$ and $r\neq 0$, the leading voltage dependence of the differential conductance is linear in V. Hence $F(V,T)$ at low temperature and low voltage does not reduce to a function of V/T, in contrast to the Kondo model. Asymptotic dependence on V/T is recovered when at least one of $E_f^{(0)}$ or r is zero, in which case the low-temperature and low-voltage scaling function reads

$$F^{RLM}(V,T)=\frac{3}{\pi^2}\left(\frac{1}{4}+3r^2\right)\left(\frac{eV}{k_BT}\right)^2. \tag{5.28}$$

Contrary to the Kondo case, Eq. (5.28) is not universal. Rather, it depends on the parameter r, which is model dependent. Moreover, with the exception of the case $r=\pm 1/2$, $F^{RLM}(V,T)$ is smaller by a factor of $1/4+3r^2<1$ than the corresponding Kondo-model result. We note that, for nearly 60% of the parameter range in r, this factor is smaller than one-half. For $r=0$, it is equal to one-quarter. Thus, measurement of the scaling function of Eq. (5.13) should allow a clear distinction between Kondo-assisted and resonant tunneling, provided E_f sufficiently deviates from $\pm eV/2$.

The response to an applied magnetic field completes the distinction between Kondo-assisted and resonant tunneling. In the resonant-level model, a nonzero magnetic field splits the energy of the localized level according to $E_f\to E_{f,\sigma}=E_f-\frac{1}{2}\sigma\mu_B g_i H$. Each of the two spin species then carries a current that is equal to half the expression in Eq. (5.23), only with E_f replaced by $E_f-\frac{1}{2}\sigma\mu_B g_i H$. The total electric current is equal to the sum of the two spin contributions.

At $T=0$, the generic differential-conductance curve for a nonzero magnetic field is a superposition of four distinct Lorentzians. For either $E_f=0$ or $E_f=\pm eV/2$, however, the zero-field curve is simply split into two symmetric Lorentzians centered about $eV=\pm\mu_B g_i H$ (for $E_f=0$) or $eV=\pm\frac{1}{2}\mu_B g_i H$ (for $E_f=\pm eV/2$). In particular, for $E_f=\pm eV/2$ and a sufficiently large magnetic field, the zero-bias anomaly is split by $\mu_B g_i H$, which is half the magnetic splitting for the Kondo impurity. Thus, while the low-temperature scaling function for $E_f=\pm eV/2$ is identical to that of the Kondo model, the magnetic splitting is smaller by a factor of 2. The situation is reversed for $E_f=0$. Here the magnetic splitting $2\mu_B g_i H$ is the same as for the Kondo model, but the scaling function is smaller by a factor of 4. Combined, the low-temperature scaling function and the splitting with an applied magnetic field fully distinguish the differential conductance for our Kondo model from that due to ordinary resonant tunneling.

VI. SPIN CURRENT

Next we compute the Kondo-assisted spin current. While $I_c(V)$ measures the total electric current across the junction, the spin current measures the difference in currents between the spin-up and spin-down carriers. In the Kondo model, spin-up and spin-down electrons are coupled via the spin-flip processes. As we shall see, this has a striking effect on the spin current, which as a result is a symmetric function the applied bias, and its direction is determined by the asymmetry in the transverse coupling to the left and right leads.

A. Derivation

The derivation of the time-averaged spin current $I_s(V)$ is similar to that of the charge current in the previous section. In the scattering-state approach, one implements the same two basic steps, i.e., (i) expanding the operator $\hat{I}_s'$ in terms of the scattering-state operators and (ii) averaging the resulting expression with respect to $e^{-\beta(\mathcal{H}'-Y')}$. The diagrammatic calculation also resembles that of the charge current and is detailed below.

By analogy with the function $G^{>}_{fk,a}(t,t')$ of Eq. (5.4), we begin by defining the functions

$$G^{>}_{sfk,a}(t,t')=\langle[\psi^{\dagger}_{sf,k}(t)+\psi_{sf,k}(t)]\hat{a}(t')\rangle, \tag{6.1}$$

$$G^{>}_{sfk,b}(t,t')=\langle[\psi^{\dagger}_{sf,k}(t)-\psi_{sf,k}(t)]\hat{b}(t')\rangle, \tag{6.2}$$

which determine the spin current according to

$$I_s(V)=i\frac{J^-}{2\hbar\sqrt{\pi aL}}\sum_k G^{>}_{sfk,a}(t,t) - \frac{J^+}{2\hbar\sqrt{\pi aL}}\sum_k G^{>}_{sfk,b}(t,t). \tag{6.3}$$

Switching to energy variables and applying perturbation theory with respect to $J_{\perp}^{LR}$, J^+, J^-, and H, one obtains

$$\frac{1}{\sqrt{L}}\sum_k G^{>}_{sfk,a}(\epsilon)=\frac{J^+}{2v_F\hbar\sqrt{\pi a}}[G^{>}_{ba}(\epsilon)+2if(-\epsilon)G^{a}_{ba}(\epsilon)], \tag{6.4}$$

$$\frac{1}{\sqrt{L}}\sum_k G^{>}_{sfk,b}(\epsilon)=i\frac{J^-}{2v_F\hbar\sqrt{\pi a}}[G^{>}_{ab}(\epsilon)+2if(-\epsilon)G^{a}_{ab}(\epsilon)], \tag{6.5}$$

where the wideband-limit relation of Eq. (4.32) has been used. The spin current follows from combining Eqs. (6.4) and (6.5) with Eq. (6.3), which gives

$$I_s(V)=\frac{\Gamma_L-\Gamma_R}{8\pi\hbar}\times\int_{-\infty}^{\infty}[iG^{>}_{ba}(\epsilon)-iG^{>}_{ab}(\epsilon)+4f(-\epsilon)G^{a}_{ab}(\epsilon)]d\epsilon. \tag{6.6}$$

Here Γ_L and Γ_R are equal to $(J_{\perp}^{LL})^2/4\pi a\hbar v_F$ and $(J_{\perp}^{RR})^2/4\pi a\hbar v_F$, respectively. Finally, upon inserting the explicit expressions for $G^{>}_{ba}$, $G^{>}_{ab}$, and G^{a}_{aa}, one arrives at

$$I_s(V)=\mu_B g_i H\frac{(\Gamma_L-\Gamma_R)\Gamma_1}{2\pi\hbar}\int_{-\infty}^{\infty}d\epsilon[f_{eff}(\epsilon)-f(\epsilon)]\times\frac{\epsilon}{|(\epsilon+i\Gamma_a)(\epsilon+i\Gamma_b)-(\mu_B g_i H)^2|^2}, \tag{6.7}$$

where $f_{eff}(\epsilon)$ is the effective distribution function of Eq. (4.35). As for the charge current, an identical result is obtained using the scattering-state approach.

B. Master equation

Several facts are apparent from Eq. (6.7). First, no spin current can flow if H is equal to zero. This is to be expected since the two spin orientations are equivalent for $H=0$, and hence the spin-up and spin-down currents are identical in the absence of a magnetic field. Second, $I_s(V)$ is proportional to $\Gamma_L-\Gamma_R$, which implies that $|J_{\perp}^{LL}|$ must differ from $|J_{\perp}^{RR}|$ in order for a spin current to flow. Most surprising is the fact that the direction of the spin current is determined by $J_{\perp}^{LL}$, $J_{\perp}^{RR}$, and the sign of H, and is independent of the sign of V.

To understand how these features come about, it is useful to consider the limit where $eV>\mu_B g_i H$ and $eV-\mu_B g_i H,\mu_B g_i H\gg k_BT,\Gamma_a,\Gamma_b$. In this case we are able to derive the spin-current result by a master equation, which relies on the fact that the resonance widths Γ_a and Γ_b are much smaller than $eV-\mu_B g_i H$ and $\mu_B g_i H$. To make the physical picture explicit, we use the following representation of the transformed Hamiltonian in terms of the d fermion rather than the $\hat{a}$ and $\hat{b}$ Majorana fermions [see Eq. (3.15)]:

$$\begin{aligned}\mathcal{H}'=&\mathcal{H}_0'+\mu_B g_i H(d^{\dagger}d-1/2)\\&+\frac{J_{\perp}^{LL}}{2\sqrt{2\pi a}}[\psi^{\dagger}_{sf}(0)d^{\dagger}+d\psi_{sf}(0)]\\&+\frac{J_{\perp}^{RR}}{2\sqrt{2\pi a}}[\psi_{sf}(0)d^{\dagger}+d\psi^{\dagger}_{sf}(0)]\\&+\frac{J_{\perp}^{LR}}{2\sqrt{2\pi a}}[\psi^{\dagger}_{f}(0)d^{\dagger}+\psi^{\dagger}_{f}(0)d+d^{\dagger}\psi_f(0)+d\psi_f(0)].\end{aligned} \tag{6.8}$$

Here $\mathcal{H}_0'$ is the free kinetic-energy part of $\mathcal{H}'$.

From the definitions of the d fermion, Eq. (3.12), and the canonical transformation U, one recognizes that an empty d level corresponds to the spin-up ($\tau^z=\uparrow$) impurity state, whereas an occupied d level represents the spin-down ($\tau^z=\downarrow$) state. Let $P_{\uparrow}(t)$ be the probability for having an empty d level at time t, and let $P_{\downarrow}(t)$ denote the probability for having an occupied level. Since the d level is either occupied or unoccupied, the sum of the two probabilities is equal to 1: $P_{\uparrow}(t)+P_{\downarrow}(t)=1$.

The different rates for transitions between the spin-up and spin-down impurity configurations can be read off from Eq. (6.8) using Fermi's golden rule. Altogether there are eight different terms in Eq. (6.8) that flip the impurity spin; however, only some of them contribute in the limit considered here. For example, since the energy of the spin-up state is lower by $\mu_B g_i H$ than that of the spin-down state (assuming $H>0$), there is no thermal energy to flip the impurity spin from up to down. Only the voltage can provide the necessary energy for such a spin flip, by tunneling an electron from the left lead to the right one. Thus, $\psi_f(0)d^{\dagger}$, which describes this process, is the only allowed transition when the impurity spin is up. In contrast, nearly all spin-flip processes are active when the impurity spin is down. The only forbidden process in this case is $\psi^{\dagger}_f(0)d$, which corresponds to tunneling of an electron from the right lead to the left one. Such a process is prohibited by the large voltage barrier for tunneling from right to left. Collecting the different transition rates for each impurity state, the resulting master equations for $P_{\uparrow}(t)$ and $P_{\downarrow}(t)$ read

$$\frac{dP_{\uparrow}(t)}{dt}=P_{\downarrow}(t)\frac{1}{2\hbar}[\Gamma_1+\Gamma_L+\Gamma_R]-P_{\uparrow}(t)\frac{\Gamma_1}{2\hbar}, \tag{6.9}$$

$$\frac{dP_{\downarrow}(t)}{dt}=P_{\uparrow}(t)\frac{\Gamma_1}{2\hbar}-P_{\downarrow}(t)\frac{1}{2\hbar}[\Gamma_1+\Gamma_L+\Gamma_R]. \tag{6.10}$$

Note that the effect of H in this limit is to block intralead spin-flip scattering when the impurity spin is up. The large bias enables the spin to flip freely in both directions, by tunneling an electron from the left lead to the right one.

Hence the asymmetry between the spin-up and spin-down impurity states is reflected in the intralead processes. Indeed, by inverting the sign of V one changes the direction of tunneling, but Eqs. (6.9) and (6.10) remain intact. On the other hand, flipping the sign of H interchanges the roles of $P_{\uparrow}(t)$ and $P_{\downarrow}(t)$.

The steady-state solution of Eqs. (6.9) and (6.10) is readily obtained by setting the left-hand sides equal to zero. Together with the requirement that $P_{\uparrow}$ and $P_{\downarrow}$ add up to 1, this leads to

$$P_{\uparrow}=\frac{\Gamma_a+\Gamma_b-\Gamma_1/2}{\Gamma_a+\Gamma_b}, \quad P_{\downarrow}=\frac{1}{2}\frac{\Gamma_1}{\Gamma_a+\Gamma_b}. \tag{6.11}$$

The apparent difference between $P_{\uparrow}$ and $P_{\downarrow}$ simply reflects the different lifetimes for the two impurity configurations in the presence of an applied magnetic field.

To determine the spin current and also the charge current from the probabilities $P_{\uparrow}(t)$ and $P_{\downarrow}(t)$, we need to compute the time derivatives of $N_{sf}(t)$ and $N_f(t)$, respectively. Bearing in mind that (i) tunneling of an electron from right to left is forbidden for large positive voltage bias [i.e., no $\psi_f^{\dagger}(0)$ processes are allowed within Eq. (6.8)] and (ii) intralead spin flips are suppressed when the impurity spin is up [i.e., no $\psi_{sf}^{\dagger}(0)d^{\dagger}$ and $\psi_{sf}(0)d^{\dagger}$ processes are permitted within Eq. (6.8)] one obtains

$$\frac{dN_f(t)}{dt}=-\frac{1}{2\hbar}\Gamma_1[P_{\uparrow}(t)+P_{\downarrow}(t)], \tag{6.12}$$

$$\frac{dN_{sf}(t)}{dt}=\frac{1}{2\hbar}(\Gamma_R-\Gamma_L)P_{\downarrow}(t). \tag{6.13}$$

Substituting the steady-state value for $P_{\downarrow}$, Eq. (6.11), then gives

$$I_c=-e\frac{dN_{sf}(t)}{dt}=\frac{e}{2\hbar}\Gamma_1, \tag{6.14}$$

$$I_s=-\frac{dN_{sf}(t)}{dt}=\frac{1}{4\hbar}\frac{\Gamma_1(\Gamma_L-\Gamma_R)}{\Gamma_a+\Gamma_b}. \tag{6.15}$$

In the limit $eV-\mu_B g_i H, \mu_B g_i H \gg k_B T, \Gamma_a, \Gamma_b$, Eqs. (6.14) and (6.15) coincide with the exact expressions, Eqs. (5.7) and (6.7), respectively. Thus, the mechanism for creating a spin current involves (i) a magnetic field that polarizes the impurity spin, (ii) a sufficiently large voltage bias that provides the energy for flipping the impurity spin in both directions, and (iii) an asymmetry between the intralead spin-flip processes for the left and right leads. Although the spin current is triggered by the application of a voltage bias, its direction is determined by the sign of H and the asymmetry in the intralead spin-flip scattering. Indeed, the even dependence of the spin current on V can be seen on a formal level, by noting that V and $-V$ are connected within Y_0' via the particle-hole transformation $\psi_f \leftrightarrow -\psi_f^{\dagger}$. As the Hamiltonian $\mathcal{H}'$ and the number operator $\hat{N}_{sf}$ are both invariant under this transformation, the spin current is independent of the sign of V.

Although Eqs. (6.14) and (6.15) apply only to the solvable point, the even dependence of the spin current on V and the proportionality to $\Gamma_L-\Gamma_R$ can be seen already in the original Hamiltonian of Eq. (2.2), using the same arguments as for the solvable point. We illustrate this point in Fig. 5, where the limit of a large magnetic field and an even larger voltage bias is assumed.

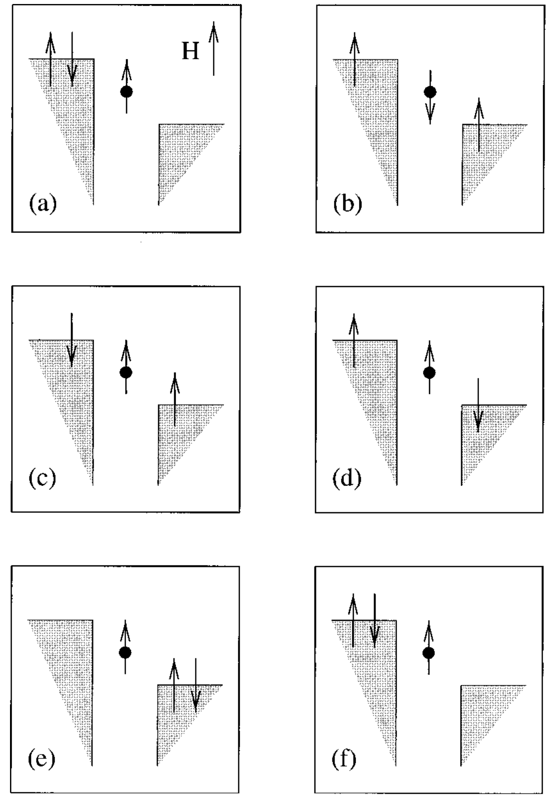

FIG. 5. Schematic description of the mechanism for creating a spin current. Assuming a large magnetic field and an even larger voltage bias, an impurity polarized in the direction of the field (a) can only be flipped by tunneling an electron across the junction (b). As the opposite spin flip has no energy barrier to overcome, several spin-flip processes are available. These include (i) flipping a left-lead electron from spin up to spin down (c), (ii) flipping a right-lead electron from spin up to spin down (d), (iii) tunneling a second electron from left to right (e), and (iv) the same electron that tunneled in (b) from left to right can actually tunnel back (f). Of the four sequences, only (c) produces a positive spin current, while (d) produces a negative spin current. Since the respective rates for processes (i) and (ii) are proportional to $(J_{\perp}^{LL})^2$ and $(J_{\perp}^{RR})^2$, the total spin current is proportional to $(J_{\perp}^{LL})^2-(J_{\perp}^{RR})^2$.

In Fig. 5(a) we begin at an instant in time in which the impurity spin is polarized in the up direction (we assume $H>0$). Due to the large Zeeman splitting, the impurity can be flipped from up to down only by tunneling an electron across the junction, Fig. 5(b). The opposite spin flip has no Zeeman energy barrier to overcome; hence the impurity spin can be flipped back by any of the following four processes: (i) scattering a spin-up electron on the left lead to a spin-down electron on the same lead, Fig. 5(c); (ii) scattering a spin-up electron on the right lead to a spin-down electron on the same lead, Fig. 5(d); (iii) tunneling a second electron from the left lead to the right one, Fig. 5(e); and (iv) the original electron that tunneled in Fig. 5(b) from left to right can actually tunnel back, Fig. 5(f).

Of these four processes, only the former two contribute to

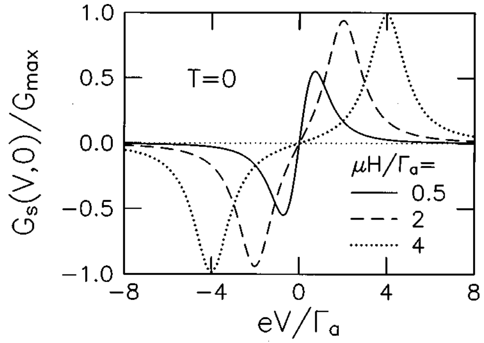

FIG. 6. The differential conductance for the spin current, $G_s(V,T)=dI_s/dV$, vs V, for $T=0$, $\Gamma_a=\Gamma_b$, and different values of the magnetic field. As the spin current is even in the applied bias, $G_s(V,T)$ is an odd function of V, with resonances (either a maximum or a minimum) at $eV=\pm\mu_B g_i H$. Here $G_{max}=e(\Gamma_L-\Gamma_R)\Gamma_1/8\pi\hbar\Gamma_a^2$ and $\mu=\mu_B g_i$. The maximal peak height for $\Gamma_a=\Gamma_b$ is equal to $|G_{max}|$ and is approached for large magnetic fields.

the spin current. Process (iv) produces neither a spin current nor a charge current, while process (iii) results in a net charge current but no spin current. This is seen from the fact that both a spin-up and a spin-down electron have been effectively transferred from left to right in going from Fig. 5(a) to Fig. 5(e). The remaining two processes result in either a positive spin current, Fig. 5(c), or a negative spin current, Fig. 5(d), depending on which spin carrier has been effectively transferred from left to right in going from Fig. 5(a). Given that the rates for (i) and (ii) are proportional to $(J_\perp^{LL})^2$ and $(J_\perp^{RR})^2$, respectively, the total spin current is thus proportional to $(J_\perp^{LL})^2-(J_\perp^{RR})^2$.

Note that the role of V in this scenario is to enable the first spin flip of the sequence, i.e., the one starting from an impurity spin parallel to the applied magnetic field. The sign of the spin current is determined, however, by the opposite spin flip, through the difference in rates for the two intralead processes. As a result, $I_s(V)$ has the same sign as $H[(J_\perp^{LL})^2-(J_\perp^{RR})^2]$, irrespective of the direction of the applied bias.

We further emphasize that the above picture is independent of the longitudinal couplings $J_z^{\alpha\beta}$, as the probability for a longitudinal Kondo scattering is independent of both the spin of the scattered electrons and the orientation of the impurity spin. Thus, the mechanism for creating a spin current relies solely on spin-flip scattering.

C. Differential conductance

We now return to the exact expression for the spin current, Eq. (6.7). In Fig. 6 we have plotted the differential conductance for the spin current, $G_s(V,T)=dI_s/dV$, as a function of bias, for zero temperature and different values of the magnetic field. For conciseness, we have focused on the effective one-channel limit $\Gamma_a=\Gamma_b$, which is expected to be the most relevant case.

Since the spin current is even in the applied bias, the differential conductance is an odd function of V. This should provide a distinct experimental signature of the Kondo effect. In particular, $G_s(V,T)$ has a resonance at $eV=\mu_B g_i|H|$—either a maximum if $H(\Gamma_L-\Gamma_R)>0$ or a minimum if $H(\Gamma_L-\Gamma_R)<0$. One can understand the origin of this resonance in terms of the mechanism for creating a spin current. For $\mu_B g_i H-eV,\mu_B g_i H\gg k_BT,\Gamma_a,\Gamma_b$, there is not enough energy to flip the impurity spin from up to down. Consequently, the impurity is frozen in the spin-up configuration, which blocks any spin current from flowing. On the other hand, for $eV-\mu_B g_i H,\mu_B g_i H\gg k_BT,\Gamma_a,\Gamma_b$ the voltage is sufficiently large for the impurity spin to flip, allowing a spin current to flow. Thus, the mechanism for creating a spin current is activated as eV sweeps through $\mu_B g_i H$, producing a resonance in the differential conductance at $eV=\mu_B g_i H$.

A natural question to ask is, how large can the spin differential conductance be? It is known that the charge differential conductance for this system is bounded by $e^2/\pi\hbar$, i.e., one e^2/h quanta per spin channel. For $\Gamma_a=\Gamma_b$, the maximal peak height is approached for $\mu_B g_i H\gg\Gamma_a,k_BT$ and is equal to

$$\frac{e}{8\pi\hbar}\frac{|\Gamma_L-\Gamma_R|\Gamma_1}{\Gamma_a^2}. \tag{6.16}$$

As a function of Γ_1/Γ_a, it takes the optimal value of roughly $0.385(e/2\pi\hbar)$, which marks the upper bound on $|G(V,T)|$ for $\Gamma_a=\Gamma_b$. Larger values of $|G(V,T)|$ are possible if $\Gamma_a\neq\Gamma_b$. For example, $|G(V,T)|$ can be as large as $e/2h$, for $\Gamma_a=3\Gamma_b$ and $\mu_B g_i H\gg\Gamma_a,k_BT$. This value actually corresponds to half the maximal differential conductance one would get if there was only one spin channel in the problem.

VII. CHARGE-CURRENT NOISE

Thus far our discussion has focused on properties of the time-averaged current. Another quantity of interest is the charge-current noise, which corresponds to fluctuations about the average current. The noise spectrum $S(\Omega)$ measures pair excitations of the system and, as such, provides information about dynamical properties that cannot be attained from the time-averaged current. A classical example is the electric charge of the current carriers. In this section we show that the noise spectra contains perhaps the most direct and unambiguous evidence for the many-body interactions in our Kondo model. Most notably, it features signatures of pair-tunneling processes that cannot be traced in the time-averaged current.

A. Derivation

The charge-current noise spectrum $S(\Omega)$ is defined by the correlation function

$$S(\Omega)=\int_{-\infty}^{\infty}e^{i\Omega t}[\langle\{\hat{I}_c'(t),\hat{I}_c'(0)\}\rangle-2\langle\hat{I}_c'(t)\rangle\langle\hat{I}_c'(0)\rangle]dt. \tag{7.1}$$

Here the curly brackets in the leftmost average denote the anticommutator of the charge current $\hat{I}_c'$ at time t and that at time $t=0$. Similar to the derivation of the average current, also $S(\Omega)$ can be computed in two distinct ways, which are briefly outlined below.

In the scattering-state approach, after $\hat{I}_c'$ has been expanded in terms of the scattering-state operators using Tables II and III, the explicit time dependence of $\hat{I}_c'(t)$ is introduced by replacing all $c^{\dagger}_{\nu,k}$ and $c_{\nu,k}$ operators in $\hat{I}'_c$ with $c^{\dagger}_{\nu,k}(t) = e^{i\epsilon_k t/\hbar} c^{\dagger}_{\nu,k}$ and $c_{\nu,k}(t) = e^{-i\epsilon_k t/\hbar} c_{\nu,k}$, respectively. This in turn allows us to express the anticommutator $\{\hat{I}'_c(t), \hat{I}'_c(0)\}$ entirely in terms of scattering-state operators. Once this step has been accomplished, averaging with respect to $e^{-\beta(\mathcal{H}'-Y')}$ is readily carried out using Eqs. (5.3), as is the integral over t. The latter step provides us with $S(\Omega)$.

An identical result is obtained for the noise spectrum when diagrammatic techniques are employed. The starting point for this approach is the function

$$I^{>}(t,t') = \langle \hat{I}'_c(t) \hat{I}'_c(t') \rangle, \tag{7.2}$$

which enters Eq. (7.1) in the following manner:

$$S(\Omega) = \int_{-\infty}^{\infty} e^{i\Omega t} [I^{>}(t,0) + I^{>}(0,t) - 2\langle \hat{I}'_c(t)\rangle \langle \hat{I}'_c(0)\rangle] dt. \tag{7.3}$$

Diagrammatically, $I^{>}(t,t')$ is evaluated in a rather standard manner from the current-current bubble diagram, the only exception here being that, because $\mathcal{H}'$ contains Majorana fermions and does not conserve the number of ψ fermions, all possible contractions must be taken into account. $I^{>}(t,t')$ therefore breaks into products of single-particle response functions, which are comprised of $G^{>}_{aa}(t,t')$ and $G^{>}_{fk,a}(t,t')$ [Eqs. (4.25) and (5.4), respectively], together with

$$G^{>}_{fk,fk'}(t,t') = \langle [\psi^{\dagger}_{f,k} + \psi_{f,k}](t) [\psi^{\dagger}_{f,k'} + \psi_{f,k'}](t') \rangle \tag{7.4}$$

and

$$G^{>}_{a,fk}(t,t') = \langle \hat{a}(t) [\psi^{\dagger}_{f,k}(t') + \psi_{f,k}(t')] \rangle. \tag{7.5}$$

Specifically, using Eq. (4.32) one has

$$\begin{aligned} I^{>}(t,t') = {} & \langle \hat{I}'_c(t)\rangle \langle \hat{I}'_c(t')\rangle + \frac{e^2}{\hbar}\Gamma_1 v_F \\ & \times \frac{1}{L}\sum_{k,k'} [G^{>}_{fk,fk'}(t,t') G^{>}_{aa}(t,t') \\ & - G^{>}_{fk,a}(t,t') G^{>}_{a,fk'}(t,t')]. \end{aligned} \tag{7.6}$$

Using Eq. (7.6), the noise can be expressed in terms of the single-particle response functions mentioned above. These in turn are evaluated in the Fourier representation using perturbation theory with respect to $J_{\perp}^{\alpha\beta}$ and H. Skipping the details of the algebra, we quote here only the end result for the noise:

$$\begin{aligned} S(\Omega) = {} & \frac{e^2}{\hbar}\Gamma_1 \int_{-\infty}^{\infty} \frac{d\epsilon}{\pi} \{ \Gamma_1 g(\epsilon) g(\epsilon - \hbar\Omega) \\ & + G^{>}_{aa}(\epsilon)[f_{eff}(\epsilon+\hbar\Omega) + f_{eff}(\epsilon-\hbar\Omega)]\}, \end{aligned} \tag{7.7}$$

with

$$g(\epsilon) = G_{aa}(\epsilon - i\eta)[f(\epsilon - eV) - f(\epsilon + eV)]. \tag{7.8}$$

Here $f_{eff}(\epsilon)$ is the effective distribution function defined in Eq. (4.35).

Equations (7.7) and (7.8) are the central result of this section. Together they provide us with an exact expression for the noise spectrum, for arbitrary frequency Ω. We devote the remainder of this section to evaluation and analysis of these equations, starting with the $\Omega=0$ component of the noise spectrum.

B. Zero-frequency noise

Before proceeding to examine the zero-frequency noise, we briefly review several standard limits which will be used as a reference. In the case of uncorrelated tunneling events obeying Poisson statistics,[35] the noise-to-current ratio is $2e$, which we refer to hereafter as the Poisson limit or the "full" shot noise. For a noninteracting quantum-mechanical electron gas incident upon a barrier with energy-independent transmission probability $\mathcal{T}$, there is a suppression of the noise-to-current ratio[36–41] from the Poisson result to $2e(1-\mathcal{T})$. Inclusion of energy dependence in the transmission probability amounts to replacing $\mathcal{T}$ in $2e(1-\mathcal{T})$ with an effective transmission coefficient $\mathcal{T}_{eff}$:

$$S(0)/I_c = 2e(1-\mathcal{T}_{eff}), \tag{7.9}$$

with

$$\mathcal{T}_{eff} = \frac{1}{\int_{\mu_R}^{\mu_L} \mathcal{T}(\epsilon) d\epsilon} \int_{\mu_R}^{\mu_L} \mathcal{T}^2(\epsilon) d\epsilon. \tag{7.10}$$

Thus, the zero-temperature noise-to-current ratio for a noninteracting system is always bounded by the Poisson limit, the latter being valid only in the limit $\mathcal{T}_{eff} \to 0$.

A generic feature of the noise-to-current ratio for our model is that it approaches the Poisson limit of $2e$ at large bias. This can be seen from the fact that Eqs. (7.7) and (7.8) with $\Omega=0$ and $T=0$ can be recast, after some manipulations, in the form

$$S(0) = 2eI_c(V) + \frac{e^2\Gamma_1^2}{\pi\hbar} \int_{-eV}^{eV} \mathrm{Re}\{G^2_{aa}(\epsilon + i\eta)\} d\epsilon. \tag{7.11}$$

For large V, the second term drops out in Eq. (7.11), as $G^2_{aa}(\epsilon+i\eta)$ is analytic in the upper half plane and falls asymptotically like $1/\epsilon^2$. Consequently, the unbounded integral of $\mathrm{Re}\{G^2_{aa}(\epsilon+i\eta)\}$ identically vanishes, leaving only the first term in Eq. (7.11), which is the Poisson result. In a similar fashion, $S(0)/I_c$ can be shown to approach the Poisson limit at large bias for arbitrary temperature.

1. $T=0$, $H=0$

The zero-temperature, zero-field noise for our model is summarized in Fig. 7(a). Initially, there is a suppression of the shot noise near zero bias, but eventually it approaches the "full" shot noise $S(0)/I_c = 2e$ for voltages much larger than Γ_a. This can be understood quantitatively from the expressions for the noise and the noise-to-current ratio:

$$S(0) = 2\frac{e^2}{\pi\hbar}\Gamma_1 \left[\arctan\left(\frac{eV}{\Gamma_a}\right) - \frac{eV\Gamma_1}{(eV)^2 + \Gamma_a^2} \right] \tag{7.12}$$

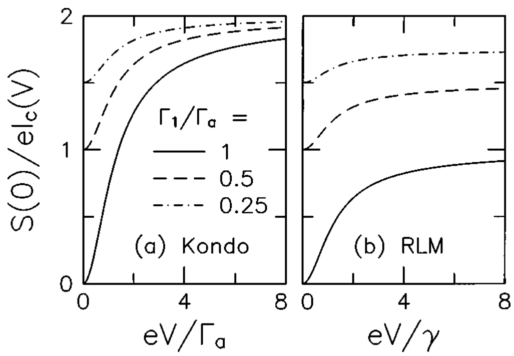

FIG. 7. The zero-temperature, zero-field noise-to-current ratio (a) for our Kondo model and (b) for the noninteracting resonant-level model with $E_f=0$. Corresponding model parameters were adjusted to produce identical zero-temperature I-V curves for the two models (i.e., $\Gamma_a=\gamma$ and $\Gamma_1=4\gamma_L\gamma_R/\gamma$). For the Kondo model, $S(0)/I_c(V)$ is equal to $2e(1-\Gamma_1/\Gamma_a)$ for $V\ll\Gamma_a$, and approaches the Poisson limit $2e$ for $\Gamma_a\ll eV$. For the resonant-level model, the noise-to-current ratio also starts at $2e(1-\Gamma_1/\Gamma_a)$, but saturates at $e(2-\Gamma_1/\Gamma_a)<2e$ for large voltages.

and

$$\frac{S(0)}{I_c(V)}=2e\left[1-\frac{\Gamma_1 eV}{\arctan(eV/\Gamma_a)[(eV)^2+\Gamma_a^2]}\right]. \quad (7.13)$$

For voltages small compared to Γ_a, Eq. (7.13) reduces to $2e(1-\Gamma_1/\Gamma_a)$. This is consistent with the noninteracting case, in the sense that $\Gamma_1/\Gamma_a=G(0,0)\pi\hbar/e^2$ can be interpreted as the zero-energy transmission probability per spin channel. Specifically, $S(0)/I_c$ vanishes at small voltages for $\Gamma_1=\Gamma_a$, in accordance with the limit of perfect zero-temperature transmission. Upon increasing V, the noise-to-current ratio monotonically increases until it saturates at the Poisson limit for $eV\gg\Gamma_a$. The effect of decreasing Γ_1/Γ_a is also to increase $S(0)/I_c$. In the limit of weak tunneling, $\Gamma_1/\Gamma_a\ll 1$, the ratio $S(0)/I_c$ approaches the ''full'' shot noise for arbitrary voltage bias, in agreement with the limit $\mathcal{T}_{eff}\ll 1$ for the noninteracting case.

The noise curves in Fig. 7(a) are qualitatively similar to those for the $E_f=0$ resonant-level model, shown in Fig. 7(b). At zero frequency, the noise for the $E_f=0$ resonant level is obtained from Eqs. (7.9) and (7.10) using a Lorentzian form for the transmission probability:

$$\mathcal{T}(\epsilon)=\frac{\gamma_L\gamma_R}{\epsilon^2+(\gamma/2)^2}. \quad (7.14)$$

Thus, there is a suppression of the shot noise even for $V\to\infty$, due to the factor of $1-\mathcal{T}_{eff}$ in Eq. (7.9). For $\mathcal{T}(\epsilon)$ of Eq. (7.14), $\mathcal{T}_{eff}$ is equal to $2\gamma_L\gamma_R/\gamma^2$ at large bias.[42]

The reason why the resonant-level model has suppressed noise at large bias but the Kondo model does not can be understood from a simple master equation for the charge current. For the resonant-level model, the spin-σ current from the left lead to the level is given at large bias by

$$I_{L\sigma}(t)=\frac{e\gamma_L}{\hbar}[1-n_\sigma(t)], \quad (7.15)$$

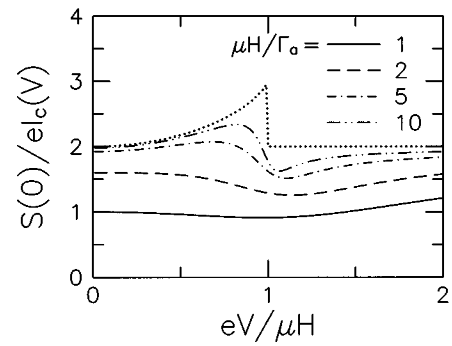

FIG. 8. The zero-temperature noise-to-current ratio for $\Gamma_a=\Gamma_b=\Gamma_1$ and different values of the magnetic field. Here $\mu=\mu_B g_i$. For intermediate to large magnetic fields, there is a minima in the noise-to-current ratio above $eV=\mu_B g_i H$. For $\mu_B g_i H/\Gamma_a>4.25$, a window opens in which $S(0)/I_c(V)$ exceeds the Poisson limit. Finally, for $\mu_B g_i H\gg\Gamma_a$, the noise-to-current ratio approaches the dotted curve which has a peak value of $S(0)/I_c=3e$ and which is given for $eV<\mu_B g_i H$ by the ratio of Eq. (7.19) to Eq. (7.18).

where $n_\sigma(t)$ is the occupancy of the $f_\sigma^\dagger$ state at time t. Hence the noise measures not only the Poissonian tunneling attempts from the lead, but also the temporal fluctuations in the occupancy of the level. In particular, if the level is occupied at a given instance, then tunneling to the level is forbidden by Pauli's exclusion principle until it becomes vacant again. This induces temporal correlations between successive tunneling events, causing suppression of the shot noise below the Poisson limit.

In the Kondo model, the localized fermions are replaced by Majorana fermions, which are not subject to any exclusion principle. Consequently, the current at large bias is given by Eq. (6.14) and is free of any damping term analogous to $1-n_\sigma(t)$. Physically, this reflects the lack of any fundamental restriction on repeated flipping of the impurity spin. The only contribution to the shot noise in this case comes from the random Poissonian tunneling attempts from the lead, which give $S(0)=2eI_c$.

2. $T=0$, $H\neq 0$

Next we switch on a nonzero magnetic field. Figures 8 and 9 display the noise-to-current ratio for zero temperature and nonzero magnetic field. [See Appendix D, Eq. (D5), for

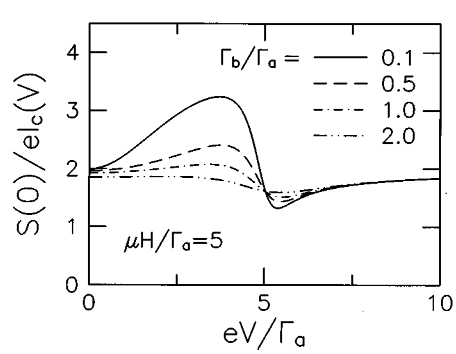

FIG. 9. The zero-temperature noise-to-current ratio for $\mu_B g_i H=5\Gamma_a$, $\Gamma_a=\Gamma_1$, and different ratios of Γ_b to Γ_a. The excess noise increases as Γ_b/Γ_a decreases. Specifically, $S(0)/I_c(V)$ approaches the asymptotic peak value of $2e+2e\Gamma_1/(\Gamma_a+\Gamma_b)$, in the limit of a large magnetic field.

an explicit analytic expression.] The most intriguing feature of these plots is the enhancement of $S(0)/I_c$ for sufficiently large magnetic fields, as eV approaches $\mu_B g_i H$ from below. In particular, the noise can actually exceed the Poisson value of $2eI_c$. From Figs. 8 and 9 we see that this effect is more pronounced for fields large relative to the Kondo scales Γ_a and Γ_b, and that the size of the excess noise increases with Γ_a/Γ_b. As noted above, it is impossible to achieve a noise-to-current ratio larger than $2e$ from a noninteracting electron model. Thus, this is a clear signature for the many-body phenomena of this problem. Moreover, there is no analogous indication for many-body physics in the differential conductance, which can actually be reproduced for $\Gamma_a=\Gamma_b$ from the noninteracting resonant-level model.

The key to understanding the noise curves in Figs. 8 and 9 is that tunneling processes involving just a single spin-flip scattering are energetically disallowed for $eV<\mu_B g_i H$. The voltage can provide an excess energy of eV, which is insufficient to overcome the large Zeeman splitting at zero temperature. Thus, the only way to get a current is by virtual processes in which the impurity spin is flipped twice, some of which involve the transfer of two electrons across the junction, while others involve the usual transfer of a single electron. As the effective charge for pair tunneling is $2e$ instead of e, the maximal possible noise is $2(2e)I_c$ rather than $2eI_c$.

This argument can be made quantitative by computing the rates for the one- and two-electron processes, using Fermi's golden rule and the Hamiltonian of Eq. (6.8). Assuming $\mu_B g_i H$ is positive and large compared to Γ_a and Γ_b, the d fermion is unoccupied (spin up) for $\mu_B g_i H \gg k_B T$. Flipping the impurity spin back and forth corresponds to the creation and annihilation of a d fermion, which costs an energy of $\mu_B g_i H$ in the intermediate state. As the impurity energy is the same for the initial and final states, conservation of energy implies that the conduction-electron energy is also unchanged between the initial and final states.

From Eq. (6.8), there are four different terms that create a d fermion and four different terms that annihilate one, giving a total of 16 second-order processes that flip the impurity back and forth. We are interested in those processes that conserve energy and carry current at the same time, of which there are only five processes. Specifically, the sequence of terms $\psi_f(0)d^\dagger$ followed by $\psi_f(0)d$ annihilates a pair of flavor fermions, which corresponds to tunneling of two electrons from left to right [see Eqs. (3.5)]. The other four sequences involve one $\psi_f(0)$ operator and one spin-flavor operator—either $\psi_{sf}(0)$ or $\psi_{sf}^\dagger(0)$—and therefore decrease the number of flavor fermions only by 1. This corresponds to tunneling of a single electron. Hence to second order there are two types of contributions to the current: one-electron and two-electron tunneling processes.

Using Fermi's golden rule, the corresponding one-electron (R_1) and two-electron (R_2) tunneling rates are found to be

$$R_1=\frac{\Gamma_1^2}{4\pi H}\left[\frac{v}{1-v^2}+\frac{1}{2}\ln\left(\frac{1-v}{1+v}\right)\right], \tag{7.16}$$

$$R_2=\frac{\Gamma_1\Gamma_2}{2\pi H}\left[\frac{v}{1-v^2}+\frac{1}{2}\ln\left(\frac{1-v}{1+v}\right)\right] + \frac{\Gamma_1\Gamma_b}{2\pi H}\left[\frac{v}{1-v^2}-\frac{1}{2}\ln\left(\frac{1-v}{1+v}\right)\right], \tag{7.17}$$

where $v=eV/\mu_B g_i H<1$ is the ''reduced'' voltage, and Γ_2 is equal to $\Gamma_a-\Gamma_1$ (see Table I). In terms of the tunneling rates, the charge current and the zero-frequency noise are given by

$$I_c=eR_1+2eR_2, \tag{7.18}$$

$$S(0)=2e^2R_1+2(2e)^2R_2. \tag{7.19}$$

In the above we have assumed that the one- and two-electron tunneling events are uncorrelated, and hence the noise and the current are both additive, with the one- and two-electron contributions each obeying the relation $S(0)=2QI_c$. Here Q is the net charge transferred across the junction, i.e., $Q=e$ for one-electron tunneling and $Q=2e$ for pair tunneling.

Equations (7.18) and (7.19) are correct to fourth order in the transverse couplings, which is the lowest nonvanishing order for the current and noise when $eV<\mu_B g_i H$. They can also be obtained from the exact expressions, Eqs. (5.7) and (7.11), by taking the limit $\Gamma_a,\Gamma_b\ll\mu_B g_i H$. From the exact expressions one can see that the apparent divergences in Eqs. (7.16) and (7.17) as eV approaches $\mu_B g_i H$ from below are cut off by higher order contributions once $\mu_B g_i H-eV$ becomes comparable to the largest of Γ_a and Γ_b. In terms of the ''reduced'' voltage, v, this cutoff can be made arbitrarily close to 1 by considering a sufficiently large magnetic field.

The dotted curve in Fig. 8 shows the asymptotic noise-to-current ratio, for a large magnetic field. For $eV<\mu_B g_i H$, the curve is given by the ratio of Eq. (7.19) to Eq. (7.18). The maximal value for $S(0)/I_c$ is approached in the limit $v\to 1^-$ and is equal to $2e+2e\Gamma_1/(\Gamma_a+\Gamma_b)$. The upper bound for $S(0)/I_c$ is therefore $4e$ instead of $2e$, corresponding to the case where only pair-tunneling processes are present. In terms of the original model parameters, this case corresponds to $J_\perp^{LL}=J_\perp^{RR}=0$.

Once $eV>\mu_B g_i H$, the voltage can supply the necessary energy to flip the impurity spin from up to down. This is manifest in Figs. 8 and 9 in a quick drop in the noise-to-current ratio, below the Poisson value of $2e$. As explained in the previous subsection, the Poisson limit is recovered for very large voltages, i.e., $\mu_B g_i H\ll eV$.

One may ask, how robust is this enhancement of the noise-to-current ratio? Similar to the spin-current case, the mechanism for pair tunneling can already be seen in the original Hamiltonian of Eq. (2.2), provided J_z^{LR} is zero. For a large magnetic field, energy conservation prohibits any direct tunneling across the junction. Consequently, the lowest-order tunneling processes involve two electrons, where the impurity spin is flipped twice. Of the 16 different processes that flip the impurity spin back and forth, only five conserve energy and carry current at the same time. The first three processes in the latter category are described by the sequences (c), (d), and (e) in Fig. 5. In each of these cases the impurity is first flipped by tunneling an electron from left to right (assuming $V>0$) and then flipped back either via an in-

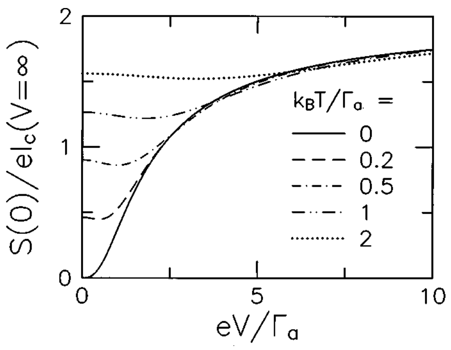

FIG. 10. The zero-frequency charge-current noise $S(0)$ for $H=0$, $\Gamma_a=\Gamma_1$, and different temperatures. Here $I_c(V=\infty)=e\Gamma_1/2\hbar$ denotes the charge current at large voltage bias. In accordance with the fluctuation-dissipation theorem, $S(0)$ is equal to $4k_BTG(0,T)$ at zero bias. For sufficiently large bias, it crosses over from the Nyquist-Johnson noise to the shot noise.

tralead spin flip [Figs. 5(c) and 5(d)] or by tunneling a second electron across the junction [Fig. 5(e)]. The remaining two processes are similar to those in Figs. 5(c) and 5(d), but the order of spin flips is reversed: first the impurity spin is flipped via an intralead scattering, and only then is it flipped back by tunneling an electron from left to right. The enhancement of the noise-to-current ratio comes from the sequence of Fig. 5(e), in which a charge of $2e$ is transferred across the junction. This phenomena should occur in any system where direct tunneling is forbidden by energy conservation and there are two-electron virtual processes.

3. Finite temperature

While at zero temperature one is dealing with pure shot noise, at finite temperature there are also thermal fluctuations that contribute to the noise. For small voltages $eV \ll k_BT$, thermal fluctuations dominate the zero-frequency noise. Specifically, from the fluctuation-dissipation theorem[43] it is known that $S(0)=4k_BTG(0,T)$ at zero bias. In the opposite limit $eV \gg k_BT$, one expects a crossover from the Nyquist-Johnson noise to the shot-noise result. This is illustrated in Fig. 10, for zero magnetic field and $\Gamma_1=\Gamma_a$. At zero voltage, $S(0)$ increases monotonically with temperature from $S(0)=0$ at $T=0$ to $S(0)=e^2\Gamma_1/\hbar$ at $k_BT \gg \Gamma_a$. As a function of voltage, $S(0)$ gradually collapses onto the zero-temperature shot noise, leaving only a single curve in Fig. 10 for sufficiently large voltage bias. The crossover to the shot-noise result occurs as eV becomes several times larger than k_BT.

Both the zero-voltage and the large-voltage limits can be seen analytically from Eqs. (7.7) and (7.8), after setting Ω equal to zero. Specifically, for zero voltage the first term in Eq. (7.7) drops out and $f_{eff}(\epsilon)$ reduces to $f(\epsilon)$. After manipulating Eqs. (4.34)–(4.37) for $G^{>}_{aa}(\epsilon)$ one obtains

$$S(0)=4\frac{e^2\Gamma_1}{\pi\hbar}\int_{-\infty}^{\infty}A_a(\epsilon)f(-\epsilon)f(\epsilon)d\epsilon=4k_BTG(0,T), \tag{7.20}$$

which is the fluctuation-dissipation theorem.

In the opposite limit $eV \gg k_BT,\Gamma_a,\Gamma_b,\mu_Bg_iH$, the first term in Eq. (7.7) approaches the unbounded integral of $G^2_{aa}(\epsilon-i\eta)$, which is identically zero [see discussion following Eq. (7.11)]. In the second term, $f_{eff}(\epsilon)$ is equal to one-half in the dominant integration range, and hence

$$S(0)\approx\frac{e^2\Gamma_1}{\pi\hbar}\int_{-\infty}^{\infty}G^{>}_{aa}(\epsilon)d\epsilon=\frac{e^2}{\hbar}\Gamma_1. \tag{7.21}$$

Evidently, Eq. (7.21) is independent of temperature, indicating that thermal noise is unimportant at sufficiently large bias. A complete expression for $S(0)$ for arbitrary temperature and zero magnetic field is provided in Appendix D, Eq. (D6).

C. Finite frequencies

Thus far our discussion has focused on the zero-frequency noise. The most interesting aspect of the finite-frequency noise spectrum $S(\Omega)$ is the appearance of singularities at zero temperature at certain frequencies. For a noninteracting gas incident upon a barrier, $S(\Omega)$ has three characteristic singularities:[44] one singularity at zero frequency and two symmetric singularities at $\Omega=\pm eV/\hbar$. The noise spectrum is continuous in all three locations, but has discontinuous derivatives with respect to Ω.

The origin of the singularities in $S(\Omega)$ is in the sharpness of the Fermi surfaces at zero temperature. This is best seen by working in the scattering-state basis, where the Hamiltonian is diagonal. For a general noninteracting problem, such as the resonant-level model, the current operator is bilinear in scattering-state operators. Hence the noise correlation function, Eq. (7.1), measures particle-hole excitations. A particle-hole excitation involves two Fermi functions: one function $f(\epsilon_1-\mu_1)$ for the availability of the particle and another function $1-f(\epsilon_2-\mu_2)$ for the availability of the hole. The frequency Ω probes the energy of the excitation. At zero temperature, there will be an abrupt change in the product of the two Fermi functions as one sweeps through $\hbar\Omega=\mu_2-\mu_1$, corresponding to the threshold energy for creating a particle-hole excitation. Thus, if μ_1 is equal to μ_2, as in the case of a particle and a hole that originate from the same lead, there will be a singularity in the noise spectrum at $\Omega=0$. In the case of excitations that involve two opposite leads, the singularities occur at $\Omega=\pm eV/\hbar$. In a general multilead system, the noise will typically have singularities at all possible chemical-potential differences.

A similar picture applies to the nonequilibrium Kondo model. Here the elementary excitations of the system are the scattering states for the flavor and spin-flavor channels, which differ from both the physical electrons and the refermionized ψ fermions. The new ingredient in this case comes from the structure of the charge-current operator, which is still bilinear in the scattering-state operators, but includes also particle-particle ($c^\dagger c^\dagger$) and hole-hole (cc) combinations of scattering states. Accordingly, the current-current correlation function of Eq. (7.1) measures three distinct types of scattering-state pair excitations: particle-hole, particle-particle, and hole-hole excitations, each of which has a different characteristic threshold energy. Consequently, $S(\Omega)$ for the Kondo model develops singularities when $\pm\hbar\Omega$ is equal either to the difference or to the *sum* of the two chemical potentials for the relevant scattering-state fermions.

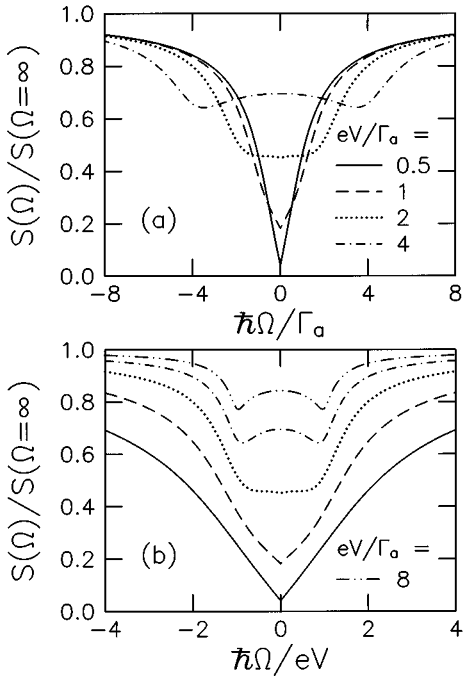

FIG. 11. The zero-temperature charge-current noise spectrum $S(\Omega)$ for $\Gamma_1=\Gamma_a$, $H=0$, and different voltage bias V (a) plotted vs $\hbar\Omega/\Gamma_a$ and (b) plotted vs $\hbar\Omega/eV$. Here $S(\Omega=\infty)=e^2\Gamma_1/\hbar$ is the noise at large frequencies. For $\Gamma_1=\Gamma_a$, there are three distinct frequencies where $S(\Omega)$ has singularities: $\Omega=0$, where the slope of $S(\Omega)$ is discontinuous, and $\Omega=\pm 2eV/\hbar$, where the third derivative of $S(\Omega)$ with respect to Ω is discontinuous. The effect of a voltage is to weaken the singularity at $\Omega=0$, making it indiscernible at large bias. For sufficiently large bias, two symmetric minima develop at $\Omega=\pm eV/\hbar$.

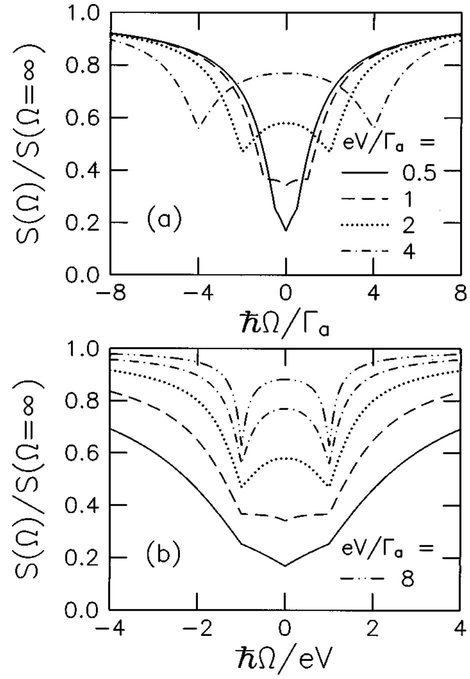

FIG. 12. The same zero-temperature charge-current noise spectra as in Fig. 11, but with $\Gamma_1=0.5\Gamma_a$. For either $\Gamma_1\neq\Gamma_a$ or $H\neq 0$, the noise spectrum has two additional singularities at $\Omega=\pm eV/\hbar$, where the slope of $S(\Omega)$ is discontinuous.

In Figs. 11 and 12 we have plotted the zero-temperature noise as a function of frequency, for two different sets of model parameters. In both figures the magnetic field is equal to zero; however, Γ_1 in Fig. 11 is equal to Γ_a. From Tables II and III one can see that $\hat{I}'_c$ involves only flavor scattering-state operators when $\Gamma_1=\Gamma_a$, but contains also spin-flavor operators if either $\Gamma_1\neq\Gamma_a$ or $H\neq 0$. As we shall see, this changes the number of singularities in the noise spectrum in going from Fig. 11 to Fig. 12. A complete analytical expression for the noise spectra at zero temperature and zero magnetic field is detailed in Appendix D, Eq. (D7).

We begin with the limit of low frequencies. In the previous subsections we have described in detail the zero-frequency noise. In both Figs. 11 and 12 one sees that the noise actually has a cusp at $\Omega=0$, where $S(\Omega)$ varies like the absolute value of Ω. This cusp is the analog of the zero-frequency singularity in the noninteracting case. It stems from particle-hole excitations for the flavor-channel scattering states, i.e., from the terms $c^{\dagger}_{f,k}c_{f,k'}$ in $\hat{I}'_c$. As the voltage is increased, it appears as if this singularity is washed out. However, careful analysis of Eq. (D7) shows that the noise at small frequencies always has the singular component

$$S_{singular}(\Omega\approx 0)=\frac{2e^2\Gamma_1^2}{\pi}A_a^2(eV)|\Omega|. \tag{7.22}$$

Here $A_a(\epsilon)$ is the spectral function for the $\hat{a}$ Majorana fermion. For $eV>\Gamma_a$, $A_a^2(eV)$ diminishes as $\Gamma_a^2/(eV)^4$, which explains the rapid weakening of the singularity as the voltage is increased.

Although it may not be apparent from Figs. 11 and 12, there are actually additional singularities in the noise spectrum at $\Omega=\pm 2eV/\hbar$. These, however, are higher-order singularities, featuring a discontinuity in the third derivative of $S(\Omega)$ with respect to Ω. To analyze the latter singularities it is necessary to expand Eq. (D7) about $\Omega=\pm 2eV/\hbar$ to third order in $\delta_{\pm}=\Omega\mp 2eV/\hbar$, which reveals the nonanalytic term

$$S_{singular}(\Omega\approx\pm 2eV/\hbar)=\frac{e^2\hbar^2}{12\pi}\frac{\Gamma_1^2}{[(eV)^2+\Gamma_a^2]^2}|\delta_{\pm}|^3. \tag{7.23}$$

As explained above, it is impossible to obtain any kind of singularities at $\pm 2eV/\hbar$ from a noninteracting electron model. Moreover, the present singularities originate from the terms $c^{\dagger}_{f,k}c^{\dagger}_{f,k'}$ and $c_{f,k}c_{f,k'}$ in the charge-current operator, which bear no contribution to the time-averaged current. Hence the processes underlying these unconventional singularities cannot be probed through the time-averaged current.

We note that a similar factor of 2 in the location of singularities was recently found in the noise spectrum for static impurity scattering in a $g=1/2$ Luttinger liquid,[45] where it was interpreted as measuring the charge of the current carriers ($2e^*$ for physical electrons instead of e^* for the original Laughlin quasiparticles). A similar interpretation in the present context would imply the existence of pair-tunneling processes. We emphasize, however, that while the singularities at $\pm 2eV/\hbar$ are naturally understood in terms of particle-particle and hole-hole excitations for the scattering-state fermions, it is difficult to interpret them in terms of the actual conduction electrons in the system. Indeed, since $c_{f,k}$ contains both $\psi_{f,k}$ and $\psi^{\dagger}_{f,k}$ components, one cannot simply associate $c_{f,k}c_{f,k'}$ with the tunneling of two conduction electrons from left to right, as is the case for $\psi_{f,k}\psi_{f,k'}$. It remains to be seen what the underlying mechanism is for creating these singularities in terms of the physical conduction electrons.

The noise spectra in Fig. 11 have only three singularities at $\Omega=0$ and $\Omega=\pm 2eV/\hbar$. The noise is smooth and nonsingular at $\Omega=\pm eV/\hbar$, even though two symmetric minima do develop at these frequencies for sufficiently large bias. The situation is quite different when either $\Gamma_1 \neq \Gamma_a$ or if a nonzero magnetic field is switched on. In each of these cases, $\hat{I}_c$ contains mixed terms that involve one flavor and one spin-flavor scattering-state operator, each of which can either create or annihilate a scattering-state fermion. Since the corresponding chemical potentials for the flavor and spin-flavor fermions are $\mu_f=eV$ and $\mu_{sf}=0$, respectively, there are additional singularities in the noise spectrum at $\Omega=\pm eV/\hbar$. Indeed, for a zero magnetic field, expansion of Eq. (D7) about $\Omega=\pm eV/\hbar$ to linear order in $\delta_{\pm}=\Omega\mp eV/\hbar$ reveals the nonanalytic term

$$S_{singular}(\Omega \approx \pm eV/\hbar) = \frac{e^2\Gamma_1\Gamma_2}{\pi\Gamma_a^2}|\delta_{\pm}|, \tag{7.24}$$

where Γ_2 is equal to $\Gamma_a-\Gamma_1$. Hence, similar to the noninteracting case, the noise has a discontinuous slope at $\Omega=\pm eV/\hbar$.

Finally, we comment on the high-frequency limit. At high frequencies, $S(\Omega)$ approaches the asymptotic value of $e^2\Gamma_1/\hbar$. The noise does not decay as $\Omega\to\infty$ because we have chosen to work with an infinite bandwidth. For a finite bandwidth D, there will be a characteristic cutoff frequency $\Omega_c \sim D/\hbar$, beyond which $S(\Omega)$ decays to zero. Such a cutoff scale is absent for an infinite bandwidth.

VIII. IMPURITY MAGNETIZATION AND SUSCEPTIBILITY

While transport properties are the most accessible experimentally for a single impurity, theoretically one is equally interested in magnetic properties, as these provide direct information about the onset of Kondo screening. In this section, we discuss in detail the magnetic properties of the impurity spin, focusing mainly on the static susceptibility.

A. Impurity susceptibility

The time-averaged impurity magnetization follows directly from the equal-time Green function $G^{>}_{ab}(t,t)$:

$$M(H,V) = i\mu_B g_i \int_{-\infty}^{\infty} \frac{d\epsilon}{2\pi} G^{>}_{ab}(\epsilon). \tag{8.1}$$

Inserting Eqs. (4.33)–(4.37) for $G^{>}_{ab}(\epsilon)$ yields

$$M(H,V) = \mu_B g_i \left[\frac{\Gamma_1}{\Gamma_a+\Gamma_b} m(\mu_B g_i H, eV) + \frac{\Gamma_a+\Gamma_b-\Gamma_1}{\Gamma_a+\Gamma_b} m(\mu_B g_i H, 0) \right], \tag{8.2}$$

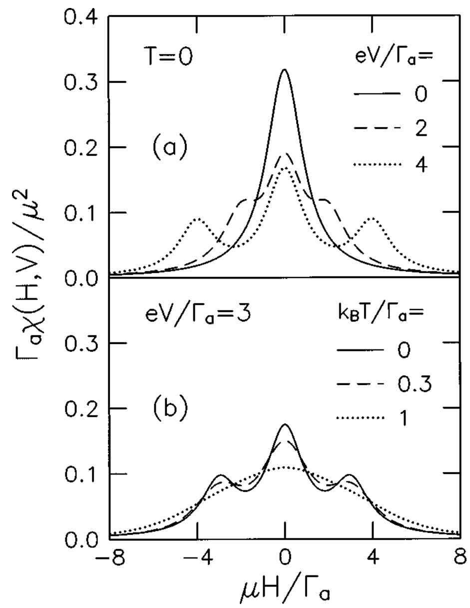

FIG. 13. The impurity susceptibility $\chi(H,V)$ as a function of H (a) for zero temperature and different voltage bias and (b) for $eV/\Gamma_a=3$ and different temperatures. In both graphs, $\Gamma_1=\Gamma_a=\Gamma_b$ and $\mu=\mu_B g_i$. As the voltage is increased, the zero-temperature susceptibility evolves from a single peak at $H=0$ to three resonances at $\mu_B g_i H = 0, \pm eV$. The effect of a temperature is to smear the $T=0$ structure, leaving only a single broad peak at sufficiently large T.

where

$$m(x,y) = -\frac{x}{\pi}\int_{-\infty}^{\infty} \frac{(\Gamma_a+\Gamma_b)\epsilon}{|(\epsilon+i\Gamma_a)(\epsilon+i\Gamma_b)-x^2|^2} f(\epsilon-y)\,d\epsilon. \tag{8.3}$$

At zero temperature, $m(x,y)$ has the simple closed-form expression

$$m(x,y) = \mathrm{Im}\left\{ \frac{x}{\pi\sqrt{4x^2-(\Gamma_a-\Gamma_b)^2}} \times \ln\left(\frac{2y+i(\Gamma_a+\Gamma_b)-\sqrt{4x^2-(\Gamma_a-\Gamma_b)^2}}{2y+i(\Gamma_a+\Gamma_b)+\sqrt{4x^2-(\Gamma_a-\Gamma_b)^2}} \right) \right\}. \tag{8.4}$$

At finite temperature, $m(x,y)$ is conveniently expressed in terms of the digamma function; see Appendix D, Eq. (D8).

Equation (8.2) for the magnetization has the following physical interpretation. The first term is proportional to the tunneling rate Γ_1 and, hence, explicitly involves transitions between the two leads. Indeed, this is the only term to survive when both $J_{\perp}^{LL}$ and $J_{\perp}^{RR}$ are equal to zero. Conversely, only the second term remains if $J_{\perp}^{LR}$ is zero, i.e., when the two leads are decoupled. Thus, there is a clear physical distinction between interlead processes involving $J_{\perp}^{LR}$ and intralead processes involving $J_{\perp}^{LL}$ and $J_{\perp}^{RR}$, which is further evident from the fact that only the first term in Eq. (8.2) depends on the voltage V.

Figures 13 and 14 show the impurity susceptibility as a function of field, for different temperatures and model pa-

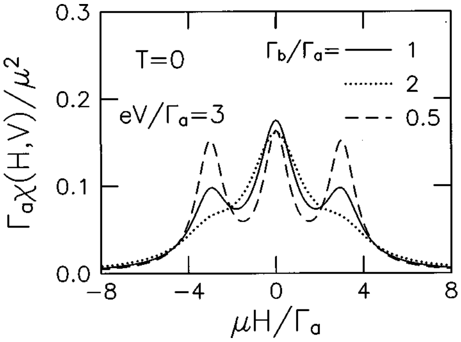

FIG. 14. The impurity susceptibility $\chi(H,V)$ as a function of H, for $T=0$, $eV/\Gamma_a=3$, and different ratios of Γ_b to Γ_a. The same general structure is found for all values of Γ_b/Γ_a; however, the peak resolution is improved as Γ_b/Γ_a is reduced.

rameters. Each term in Eq. (8.2) is responsible for different resonances in the magnetic susceptibility. This is best seen for zero temperature and $\Gamma_a=\Gamma_b$, when differentiation of the first term with respect to H gives

$$\chi_1(H,V)=\frac{(\mu_B g_i)^2}{4\pi}\left[\frac{\Gamma_1}{(\mu_B g_i H-eV)^2+\Gamma_a^2}+\frac{\Gamma_1}{(\mu_B g_i H+eV)^2+\Gamma_a^2}\right] \tag{8.5}$$

and differentiation of the second term gives

$$\chi_2(H)=\frac{(\mu_B g_i)^2}{2\pi}\,\frac{2\Gamma_a-\Gamma_1}{(\mu_B g_i H)^2+\Gamma_a^2}. \tag{8.6}$$

As a function of H, $\chi_2(H)$ has a peak at zero field, while $\chi_1(H,V)$ is peaked at $\mu_B g_i H=\pm eV$. The total susceptibility $\chi=\chi_1+\chi_2$ therefore has three separate peaks for sufficiently large voltage: one central peak at $H=0$ and two symmetric peaks at $\mu_B g_i H=\pm eV$. The same qualitative picture also applies to $\Gamma_a\neq\Gamma_b$; see Fig. 14. The main effect of $\Gamma_a\neq\Gamma_b$ is to modify the shapes of $\chi_1(H,V)$ and $\chi_2(H)$, and to alter the characteristic voltage at which the three-peak structure is resolved. Similar to the differential conductance, the effect of a temperature is to smear the zero-temperature structure. As demonstrated in Fig. 13(b), only a single broad resonance is left in the susceptibility for sufficiently large temperature.

To understand the origin of the peaks in the magnetic susceptibility, we go back to the master-equation approach of Sec. VI B. For $eV-\mu_B g_i H, \mu_B g_i H \gg k_B T, \Gamma_a, \Gamma_b$, the probabilities for finding the impurity in the spin-up and spin-down states are specified in Eq. (6.11). The corresponding impurity magnetization is equal to

$$M=\frac{\mu_B g_i}{2}(P_\uparrow-P_\downarrow)=\mu_B g_i\frac{\Gamma_a+\Gamma_b-\Gamma_1}{2(\Gamma_a+\Gamma_b)}, \tag{8.7}$$

which can also be obtained from the exact expression, Eq. (8.2), by taking the appropriate limit.

The above magnetization reflects the different lifetimes for the two spin states: only interlead spin-flip processes (Γ_1) can flip the impurity spin from up to down, whereas both interlead (Γ_1) and intralead (Γ_2 and Γ_b) processes can flip the spin from down to up. Thus, polarization of the impurity spin stems from the rapid suppression of intralead spin-flip processes for the spin-up state, as $\mu_B g_i H$ is increased from zero to $\mu_B g_i H \gg k_B T, \Gamma_a, \Gamma_b$. This produces a peak in the susceptibility at $H=0$. If one further increases H such that $\mu_B g_i H - eV \gg k_B T, \Gamma_a, \Gamma_b$, then interlead spin flips are also suppressed, and the impurity is frozen in the spin-up configuration ($P_\uparrow=1$). This produces a second-step jump in the impurity magnetization, which shows up as an additional peak in the susceptibility at $\mu_B g_i H = eV$.

B. Relating the spin susceptibility to the differential conductance

One feature which becomes apparent at the solvable point is the close relation between the magnetic susceptibility $\chi(H,V)$ and the differential conductance $G(V,H)$. Specifically, for $\Gamma_a=\Gamma_b$ one has the identity

$$\chi(H,V)=\frac{\hbar(\mu_B g_i)^2}{e^2\Gamma_1}\left[\frac{\Gamma_1}{\Gamma_a+\Gamma_b}G(V,H)+\frac{\Gamma_a+\Gamma_b-\Gamma_1}{\Gamma_a+\Gamma_b}G(0,H)\right], \tag{8.8}$$

which gives

$$\chi(H,V)-\chi(H,0)=\frac{\hbar(\mu_B g_i)^2}{e^2(\Gamma_a+\Gamma_b)}[G(V,H)-G(0,H)]. \tag{8.9}$$

Hence, up to rescaling, the impurity susceptibility and the differential conductance share the same voltage dependence for $\Gamma_a=\Gamma_b$. Although Eq. (8.9) is no longer exact for $\Gamma_a\neq\Gamma_b$, it remains a good approximation for arbitrary Γ_a and Γ_b, if $|\Gamma_a-\Gamma_b|$ is small compared to $\mu_B g_i H$. This suggests that one can actually use the differential conductance as a probe for the voltage dependence of the impurity susceptibility, thus opening the door to susceptibility-like experiments on a single impurity.

C. Two-channel limits

Finally, it is worthwhile to consider how a finite bias affects the overscreening of the impurity spin in each of the two-channel limits of our model, as measured through the impurity susceptibility. In the Emery-Kivelson solution of the two-channel Kondo model,[13] the impurity response to a local field is singular as $T,H\to 0$. Specifically, for $T=0$ and $H\to 0$ the magnetic susceptibility diverges logarithmically as[13]

$$\chi(H)\approx 2\frac{(\mu_B g_i)^2}{\pi\Gamma}\ln\left(\frac{\Gamma}{\mu_B g_i H}\right), \tag{8.10}$$

while for $H=0$ and $T\to 0$ it diverges as

$$\chi(0)=\frac{(\mu_B g_i)^2}{\pi\Gamma}\ln\left(\frac{1.13\Gamma}{k_B T}\right). \tag{8.11}$$

Here Γ is the relevant Kondo scale, i.e., Γ_a or Γ_b, depending on the two-channel limit under consideration.

Consider now the effect of a finite bias. In the first two-channel limit $\Gamma_a=0$, the two leads are decoupled. Consequently, V has no effect on physical quantities, and Eqs.

(8.10) and (8.11) remain intact. In the opposite limit $\Gamma_b = 0$, the divergences in the susceptibility are reduced by a factor of $1-\Gamma_1/\Gamma_a$, which is equal to zero for $\Gamma_1=\Gamma_a$. In the latter case, a finite voltage entirely cuts off the divergence in χ, which instead saturates at

$$\chi(H\to 0,T\to 0)=\frac{(\mu_B g_i)^2}{\pi\Gamma_a}\ln\left[1+\left(\frac{\Gamma_a}{eV}\right)^2\right]. \quad (8.12)$$

Hence, for $\Gamma_b=0$ and $\Gamma_1=\Gamma_a$, the effect of a voltage on the impurity susceptibility is similar to that of a local magnetic field.

IX. CONCLUSIONS

In this paper, we have presented an exact solution to the nonequilibrium Kondo problem based on a special point in the parameter space of the model where both the Hamiltonian $\mathcal{H}$ and the operator describing the nonequilibrium distribution, Y, can be diagonalized simultaneously. This enabled the calculation of a large number of experimentally observable quantities. In the process of solving the problem, we have also demonstrated by explicit calculation the equivalence of two alternative approaches to nonequilibrium: a many-body scattering-state-operator approach[17] and the more conventional perturbation theory based on nonequilibrium Green functions. Both formulations rely on describing the nonequilibrium condition by an operator Y_0, which plays the role of μN in the equilibrium theory. Below we summarize our main results.

The charge current and differential conductance are the most widely studied observables in the nonequilibrium Kondo problem. Our solution shows the standard zero-bias anomaly and its splitting under an applied magnetic field, which actually very few other approaches have been able to describe in the strong-coupling regime. Most important, because of the analytic nature of our solution, we are able to analyze in detail the scaling properties of the differential conductance at low temperature and low voltage. In particular, we obtained the universal low-temperature scaling curve and the finite-temperature corrections to it, both of which bear direct relevance to quantitative comparisons with experiments.

Contrary to the charge current, the spin current has not been studied before in the context of the nonequilibrium Kondo problem. In computing the spin current and the associated differential conductance, we find that the spin current for this model is actually even in the applied voltage. Its direction depends solely on the sign of the magnetic field and the asymmetry in the transverse coupling to the left and right leads, which provides a distinct experimental signature for tunneling through a Kondo impurity. A simple physical picture is given for this effect in terms of the different possible tunneling processes. Although the spin current has not been studied experimentally to date, there is no reason why it cannot be measured in light of the present interest in spin-polarized transport.

Similar to the spin current, the charge-current noise has not been studied before in this problem. The noise spectrum measures pair excitations of the system. With the noise one is able to see new physics which is not observable in the differential conductance. In particular, for a large magnetic field at zero temperature, the noise-to-current ratio $S(0)/I_c$ exceeds the Poisson value of $2e$ and can be as large as $4e$. We explain this effect by virtual processes involving tunneling of pairs of electrons. This provides a simple mechanism for the enhancement of the noise-to-current ratio in interacting mesoscopic systems.

Pair processes of a different kind are observed in the finite-frequency noise spectrum. As a function of frequency, the noise has a new set of singularities at $\hbar\Omega=\pm 2eV$, which are twice as large as the conventional frequencies.[44] These new singularities are understood in terms of the current operator, which contains components describing the simultaneous creation or annihilation of pairs of scattering states. The scattering states are the elementary excitations of the Hamiltonian; however, unlike in conventional noninteracting systems, they do not correspond to any fixed number of physical electrons. Although the new singularities at $\hbar\Omega=\pm 2eV$ are too smooth to be detected experimentally, they clearly illustrate the complex nature of the tunneling current.

Finally, we have computed the impurity magnetization and susceptibility as a function of magnetic field and voltage. While it appears unlikely that the magnetization and susceptibility of a single impurity can be measured experimentally, from a theoretical point of view they are perhaps the most direct measurement of the screening of the impurity by the conduction electrons. By examining the susceptibility as a function of voltage and field, we are able to identify two distinct processes—intralead and interlead—which are responsible for different peaks in the susceptibility curve. Each peak occurs at a field where a certain spin-flip mechanism is suppressed. Intralead spin flips are suppressed for $\mu_B g_i H > 0$, whereas interlead spin flips are suppressed for $\mu_B g_i H > eV$.

Although the solvable point is only one point in the parameter space of the nonequilibrium Kondo problem, we expect it to correctly describe the strong-coupling regime of the model for arbitrary antiferromagnetic coupling constants. In particular, our predictions for the scaling curve should be quantitatively correct. As one of the parameters k_BT, eV, or $\mu_B g_i H$ becomes of order of the Kondo scale, our results are expected to remain qualitatively correct, but not necessarily quantitative. For example, the differential conductance observed experimentally[8,9] shows a splitting in a magnetic field similar to the one obtained in our calculation; however, one cannot quantitatively fit our solution to the experimental curves.[46] As one leaves the scaling regime—i.e., k_BT, eV, or $\mu_B g_i H$ becomes considerably larger than the Kondo scale—it remains to be seen which of our results continue to apply to a generic Kondo Hamiltonian. We expect the spin current to remain an even function of the applied bias, with a characteristic peak in the differential conductance at $eV = \mu_B g_i H$. On the other hand, we do not recover the standard logarithmic temperature dependence of the conductance at high temperature. It is particularly interesting to see if our predictions for the enhancement of the noise carry over to the standard Kondo Hamiltonian and whether they can be detected experimentally.

It is our hope that the concepts and techniques used in this paper will prove useful in studying other interacting nonequilibrium problems and in obtaining other solvable points. Especially intriguing is the possibility of combining the

Y-operator formalism with powerful approaches such as the Bethe ansatz and conformal field theory; however, this hinges on the ability of the latter approaches to construct the appropriate many-body scattering states. It remains to be seen to what extent existing solutions of the equilibrium Kondo problem[11] can be reformulated in terms of the many-body scattering states.

ACKNOWLEDGMENTS

We gratefully acknowledge discussions with Vic Emery, Matthias Hettler, Kevin Ingersent, Khandker Muttalib, and Robert Smith. A.S. is thankful to John Wilkins for an inspiring discussion about Majorana fermions. Portions of this work carried out at Florida were supported by NSF Grant No. DMR9357474, the NHMFL, and the Research Corporation. Portions of the work carried out at Ohio State (A.S.) were supported by OSU and by a grant from the U.S. Department of Energy, Office of Basic Energy Sciences, Division of Materials Research.

APPENDIX A: MAPPING OF THE EFFECTIVE ONE-CHANNEL LIMIT ONTO THE ORDINARY ONE-CHANNEL HAMILTONIAN

In this appendix, we show that the effective one-channel limit of Eq. (2.19) is equivalent in equilibrium to the ordinary one-channel Kondo Hamiltonian. Specifically, using the notation of Eq. (2.16) we present an exact mapping of the Hamiltonian

$$\mathcal{H}=\mathcal{H}_{kin}+J_{z1}s_1^z\tau^z+J_{\perp 1}(s_1^x\tau^x+s_1^y\tau^y)+J_{z2}s_2^z\tau^z \tag{A1}$$

onto the standard single-channel Kondo Hamiltonian. Here $\mathcal{H}_{kin}$ is the kinetic energy for the $\psi_{1\sigma}$ and $\psi_{2\sigma}$ fields, and J_{z1}, J_{z2}, and $J_{\perp 1}$ are arbitrary coupling constants. For conciseness, we have omitted the local magnetic field acting on the impurity spin from Eq. (A1). Such a term, though, can be trivially incorporated. The mapping is obtained in the framework of bosonization.

To bosonize the fermion fields $\psi_{1\sigma}$ and $\psi_{2\sigma}$, we employ the same representation of Sec. III, with the indices L and R corresponding to 1 and 2, respectively. This leads to the following representation of Eq. (A1):

$$\begin{aligned}\mathcal{H}=&\frac{\hbar v_F}{4\pi}\sum_{\nu=1\uparrow,1\downarrow,2\uparrow,2\downarrow}\int_{-\infty}^{\infty}[\nabla\Phi_\nu(x)]^2dx\\&+i\frac{J_{\perp 1}}{4\pi a}[e^{i(\chi_{1\uparrow}-\chi_{1\downarrow})}\tau^- - e^{-i(\chi_{1\uparrow}-\chi_{1\downarrow})}\tau^+]\\&+\frac{J_{z1}}{4\pi}[\nabla\Phi_{1\uparrow}(0)-\nabla\Phi_{1\downarrow}(0)]\tau^z\\&+\frac{J_{z2}}{4\pi}[\nabla\Phi_{2\uparrow}(0)-\nabla\Phi_{2\downarrow}(0)]\tau^z,\end{aligned} \tag{A2}$$

with $\chi_\nu=\Phi_\nu(0)-\varphi_\nu$.

The Hamiltonian of Eq. (A2) is converted to a standard one-channel Kondo Hamiltonian through a series of transformations. We begin with the canonical transformation $\mathcal{H}'=U_1\mathcal{H}U_1^\dagger$, in which

$$U_1=\exp[i\theta_1(\chi_{1\uparrow}-\chi_{1\downarrow})\tau^z+i\theta_2(\chi_{2\uparrow}-\chi_{2\downarrow})\tau^z] \tag{A3}$$

is defined by the two angles of rotation

$$\theta_1=\frac{J_{z1}}{4\pi\hbar v_F}\quad\text{and}\quad\theta_2=\frac{J_{z2}}{4\pi\hbar v_F}. \tag{A4}$$

This brings us to

$$\begin{aligned}\mathcal{H}'=&\frac{\hbar v_F}{4\pi}\sum_{\nu=1\uparrow,1\downarrow,2\uparrow,2\downarrow}\int_{-\infty}^{\infty}[\nabla\Phi_\nu(x)]^2dx\\&+i\frac{J_{\perp 1}}{4\pi a}[e^{i(1-\theta_1)(\chi_{1\uparrow}-\chi_{1\downarrow})-i\theta_2(\chi_{2\uparrow}-i\chi_{2\downarrow})}\tau^-\\&-e^{-i(1-\theta_1)(\chi_{1\uparrow}-\chi_{1\downarrow})+i\theta_2(\chi_{2\uparrow}-\chi_{2\downarrow})}\tau^+].\end{aligned} \tag{A5}$$

While the longitudinal Kondo terms have been conveniently removed from Eq. (A5), the exponential terms acquired an explicit dependence on the angles θ_1 and θ_2. To overcome the latter difficulty, we introduce a new set of boson fields

$$\tilde{\Phi}_{1\sigma}(x)=A\Phi_{1\sigma}(x)-B\Phi_{2\sigma}(x), \tag{A6}$$

$$\tilde{\Phi}_{2\sigma}(x)=B\Phi_{1\sigma}(x)+A\Phi_{2\sigma}(x), \tag{A7}$$

where

$$A=\frac{1-\theta_1}{\sqrt{(1-\theta_1)^2+\theta_2^2}}, \tag{A8}$$

$$B=\frac{\theta_2}{\sqrt{(1-\theta_1)^2+\theta_2^2}}. \tag{A9}$$

Similar combinations are defined for each of $\tilde{\varphi}_\nu$ and $\tilde{\chi}_\nu$. The coefficients A and B are chosen such that $\tilde{\Phi}_{1\sigma}(x)$ and $\tilde{\Phi}_{2\sigma}(x)$ maintain appropriate commutation relations:

$$[\tilde{\Phi}_{i\sigma}(x),\tilde{\Phi}_{j\sigma'}(y)]=-i\pi\delta_{i,j}\delta_{\sigma,\sigma'}\ \mathrm{sgn}(x-y). \tag{A10}$$

Conventional exponents are restored in Eq. (A5) by performing a second canonical transformation, this time to $\mathcal{H}''=U_2\mathcal{H}'U_2^\dagger$ with

$$U_2=\exp\{i[\sqrt{(1-\theta_1)^2+\theta_2^2}-1](\tilde{\chi}_{1\uparrow}-\tilde{\chi}_{2\downarrow})\tau^z\}. \tag{A11}$$

This step brings us to the Hamiltonian

$$\begin{aligned}\mathcal{H}''=&\frac{\hbar v_F}{4\pi}\sum_{\nu=1\uparrow,1\downarrow,2\uparrow,2\downarrow}\int_{-\infty}^{\infty}[\nabla\tilde{\Phi}_\nu(x)]^2dx\\&+i\frac{J_{\perp 1}}{4\pi a}[e^{i(\tilde{\chi}_{1\uparrow}-\tilde{\chi}_{1\downarrow})}\tau^- - e^{-i(\tilde{\chi}_{1\uparrow}-\tilde{\chi}_{1\downarrow})}\tau^+]\\&+\frac{\tilde{J}_z}{4\pi}[\nabla\tilde{\Phi}_{1\uparrow}(0)-\nabla\tilde{\Phi}_{1\downarrow}(0)]\tau^z,\end{aligned} \tag{A12}$$

where

$$\tilde{J}_z=4\pi\hbar v_F[1-\sqrt{(1-\theta_1)^2+\theta_2^2}]. \tag{A13}$$

At this point, we transform to a new fermion representation by introducing the fermion fields

$$\tilde{\psi}_{i\sigma}(x) = \frac{e^{i\Theta_{i\sigma}}}{\sqrt{2\pi a}} e^{-i\tilde{\Phi}_{i\sigma}(x)}. \tag{A14}$$

Here $\Theta_{i\sigma}$ are supplementary phase operators, introduced to assure that the different fermion species of Eq. (A14) anticommute with one another. The explicit forms of the $\Theta_{i\sigma}$ are

$$\Theta_{2\uparrow} = \frac{1}{2}\int_{-\infty}^{\infty} [\nabla\tilde{\Phi}_{2\downarrow}(x) + \nabla\tilde{\Phi}_{1\uparrow}(x) + \nabla\tilde{\Phi}_{1\downarrow}(x)]dx, \tag{A15}$$

$$\Theta_{2\downarrow} = \frac{1}{2}\int_{-\infty}^{\infty} [\nabla\tilde{\Phi}_{1\uparrow}(x) + \nabla\tilde{\Phi}_{1\downarrow}(x)]dx, \tag{A16}$$

$$\Theta_{1\uparrow} = \tilde{\varphi}_{1\uparrow} - \tilde{\varphi}_{1\downarrow} = \frac{1}{2}\int_{-\infty}^{\infty} \nabla\tilde{\Phi}_{1\downarrow}(x)dx, \tag{A17}$$

and $\Theta_{1\downarrow} = 0$. In terms of the new fermion fields, the Hamiltonian takes the form

$$\mathcal{H}'' = \mathcal{H}''_{kin} + \tilde{J}_z \tilde{s}_1^z \tau^z + J_{\perp 1}(\tilde{s}_1^x \tau^x + \tilde{s}_1^y \tau^y), \tag{A18}$$

where $\mathcal{H}''_{kin}$ is the kinetic energy of the $\tilde{\psi}_{1\sigma}$ and $\tilde{\psi}_{2\sigma}$ fields, and $\tilde{s}_1^\lambda$ are the spin densities at the origin for the $\tilde{\psi}_{1\sigma}$ fermions [obtained by replacing $\psi_{i\sigma}(0)$ with $\tilde{\psi}_{1\sigma}(0)$ in Eq. (2.18)].

Equation (A18) is just a standard one-channel Kondo Hamiltonian, in which the $\tilde{\psi}_{1\sigma}$ fermions undergo a Kondo spin-exchange interaction with the impurity spin. The $\tilde{\psi}_{2\sigma}$ fermions are decoupled from the impurity. The effective longitudinal coupling in this new representation is $\tilde{J}_z$, which generally depends on both J_{z1} and J_{z2} [see Eq. (A13)]. For $J_{z1}, J_{z2} \ll 1$, it reduces to J_{z1}.

In equilibrium, this establishes the equivalence of the effective one-channel limit of Eq. (2.19) and the standard one-channel Kondo effect. This result, however, does not carry over to the nonequilibrium case, where a simultaneous mapping of the Y_0 operator is required. When expressed in terms of the fermion fields $\psi_{1\sigma}$ and $\psi_{2\sigma}$, Y_0 contains bilinear combinations that do not transform simply under the operations U_1 and U_2. Consequently, one can no longer formally map the effective one-channel limit of Eq. (2.19) onto the standard one-channel Kondo impurity in the presence of a finite bias.

APPENDIX B: DERIVATION OF THE SCATTERING-STATE OPERATORS

In this appendix, we present a detailed solution of the scattering-state operators, as defined by Eq. (4.6). Our objective is twofold: to obtain exact, closed-form expressions for the scattering-state operators and to illustrate at the same time the type of machinery necessary for tackling operator equations such as Eq. (4.6).

To this end, we separate the Hamiltonian of Eq. (4.4) into three parts

$$\mathcal{H}'_0 = \sum_{\nu=f,sf}\sum_k \epsilon_k \psi^\dagger_{\nu,k}\psi_{\nu,k}, \tag{B1}$$

$$\begin{aligned}\mathcal{H}'_1 = {} & i\frac{J^+}{2\sqrt{\pi a L}}\sum_k (\psi^\dagger_{sf,k} + \psi_{sf,k})\hat{b} \\ & + \frac{J_\perp^{LR}}{2\sqrt{\pi a L}}\sum_k (\psi^\dagger_{f,k} - \psi_{f,k})\hat{a} \\ & + \frac{J^-}{2\sqrt{\pi a L}}\sum_k (\psi^\dagger_{sf,k} - \psi_{sf,k})\hat{a},\end{aligned} \tag{B2}$$

$$\mathcal{H}'_2 = -i\mu_B g_i H \hat{a}\hat{b}. \tag{B3}$$

Each of the above components is assigned a Liouville operator $\mathcal{L}_n$, which acts on a general operator $\hat{O}$ according to

$$\mathcal{L}_n \hat{O} = [\hat{O}, \mathcal{H}'_n]. \tag{B4}$$

Using $\mathcal{L} = \mathcal{L}_0 + \mathcal{L}_1 + \mathcal{L}_2$, Eq. (4.6) is rewritten as

$$(\mathcal{L} + \epsilon_k + i\eta)c^\dagger_{\nu,k} = i\eta\psi^\dagger_{\nu,k}, \tag{B5}$$

which has the formal solution

$$c^\dagger_{\nu,k} = i\eta\frac{1}{\mathcal{L} + \epsilon_k + i\eta}\psi^\dagger_{\nu,k}. \tag{B6}$$

Because of the explicit way in which η enters Eq. (B6), it is inconvenient to work with this representation of Eq. (4.6). Our goal is to recast the same equation in a form more suitable for computing the scattering-state operators. This is achieved by combining the operator identity

$$\frac{1}{\mathcal{L} + \epsilon_k + i\eta} = \left[1 - \frac{1}{\mathcal{L} + \epsilon_k + i\eta}(\mathcal{L}_1 + \mathcal{L}_2)\right]\frac{1}{\mathcal{L}_0 + \epsilon_k + i\eta} \tag{B7}$$

with

$$\frac{1}{\mathcal{L}_0 + \epsilon_k + i\eta}\psi^\dagger_{\nu,k} = \frac{1}{i\eta}\psi^\dagger_{\nu,k} \tag{B8}$$

and

$$\mathcal{L}_2\psi^\dagger_{\nu,k} = 0, \tag{B9}$$

to obtain

$$c^\dagger_{\nu,k} = \psi^\dagger_{\nu,k} - \frac{1}{\mathcal{L} + \epsilon_k + i\eta}\mathcal{L}_1\psi^\dagger_{\nu,k}. \tag{B10}$$

Equation (B10) is the direct analog of the Lippmann-Schwinger equation[25] for scattering states in first quantization. Here $\psi^\dagger_{\nu,k}$ plays the role of the plain-wave boundary condition, while $\mathcal{L}_1$ and $\mathcal{L}_2$ correspond to the scattering potential. A similar equation can be derived for the scattering-state operators of a general nonequilibrium problem. The remainder of this appendix is devoted to the solution of this equation.

When taking the commutator $\mathcal{L}_1\psi^\dagger_{\nu,k}$ in Eq. (B10), it is useful to introduce two auxiliary operators

$$\hat{A} = \frac{1}{\mathcal{L} + \epsilon_k + i\eta}\hat{a} \tag{B11}$$

and

$$\hat{B}=\frac{1}{\mathcal{L}+\epsilon_k+i\eta}\,\hat{b}. \tag{B12}$$

These are related to the scattering-state operators via

$$c^{\dagger}_{f,k}=\psi^{\dagger}_{f,k}+\frac{J^{LR}_{\perp}}{2\sqrt{\pi a L}}\,\hat{A}, \tag{B13}$$

$$c^{\dagger}_{sf,k}=\psi^{\dagger}_{sf,k}+\frac{J^{-}}{2\sqrt{\pi a L}}\,\hat{A}-i\frac{J^{+}}{2\sqrt{\pi a L}}\,\hat{B}. \tag{B14}$$

By analogy with Green functions, $\hat{A}$ and $\hat{B}$ can be interpreted as the ‘‘dressed’’ (with respect to $\mathcal{L}_1$ and $\mathcal{L}_2$) counterparts of $\hat{a}$ and $\hat{b}$. Indeed, a systematic expansion in $\mathcal{L}_1$ and $\mathcal{L}_2$ corresponds to perturbation theory in $\mathcal{H}'_1$ and $\mathcal{H}'_2$, with $(\mathcal{L}_0+\epsilon_k+i\eta)^{-1}$ playing the role of the bare propagator. Concentrating on the operators $\hat{A}$ and $\hat{B}$, we evaluate them using a procedure reminiscent of the equations-of-motion technique for the calculation of ordinary Green functions. As in Dyson's equation for Green functions, we seek a closed set of equations relating $\hat{A}$ and $\hat{B}$ to themselves. Bearing this aim in mind, we substitute once again the operator identity (B7) into Eqs. (B11) and (B12), only this time in combination with

$$\frac{1}{\mathcal{L}_0+\epsilon_k+i\eta}\begin{Bmatrix}\hat{a}\\ \hat{b}\end{Bmatrix}=\frac{1}{\epsilon_k+i\eta}\begin{Bmatrix}\hat{a}\\ \hat{b}\end{Bmatrix} \tag{B15}$$

and

$$\mathcal{L}_2\hat{a}=-i\mu_B g_i\hat{b},\quad \mathcal{L}_2\hat{b}=i\mu_B g_i\hat{a}, \tag{B16}$$

to obtain

$$(\epsilon_k+i\eta)\hat{A}-i\mu_B g_i\hat{B}=\hat{a}-\frac{1}{\mathcal{L}+\epsilon_k+i\eta}\,\mathcal{L}_1\hat{a}, \tag{B17}$$

$$(\epsilon_k+i\eta)\hat{B}+i\mu_B g_i\hat{A}=\hat{b}-\frac{1}{\mathcal{L}+\epsilon_k+i\eta}\,\mathcal{L}_1\hat{b}. \tag{B18}$$

While the left-hand sides of Eqs. (B17) and (B18) contain only $\hat{A}$ and $\hat{B}$, the rightmost term in each equation is a new, unknown quantity that needs to be simplified. We focus initially on the rightmost term in Eq. (B17) and write it as

$$\frac{1}{\mathcal{L}+\epsilon_k+i\eta}\,\mathcal{L}_1\hat{a}=\frac{1}{\mathcal{L}_0+\mathcal{L}_2+\epsilon_k+i\eta}\,\mathcal{L}_1\hat{a}-\frac{1}{\mathcal{L}+\epsilon_k+i\eta}\,\mathcal{L}_1\,\frac{1}{\mathcal{L}_0+\mathcal{L}_2+\epsilon_k+i\eta}\,\mathcal{L}_1\hat{a}. \tag{B19}$$

Equation (B19) is evaluated using the following steps.

(i) Implement the commutator $\mathcal{L}_1\psi^{\dagger}_{\nu,k}$.

(ii) Use the identity

$$\frac{1}{\mathcal{L}_0+\mathcal{L}_2+\epsilon_k+i\eta}\begin{Bmatrix}\psi^{\dagger}_{\nu,k'}\\ \psi_{\nu,k'}\end{Bmatrix}=\frac{1}{\epsilon_k\mp\epsilon_{k'}+i\eta}\begin{Bmatrix}\psi^{\dagger}_{\nu,k'}\\ \psi_{\nu,k'}\end{Bmatrix}. \tag{B20}$$

(iii) Take the commutators $\mathcal{L}_1\psi^{\dagger}_{\nu,k}$ and $\mathcal{L}_1\psi_{\nu,k}$.

(iv) Employ the wideband limit

$$\frac{1}{L}\sum_{k'}\frac{1}{\epsilon-\epsilon_{k'}\pm i\eta}=\frac{1}{2\pi\hbar v_F}\int\frac{d\epsilon_{k'}}{\epsilon-\epsilon_{k'}\pm i\eta}=\mp\frac{i}{2\hbar v_F}. \tag{B21}$$

At the end of these steps one arrives at

$$\begin{aligned}\frac{1}{\mathcal{L}+\epsilon_k+i\eta}\,\mathcal{L}_1\hat{a}=i\Gamma_a\hat{A}-\frac{J^{LR}_{\perp}}{2\sqrt{\pi a L}}&\times\sum_{k'}\left(\frac{\psi^{\dagger}_{f,k'}}{\epsilon_k-\epsilon_{k'}+i\eta}-\frac{\psi_{f,k'}}{\epsilon_k+\epsilon_{k'}+i\eta}\right)\\&-\frac{J^{-}}{2\sqrt{\pi a L}}\sum_{k'}\left(\frac{\psi^{\dagger}_{sf,k'}}{\epsilon_k-\epsilon_{k'}+i\eta}-\frac{\psi_{sf,k'}}{\epsilon_k+\epsilon_{k'}+i\eta}\right),\end{aligned} \tag{B22}$$

where Γ_a is defined in Eq. (4.7).

An almost identical calculation is applied to the rightmost term in Eq. (B18). It yields

$$\frac{1}{\mathcal{L}+\epsilon_k+i\eta}\,\mathcal{L}_1\hat{b}=i\Gamma_b\hat{B}-i\frac{J^{+}}{2\sqrt{\pi a L}}\times\sum_{k'}\left(\frac{\psi^{\dagger}_{sf,k'}}{\epsilon_k-\epsilon_{k'}+i\eta}+\frac{\psi_{sf,k'}}{\epsilon_k+\epsilon_{k'}+i\eta}\right), \tag{B23}$$

where Γ_b is taken from Eq. (4.8).

Substituting Eqs. (B22) and (B23) into Eqs. (B17) and (B18), a closed set of 2×2 linear equations is obtained for $\hat{A}$ and $\hat{B}$. Straightforward solution of the latter equations yields

$$\hat{A}=G_{aa}(\epsilon_k+i\eta)\hat{\alpha}_k+G_{ba}(\epsilon_k+i\eta)\hat{\beta}_k, \tag{B24}$$

$$\hat{B}=G_{ab}(\epsilon_k+i\eta)\hat{\alpha}_k+G_{bb}(\epsilon_k+i\eta)\hat{\beta}_k, \tag{B25}$$

where G_{ij} are the Majorana Green functions specified in Eq. (4.9), and $\hat{\alpha}_k$ and $\hat{\beta}_k$ are the operators defined in Eqs. (4.12) and (4.13), respectively. The final expressions for the scattering-state operators, Eqs. (4.10) and (4.11), follow from combining Eqs. (B24) and (B25) with Eqs. (B13) and (B14).

APPENDIX C: THE Y' OPERATOR

In this appendix, we show that the solution to the operator equation (4.1) is given by

$$Y'=eV\sum_k c^{\dagger}_{f,k}c_{f,k}+c, \tag{C1}$$

where c is an appropriately chosen constant (see below). To this end, we implement the commutator of Eq. (C1) with $\mathcal{H}'$:

$$[Y',\mathcal{H}'] = eV\sum_k ([c^\dagger_{f,k},\mathcal{H}']c_{f,k} + c^\dagger_{f,k}[c_{f,k},\mathcal{H}']). \tag{C2}$$

Each of the commutators on the right-hand side can be accounted for using Eq. (4.6). Hence Eq. (C2) becomes

$$[Y',\mathcal{H}'] = i\eta eV\sum_k [(\psi^\dagger_{f,k} - c^\dagger_{f,k})c_{f,k} + c^\dagger_{f,k}(\psi_{f,k} - c_{f,k})], \tag{C3}$$

which may be rewritten as

$$[Y',\mathcal{H}'] = i\eta(Y'_0 - Y') + i\eta\left[c - eV\sum_k (c^\dagger_{f,k} - \psi^\dagger_{f,k})(c_{f,k} - \psi_{f,k})\right]. \tag{C4}$$

Equation (C4) clearly reduces to Eq. (4.1) if the expression in the curly brackets is equal to zero, i.e., if c can be chosen such that it cancels the rightmost sum. Indeed, this somewhat surprising result follows from the special structure of the scattering-state operators $c^\dagger_{f,k}$. To see this we note that the operators $\hat{\alpha}_k$ and $\hat{\beta}_k$, Eqs. (4.12) and (4.13), obey

$$\hat{\alpha}^\dagger_k = \hat{\alpha}_{-k}, \quad \hat{\beta}^\dagger_k = \hat{\beta}_{-k}, \tag{C5}$$

while $G^*_{ij}(\epsilon_k + i\eta)$ is equal to $-G_{ij}(\epsilon_{-k} + i\eta)$ [see Eq. (4.9)]. From the combination of these two properties one obtains the key relation

$$c^\dagger_{f,k} - \psi^\dagger_{f,k} = \psi_{f,-k} - c_{f,-k}, \tag{C6}$$

which allows the following manipulation:

$$\begin{aligned}\sum_k (c^\dagger_{f,k} - \psi^\dagger_{f,k})(c_{f,k} - \psi_{f,k}) &= -\sum_k (c^\dagger_{f,k} - \psi^\dagger_{f,k})(c^\dagger_{f,-k} - \psi^\dagger_{f,-k}) \\ &= -\frac{1}{2}\sum_k \{c^\dagger_{f,k} - \psi^\dagger_{f,k}, c^\dagger_{f,-k} - \psi^\dagger_{f,-k}\}.\end{aligned} \tag{C7}$$

Here we have exploited the equivalence of summing over k and $-k$ in order to arrive at anticommutators. Given that $c^\dagger_{f,k} - \psi^\dagger_{f,k}$ is linear in ψ and $\psi^\dagger$ operators, each of the anticommutators above is a c number. Consequently, also the entire sum in Eq. (C7) is nothing but a constant.

Although this is sufficient to prove our point, it is satisfying to know that the sum in Eq. (C7) can be carried out explicitly. Skipping the details of the algebra, we quote here only the end result

$$\sum_k (c^\dagger_{f,k} - \psi^\dagger_{f,k})(c_{f,k} - \psi_{f,k}) = \frac{\Gamma_1}{4|\eta|}. \tag{C8}$$

Hence Eq. (C1) with $c = eV\Gamma_1/4|\eta|$ is the solution of Eq. (4.1).

Two comments should be made about the above result. First, our derivation relied solely on the special structure of the scattering-state operators $c^\dagger_{f,k}$. Since Eq. (4.10) remains intact for a general $\eta \neq 0$ (not only $\eta \to 0^+$), so does our solution for Y'. Namely, Eq. (C1) with $c = eV\Gamma_1/4|\eta|$ is the exact solution of Eq. (4.1) for arbitrary $\eta \neq 0$. Of course, only $\eta \to 0^+$ bears relevance to our discussion.

The second point to notice is that c actually diverges as $\eta \to 0$; however, this divergence is harmless. It does not enter any physical quantities.

APPENDIX D: ANALYTIC EXPRESSIONS FOR OBSERVABLES

In this appendix, we provide closed-form, analytical expressions for a comprehensive set of observables: the charge current, the differential conductance, the charge-current noise, and the impurity magnetization.

1. Charge current

The charge current for arbitrary temperature and model parameters is given by

$$\begin{aligned}I_c(V) = \frac{e\Gamma_1}{2\pi\hbar}\,\mathrm{Im}\Bigg\{&A_1\psi\left(\frac{1}{2} + \frac{\xi_1 + ieV}{2\pi k_B T}\right) - A_1\psi\left(\frac{1}{2} + \frac{\xi_1 - ieV}{2\pi k_B T}\right) + A_2\psi\left(\frac{1}{2} + \frac{\xi_2 + ieV}{2\pi k_B T}\right) \\ &- A_2\psi\left(\frac{1}{2} + \frac{\xi_2 - ieV}{2\pi k_B T}\right)\Bigg\},\end{aligned} \tag{D1}$$

where

$$\xi_{1,2} = \frac{\Gamma_a + \Gamma_b}{2} \pm \sqrt{\left(\frac{\Gamma_a - \Gamma_b}{2}\right)^2 - (\mu_B g_i H)^2} \tag{D2}$$

and

$$A_1 = \frac{\xi_1 - \Gamma_b}{\xi_1 - \xi_2}, \quad A_2 = \frac{\xi_2 - \Gamma_b}{\xi_2 - \xi_1}. \tag{D3}$$

Here $\psi(z)$ is the digamma function.[30] For a zero magnetic field, ξ_1 and ξ_2 coincide with Γ_a and Γ_b; hence Eq. (D1) reduces to Eq. (5.9). Likewise, for $\Gamma_a = \Gamma_b$ and a nonzero H, ξ_1 and ξ_2 are equal to $\Gamma_a \pm i\mu_B g_i H$, and Eq. (5.10) is obtained. Otherwise, for $\Gamma_a \neq \Gamma_b$ and a nonzero magnetic field, A_1 and A_2 are in general complex, and therefore both the real and imaginary parts of the ψ functions contribute to the charge current.

2. Differential conductance

The differential conductance $G(V,T)$ follows from differentiating Eq. (D1) with respect to V. This yields

$$G(V,T)=\frac{e^2\Gamma_1}{4\pi^2\hbar k_BT}\,\mathrm{Re}\Bigg\{A_1\psi^{(1)}\bigg(\frac{1}{2}+\frac{\xi_1+ieV}{2\pi k_BT}\bigg)+A_1\psi^{(1)}\bigg(\frac{1}{2}+\frac{\xi_1-ieV}{2\pi k_BT}\bigg)+A_2\psi^{(1)}\bigg(\frac{1}{2}+\frac{\xi_2+ieV}{2\pi k_BT}\bigg)+A_2\psi^{(1)}\bigg(\frac{1}{2}+\frac{\xi_2-ieV}{2\pi k_BT}\bigg)\Bigg\}, \tag{D4}$$

where $\psi^{(1)}(z)=d\psi/dz$ is the trigamma function.[30]

3. Charge-current noise

It is cumbersome to write down a single expression for the noise spectrum at arbitrary temperature and model parameters. We therefore restrict ourselves in the following to those particular cases discussed in the main text.

(i) For zero temperature and arbitrary model parameters, the zero-frequency noise is given by

$$S(\Omega=0,T=0)=2eI_c(V)+2\frac{e^2\Gamma_1^2}{\pi\hbar}\,\mathrm{Re}\Bigg\{\frac{A_1^2}{i\xi_1}-\frac{A_1^2}{eV+i\xi_1}+\frac{A_2^2}{i\xi_2}-\frac{A_2^2}{eV+i\xi_2}-2i\frac{A_1A_2}{\xi_1-\xi_2}\bigg[\ln\bigg(\frac{eV+i\xi_2}{eV+i\xi_1}\bigg)-\ln\bigg(\frac{\xi_2}{\xi_1}\bigg)\bigg]\Bigg\}. \tag{D5}$$

Here $I_c(V)$ is the zero-temperature charge current obtained from Eq. (D1), while $\xi_{1,2}$ and $A_{1,2}$ are defined in Eqs. (D2) and (D3), respectively.

(ii) For finite temperature and zero magnetic field, the zero-frequency noise becomes

$$S(\Omega=0,T,H=0)=2e\coth\bigg(\frac{eV}{2k_BT}\bigg)I_c(V)+2k_BT\frac{\Gamma_1}{\Gamma_a}G(V,T)+2e\frac{\Gamma_1}{\Gamma_a}\bigg[\coth\bigg(\frac{eV}{k_BT}\bigg)-\coth\bigg(\frac{eV}{2k_BT}\bigg)\bigg]I_c(V)+\frac{e^2\Gamma_1^2}{\pi^2\hbar k_BT}\coth\bigg(\frac{eV}{k_BT}\bigg)\mathrm{Im}\bigg\{\psi^{(1)}\bigg(\frac{1}{2}+\frac{\Gamma_a+ieV}{2\pi k_BT}\bigg)\bigg\}-\frac{e^2\Gamma_1^2}{2\pi^3\hbar k_BT}\,\mathrm{Re}\bigg\{\psi^{(2)}\bigg(\frac{1}{2}+\frac{\Gamma_a+ieV}{2\pi k_BT}\bigg)\bigg\}, \tag{D6}$$

where $\psi^{(2)}(z)$ is the derivative of the trigamma function, $\psi^{(2)}(z)=d\psi^{(1)}/dz$. Notice that Eq. (D6) correctly reproduces two important limits. In the limit $V\to 0$, one can replace $\coth(eV/k_BT)$ and $\coth(eV/2k_BT)$ with k_BT/eV and $2k_BT/eV$, respectively, to obtain the fluctuation-dissipation theorem $S(T)=4k_BTG(0,T)$. In the limit $T\to 0$, each of the hyperbolic cotangents is equal to 1 (assuming $eV>0$), while $\psi^{(n)}$ can be replaced with $(-1)^{n+1}[2\pi k_BT/(\Gamma_a+ieV)]^n$. Consequently, Eq. (D6) correctly reduces to Eq. (7.12).

(iii) Away from zero frequency, the noise spectrum at zero temperature and zero magnetic field is given by

$$\begin{aligned}S(\Omega,T=0,H=0)=\frac{e^2\Gamma_1^2}{2\pi\hbar\Gamma_a}\Bigg(&\mathrm{sgn}(\Omega)\bigg[\arctan\bigg(\frac{eV+\hbar\Omega}{\Gamma_a}\bigg)-\arctan\bigg(\frac{eV-\hbar\Omega}{\Gamma_a}\bigg)\\&-2\frac{\Gamma_a}{\hbar\Omega}\,\mathrm{Re}\bigg\{\ln\bigg(\frac{eV+i\Gamma_a}{eV+\hbar\Omega+i\Gamma_a}\bigg)+\ln\bigg(\frac{eV+i\Gamma_a}{eV-\hbar\Omega+i\Gamma_a}\bigg)\bigg\}\bigg]\\&+\mathrm{sgn}(\hbar\Omega-2eV)\bigg\{\arctan\bigg(\frac{\hbar\Omega-eV}{\Gamma_a}\bigg)-\arctan\bigg(\frac{eV}{\Gamma_a}\bigg)-2\frac{\Gamma_a}{\hbar\Omega}\,\mathrm{Re}\{\ln(eV-\hbar\Omega+i\Gamma_a)-\ln(eV+i\Gamma_a)\}\bigg\}\\&+\mathrm{sgn}(\hbar\Omega+2eV)\bigg\{\arctan\bigg(\frac{\hbar\Omega+eV}{\Gamma_a}\bigg)+\arctan\bigg(\frac{eV}{\Gamma_a}\bigg)-2\frac{\Gamma_a}{\hbar\Omega}\,\mathrm{Re}\{\ln(\hbar\Omega+eV+i\Gamma_a)-\ln(eV+i\Gamma_a)\}\bigg\}\Bigg)\\&+\frac{e^2\Gamma_1}{\pi\hbar\Gamma_a}(\Gamma_a-\Gamma_1)\bigg[\mathrm{sgn}(\hbar\Omega-eV)\arctan\bigg(\frac{\hbar\Omega-eV}{\Gamma_a}\bigg)+\mathrm{sgn}(\hbar\Omega+eV)\arctan\bigg(\frac{\hbar\Omega+eV}{\Gamma_a}\bigg)\bigg].\end{aligned} \tag{D7}$$

The different singularities discussed in the main text originate in Eq. (D7) from the sign functions. Specifically, the term proportional to $\mathrm{sgn}(\Omega)$ is responsible for the singularity at $\Omega=0$ [see Eq. (7.22)], the terms proportional to $\mathrm{sgn}(\hbar\Omega\mp 2eV)$ produce the singularities at $\hbar\Omega=\pm 2eV$ [see Eq. (7.23)], and the terms involving $\mathrm{sgn}(\hbar\Omega\mp eV)$ generate the singularities at $\hbar\Omega=\pm eV$ [see Eq. (7.24)]. In the limit of large frequency only the arctangent terms survive, and $S(\Omega)$ approaches the asymptotic value of $e^2\Gamma_a/\hbar$. In the opposite limit $\Omega\to 0$, the noise in Eq. (D7) reduces to Eq. (7.12).

4. Impurity magnetization

Finally, the impurity magnetization has been conveniently expressed in Eq. (8.2) in terms of the auxiliary function $m(x,y)$. At finite temperature, the latter takes the form

$$m(x,y)=\mathrm{Im}\left\{\frac{x}{\pi\Delta}\left[\psi\left(\frac{1}{2}+\frac{2y-\Delta+i\Gamma_a+i\Gamma_b}{i4\pi k_B T}\right)-\psi\left(\frac{1}{2}+\frac{2y+\Delta+i\Gamma_a+i\Gamma_b}{i4\pi k_B T}\right)\right]\right\}, \tag{D8}$$

where

$$\Delta=\sqrt{4x^2-(\Gamma_a-\Gamma_b)^2}. \tag{D9}$$

For $T\to 0$, each of the digamma functions in Eq. (D8) reduces to a logarithm, and Eq. (8.4) is properly recovered.

[1] S. Tarucha, T. Honda, and T. Saku, Solid State Commun. **94**, 413 (1995); A. Yacoby, H. L. Stormer, N. S. Wingreen, L. N. Pfeiffer, K. W. Baldwin, and K. W. West, Phys. Rev. Lett. **77**, 4612 (1996).

[2] C. T. Black, D. C. Ralph, and M. Tinkham, Phys. Rev. Lett. **76**, 688 (1996); D. C. Ralph, C. T. Black, and M. Tinkham, *ibid.* **78**, 4087 (1997); F. Braun, J. von Delft, D. C. Ralph, and M. Tinkham, *ibid.* **79**, 921 (1997).

[3] See, e.g., *The Quantum Hall Effect*, edited by R. E. Prange and S. M. Girvin (Springer-Verlag, New York, 1990). For a recent survey of the fractional quantum Hall regime see A. H. MacDonald, Solid State Commun. **102**, 143 (1997).

[4] M. A. Kastner, Phys. Today **46** (No. 1), 24 (1993).

[5] A. F. G. Wyatt, Phys. Rev. Lett. **13**, 401 (1964); R. A. Logan and J. M. Rowell, *ibid.* **13**, 404 (1964).

[6] For a comprehensive review of early experiments on tunneling through magnetic impurities see, e.g., E. L. Wolf, *Principles of Electron Tunneling spectroscopy* (Oxford University Press, Oxford, 1989), Chap. 8.

[7] J. Appelbaum, Phys. Rev. Lett. **17**, 91 (1966); P. W. Anderson, *ibid.* **17**, 95 (1966).

[8] D. C. Ralph and R. A. Buhrman, Phys. Rev. Lett. **72**, 3401 (1994).

[9] D. Goldhaber-Gordon, H. Shtrikman, D. Mahalu, D. Abusch-Magder, U. Meirav, and M. A. Kastner, Nature (London) **391**, 156 (1998).

[10] L. I. Glazman and M. E. Raikh, Pis'ma Zh. Éksp. Teor. Fiz. **47**, 378 (1988) [JETP Lett. **47**, 452 (1988)]; T. K. Ng and P. A. Lee, Phys. Rev. Lett. **61**, 1768 (1988); S. Hershfield, J. H. Davies, and J. W. Wilkins, *ibid.* **67**, 3720 (1991); Y. Meir, N. S. Wingreen, and P. A. Lee, *ibid.* **70**, 2601 (1993); T. K. Ng, *ibid.* **70**, 3635 (1993).

[11] N. Andrei, K. Furuya, and J. Lowenstein, Rev. Mod. Phys. **55**, 331 (1983); A. M. Tsvelik and P. B. Wiegmann, Adv. Phys. **32**, 453 (1983).

[12] G. Toulouse, Phys. Rev. B **2**, 270 (1970).

[13] V. J. Emery and S. Kivelson, Phys. Rev. B **46**, 10 812 (1992).

[14] A. Schiller and S. Hershfield, Phys. Rev. B **51**, 12 896 (1995). See also A. Schiller and S. Hershfield, Phys. Rev. Lett. **77**, 1821 (1996).

[15] L. P. Kadanoff and G. Baym, *Quantum Statistical Mechanics* (Benjamin, New York, 1962).

[16] L. V. Keldysh, Zh. Éksp. Teor. Fiz. **47**, 1515 (1964) [Sov. Phys. JETP **20**, 1018 (1965)].

[17] S. Hershfield, Phys. Rev. Lett. **70**, 2134 (1993).

[18] See, for example, I. Affleck and A. W. W. Ludwig, Nucl. Phys. B **360**, 641 (1991).

[19] P. W. Anderson, J. Phys. C **3**, 2436 (1970).

[20] P. Noziéres and A. Blandin, J. Phys. (Paris) **41**, 193 (1980).

[21] J. R. Schrieffer and P. A. Wolff, Phys. Rev. **149**, 491 (1966).

[22] A formal derivation of this result can be obtained within bosonization. A magnetic field acting on the conduction-electron spins adds the term $-(\mu_B g_e H_{ext}/2\pi)\int\nabla\Phi_s(x)dx$ to the Hamiltonian of Eq. (3.8). This additional magnetic term can be absorbed into the kinetic-energy part by shifting $\nabla\Phi_s(x)$ according to $\nabla\Phi_s(x)-\mu_B g_e H_{ext}/\hbar v_F\to\nabla\Phi_s(x)$, which generates two other contributions in its place: a constant term $-\frac{1}{2}(\mu_B g_e)^2\rho_0 H_{ext}^2$, corresponding to the magnetization energy of the two leads, and a renormalization of the local magnetic field according to Eq. (2.22).

[23] V. J. Emery, in *Highly Conducting One-Dimensional Solids*, edited by J. T. Devreese *et al.* (Plenum, New York, 1979); J. Sólyom, Adv. Phys. **28**, 201 (1979).

[24] F. D. M. Haldane, J. Phys. C **14**, 2585 (1981).

[25] See, e.g., K. Gottfried, *Quantum Mechanics* (Addison-Wesley, Redwood City, CA, 1989).

[26] We choose to treat the local magnetic field H as a perturbation. An alternative approach is to include this term within $\mathcal{H}_0$. Since we sum the perturbation theory exactly to all orders, both approaches are equivalent.

[27] For a clear exposition see D. C. Langreth, in *Linear and Nonlinear Electron Transport in Solids*, Vol. 17 of *NATO Advanced Study Institute, Series B: Physics*, edited by J. T. Devreese and V. E. van Doren (Plenum, New York, 1976), p. 3.

[28] In general, the greater and lesser Green functions are given by $G^{>,<}=G^r\Sigma^{>,<}G^a+G^r(G_0^r)^{-1}G_0^{>,<}(G_0^r)^{-1}G^a$, where zero subscripts denote unperturbed Green functions. Here, however, the second term drops since $(G_0^r)^{-1}G_0^{>,<}(G_0^r)^{-1}$ is zero, while $G^{r,a}$ are both regular along the real axis.

[29] K. Majumdar, A. Schiller, and S. Hershfield, Phys. Rev. B **57**, 2991 (1998).

[30] See, e.g., *Handbook of Mathematical Functions*, edited by M. Abramowitz and I. A. Stegun (Dover, New York, 1972), Chap. 6.

[31] D. C. Ralph and R. A. Buhrman, Phys. Rev. Lett. **69**, 2118 (1992).

[32] D. C. Ralph, A. W. W. Ludwig, J. von Delft, and R. A. Buhrman, Phys. Rev. Lett. **72**, 1064 (1994).

[33] M. H. Hettler, J. Kroha, and S. Hershfield, Phys. Rev. Lett. **73**, 1967 (1994).

[34] Although our model also has two-channel limits, these couple differently to the applied voltage. Specifically, for $\Gamma_a=0$ the two leads are decoupled, while for $\Gamma_b=0$ a finite voltage V breaks the picture of two equivalent channels within our model. By contrast, the Hamiltonian of Eq. (2.2) with an additional flavor index maintains two-channel symmetry even in the presence of a finite V.

[35] A. van der Ziel, *Noise in Solid State Devices and Circuits* (Wiley, New York, 1986).

[36] V. A. Khlus, Zh. Éksp. Teor. Fiz. **93**, 2179 (1987) [Sov. Phys. JETP **66**, 1243 (1987)].

[37] G. B. Lesovik, Pis'ma Zh. Éksp. Teor. Fiz. **49**, 513 (1989) [JETP Lett. **49**, 592 (1989)].

[38] B. Yurke and G. P. Kochanski, Phys. Rev. B **41**, 8184 (1990).

[39] M. Büttiker, Phys. Rev. Lett. **65**, 2901 (1990); Phys. Rev. B **46**, 12 485 (1992).
[40] R. Landauer and Th. Martin, Physica B **175**, 167 (1991); Th. Martin and R. Landauer, Phys. Rev. B **45**, 1742 (1992).
[41] For a recent review see M. J. M. de Jong and C. W. J. Beenakker, in *Mesoscopic Electron Transport*, Vol. 345 of *NATO Advanced Study Institute, Series B: Physics*, edited by L. L. Sohn, L. P. Kouwenhoven, and G. Schön (Kluwer Academic, Dordrecht, 1997), p. 225.
[42] L. Y. Chen and C. S. Ting, Phys. Rev. B **43**, 4534 (1991).
[43] J. B. Johnson, Phys. Rev. **29**, 367 (1927); H. Nyquist, *ibid.* **32**, 229 (1928).
[44] S.-R. Eric Yang, Solid State Commun. **81**, 375 (1992).
[45] C. de C. Chamon, D. E. Freed, and X. G. Wen, Phys. Rev. B **53**, 4033 (1996).
[46] For a finite magnetic field, one can actually improve the qualitative agreement with the experimental curves by considering perturbation theory about the solvable point; see Ref. 29.